Variation in style of overpressure in Scotian Shelf wells, Scotian Basin

By

Dillon White

A Thesis Submitted to

Saint Mary's University, Halifax Nova Scotia

in Partial Fulfillment of the Requirements for a

Bachelor of Science Honours Degree in Geology

October 2014, Halifax, Nova Scotia

Approved: Dr. Georgia Pe-Piper

Supervisor

Date: October, 2014

Certification

I certify that this thesis was submitted by Dillon White in fulfillment of the honours degree requirement for the Bachelor of Science Honours degree in Geology at Saint Mary's University, Halifax, Nova Scotia. This thesis truly represents the original work carried out by Mr. White under my supervision.

Dr. Georgia Pe-Piper

Professor of Geology

Variation in style of overpressure in Scotian Shelf wells, Scotian Basin

By Dillon C. White

Abstract

Overpressure is a phenomenon where pressures greatly exceed normal hydrostatic pressure and occurs in many wells within the Scotian Basin. Due to this area being actively explored for oil and gas over the last five decades, it is very important to understand where and what is causing overpressure. The main causes of overpressure are disequilibrium compaction, clay diagenesis, and hydrocarbon generation, although, the relative importance of these processes in the Scotian Basin is uncertain.

To assess and interpret the causes of variability in the style of overpressure in different wells in the Scotian Basin, velocity and density data from wireline data logs were used to produce velocity vs. density cross plots. These plots allowed the possible secondary mechanisms of overpressure generation to be visualized. XRD of < 2 μm clays from shales within overpressured wells were analyzed based on clay mineralogy to possibly find a link between overpressure and diagenesis occurring in the studied samples.

Down-well variation in velocity vs. density of shales based on wireline logs showed a wide range of velocity vs. density patterns in overpressured sections. There was an apparent regular distribution of different types observed based on velocity-density patterns.

Fractures and cementation may have an influence on velocity and density downwell. The fractures may be due to the buildup of overpressure and its eventual release. The opening of fractures would cause a decrease in velocity and that would be observable in velocity-density plots. The appearance and disappearance of smectite at certain depths in wells may be due to: a) downhole contamination by smectite cuttings from the upper sections of the wells. b) Local increase of temperature by circulating fluids causing these diagenetic transformations and c) changes in the supply of smectite by rivers that were climatically controlled.

October, 2014

Acknowledgements

I would like to thank my supervisor Dr. Georgia Pe-Piper, whom without her I would not have even thought about doing an honours, let alone complete one. Thanks to Dr. David J.W. Piper for his time, advice, and feedback on countless drafts and edits. You both provided knowledge and guidance from the beginning and right until the end and for that I am truly grateful.

I would like to thank Owen Brown of the Geological Survey of Canada (Bedford Institute of Oceanography) for his guidance and patience in the preparation of samples for XRD analysis. Thanks to Bill Leblanc of the Geological Survey of Canada (Bedford Institute of Oceanography) for running the analysis.

Thanks to the Geological Survey of Canada for providing me a workspace to complete this project. Thanks to the Canada-Nova Scotia Offshore Petroleum Board for providing samples for which part of this project is based on.

Thanks to Yuanyuan Zhang for always having the time to answer one of the many questions and provide help whenever I needed it.

Table of Contents

List of Figures

List of Tables

Chapter 1.0: Introduction

Overpressure is a phenomenon that has been recognized for decades in petroleum basins. It occurs when connate fluids cannot escape and the resulting subsurface formation fluid pressure becomes greater than hydrostatic pressure at a given depth. There are many proposed causes of overpressure, the most popular being disequilibrium compaction. This involves sediment being buried so fast that pore fluids do not have enough time to escape. The sediment is thus undercompacted and the pore fluids become overpressured by taking on part of the overburden load (Mudford 1988). Disequilibrium compaction develops in rapidly subsiding basins because subsequent rapid sedimentation tends to follow. Another cause for overpressure is clay diagenesis. Mudford (1988) describes the transformation of montmorillonite to illite by desorption of intercrystalline water as being the most commonly considered. Other diagenetic transformations have also been examined, such as the reaction from gypsum to anhydrite and smectite to illite (Osborne and Swarbrick 1997). Hydrocarbon generation from the maturation of kerogen to gas is another cause that has been looked at closely because the volume change related to this reaction is considerable (Osborne and Swarbrick 1997). Other causes include aquathermal pressuring (liquid water changing to gas due to change in temperature), and tectonic compression. The last two processes will not be looked at in this thesis. The above causes may produce overpressure independently or in combination with one another.

In order for overpressure to be generated and maintained, fluid flow must be restricted. These restrictions can take the form of salt, anhydrite, shale, and impermeable sandstones and carbonates (Wade and Maclean 1990). Some seals will not allow overpressure to escape at all, while others will have low permeability and slowly release

the built up overpressure. An improper seal will obviously allow the overpressure to escape.

Overpressure is found in many wells within the Scotian Basin. It is important to study because of the dangerous nature of drilling. When drilling into a high pressure zone, the subsurface pressure can be so high that a blowout results. This has been the case for Uniacke G-72 and West Venture N-91 that are located within the overpressure system of the Scotian Basin (Wade and Maclean 1990). This is what drives the research to understand more about overpressure.

1.1 Regional Geology of the Scotian Basin

The Scotian Basin is located offshore Nova Scotia, where it extends 1200 km from the eastern part of Georges Bank to the central Grand Banks (Wade and Maclean 1990). Figure 1.1.1 shows the wells studied in this thesis and their locations within the Scotian Basin. It is approximately 300,000 km^2 in size and formed on a passive margin that developed due to North America rifting and separating from Africa during the breakup of Pangea (CNSOPB, 2000). Development of the North Atlantic ocean basin caused sedimentation, producing interconnected Mesozoic-Cenozoic depocenters, which form a complex that is the Scotian Basin (Wade and Maclean 1990). Northeast trending grabens are thought to be the earliest form of the basin (Wade and Maclean 1990). The Scotian Basin is made up of many sub-basins including Shelburne, Sable, Abenaki, Laurentian and South Whale. These basins are interconnected areas of thick sediments that contain more than 12 km of strata that has been produced from continuous subsidence (Wade and Maclean 1990). The sub-basins are differentiated based on variations in periods of rapid subsidence (Wade and Maclean 1990).

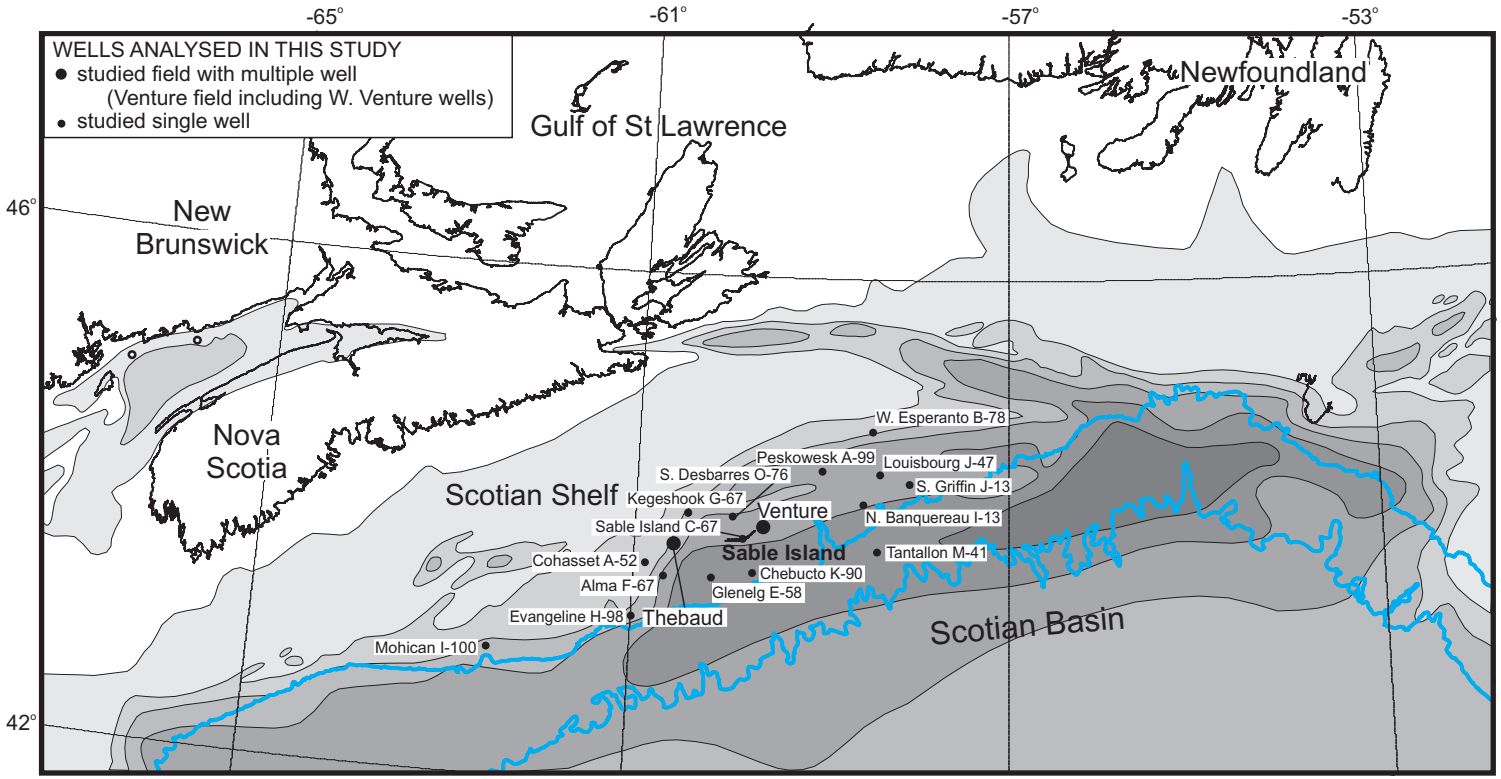

Figure 1.1.1 Map showing well locations in the Scotian Basin.

1.2 Overpressure in the Scotian Basin

Overpressure occurs in the Sable as well as the Abenaki sub-basins. Early wells and a number of later and deeper ones revealed an overpressure zone at least 10,000 km^2 in extent centered on Sable Island (Wade and Maclean 1990). The Louisbourg, Hesper, and West Esperanto wells also revealed that overpressure is found far to the east of Sable Island in the Abenaki sub-basin (Wade and Maclean 1990). It is unknown if the overpressure associated with these two systems is connected. Table 1 lists the wells used in this study, their position relative to Nova Scotia, and the year they were drilled.

Well	Geographic Position[1]	Year drilled
Alma F-67[2]	West Outboard	1983
Chebucto K-90[2]	Center Outboard	1984
Cohasset A-52	West Inboard	1985
Evangeline H-98[2]	West Outboard	1984
Glenelg E-58[2]	West Outboard	1984
Kegeshook G-67	West Inboard	1985
Louisbourg J-47[2]	East Outboard	1983
Mohican I-100	West Outboard	1971
North Banquereau I-13[2]	East Outboard	1982
Peskowesk A-99	East Inboard	1985
Sable Island C-67[2]	Center Inboard	1967
South Desbarres O-76[2]	Center Inboard	1984
South Griffin J-13[2]	East Outboard	1984
Tantallon M-41[2]	East Outboard	1986
Thebaud C-74[2]	West Inboard	1986
Thebaud I-93[2]	West Inboard	1985
Thebaud I-94[2]	West Inboard	1978
Venture B-43[2]	Center Inboard	1981
Venture B-52[2]	Center Inboard	1983
Venture H-22[2]	Center Inboard	1983
West Esperanto B-78[2]	East Inboard	1982
West Venture C-62[2]	Center Inboard	1984
West Venture N-91[2]	Center Inboard	1984

Table 1: All of the wells used to produce velocity-density cross plots. The location of the wells used in this study. The year they were drilled. 1 = Geographical position relative to Nova Scotia, 2 = Wells with overpressure.

Overpressured formations in the Scotian Basin contain abundant reservoir beds and shales are fully lithified, unlike the Gulf Coast, where there are less abundant porous reservoir beds (Wade and Maclean 1990). Studies of Sable Basin sandstones by Noguera (1987) revealed that deep diagenetic leaching of carbonate cement produced secondary porosity. This indicated that overpressure must have developed after shale diagenesis and may result from thermal expansion of pre-fluids or gas generation in a sealed system (Wade and Maclean 1990). The top of overpressure is shallowest in the southeast and gets progressively deeper and older towards the northeast (Wade and Maclean 1990).

The mechanism of overpressure generation is unknown to date but many speculations have been proposed. Some authors believe disequilibrium compaction is the cause of overpressure in the Venture field, while others believe that it is due to gas generation. Drummond (1986) believed overpressure was caused from disequilibrium compaction and thought reservoirs in the Venture field were sealed early on, thus preserving higher porosity and causing pore fluids to take on the overburden load. Mudford (1998) thought that disequilibrium compaction could not be the mechanism because prohibitive low permeability is required throughout the sedimentary section. His evidence suggested that overpressure was still developing and associated with gas generation. Later research suggests that disequilibrium compaction created the overpressure and gas generation is slightly contributing to the overall overpressure (Mudford and Best 1989, Mudford 1990, Forbes et al., 1992, Williamson, 1995).

1.3 Previous work on overpressure using velocity vs. density cross plots

Velocity-density cross plots are a fairly recent method of interpreting overpressure. Bowers (2001) was the first to implement this method and since then other authors (Hoesni 2004, O'Connor et al., 2011, Lahann and Swarbrick 2011, Tingay et al., 2013) have also adopted it. The majority of research involving velocity-density cross plotting has been done in the Malay Basin, Malaysia. This thesis marks the first time velocity-density cross plots have been used to understand overpressure across the entire Scotian Basin.

1.4 Objectives of this thesis

The objectives of this thesis are two fold. The first part is to characterize and interpret the mechanisms of overpressure generation. This will be done by creating cross plots of velocity and density data, which were obtained from well logs. The cross plots will be analyzed based on how velocity and density vary within shales and depth. Hopefully they can show us what was occurring before, leading up to, and within the overpressured interval.

The second is to understand the role of clay mineral diagenesis on overpressure. It has long been proposed that diagenesis may contribute to overpressure, albeit small. Therefore, it is important to study the affects of diagenesis on overpressure. Clay diagenesis will be studied by using a method known as X-ray Diffraction, to determine the changes in clay minerals, in overpressured and normally pressured intervals of selected wells.

Chapter 2.0: Methods

2.1 Introduction

Digital wireline log data for each well were obtained from the Geological Survey of Canada. We were interested in the depth, and the gamma, density, and velocity logs. The downloaded data were "cleaned" by only selecting data that would be used in making the required graphs. The cleaned data were put into a "shale data" worksheet where it would be sorted based on selected depths and gamma values which were obtained from the logs. The data were further cleaned by getting rid of unneeded values. It would then go into a "shale summary". Gamma values were chosen from the logs and also using the plots in MacLean and Wade (1993). These authors provided stratigraphic columns showing the location of shale. A gamma value was chosen and everything above that value was included and kept as shale data, everything below was not included. Once all the shale data were collected for each range of depth in the well, they were put into a shale summary. These steps were done for each well. Once all the shale summaries for each well were alone, they were sorted by depth from smallest to largest and plotted using Grapher™.

2.2 Data Sorting

We were looking for gamma values that would indicate shale. The data needed to be sorted in order to find appropriate gamma values. Values that were not indicating shale were omitted. Many data sets had missing gamma values at some depths, values of zero, or they were just repeated numbers. All such data were deleted. Then the following order of activities was executed.

1. Make 3 new worksheets and label them Cleaned data, Shale data, and Notes

2. Copy the data from the depth, gamma, density, neutron porosity and acoustic columns.

3. Paste data in Cleaned data worksheet. Clean up headers and delete neutron porosity column. You should be left with depth, gamma, density, and acoustic velocity.

4. Go through cleaned data and check if any of the columns have missing numbers. If they do, erase the row that has the missing numbers. For example, if there is no number in the gamma column but there are values for density and velocity, delete that row.

5. Reformat data to one decimal place.

6. Once data is cleaned, copy and paste it in the Shale data worksheet. Add a new column with the header: 1000/vel. Select the box below and put =1000/d2 into the formula bar. Press enter. Click and hold the little black square in the bottom right and drag down to the end of your data. Reformat the new data to one decimal place.

7. Using plots of gamma vs. depth (see below) and the East Coast Basin Atlas (MacLean and Wade 1993), find gamma values and areas of shale. The atlas will tell where the shale is and you just look at the log and draw a straight line through the majority of continuous squiggles. Where the line intersects the scale at the bottom will be the cut-off gamma value. If there is an area with a high velocity peak, do not include because this is likely sandstone. If the gamma reading is high but the East Coast Basin Atlas (Maclean and Wade 1993) indicates sandstone, it is probably shale mixed with the sandstone so you can include it. Anything including or above the chosen gamma value will be used; anything below will be discarded. This will create breaks in the data, which are marked by inserting two blank rows. Example: you choose a gamma value of 45 API

units and that corresponds to 4000 m depth. Then there is a gap due to a limestone bed till 4300 m. You would insert two rows at 4000.2 m indicating a break and then delete gamma values from 4000.2 m to 4300 m because they correspond to limestone not shale.

8. Once you have gamma values and breaks in the data sort the data by gamma from largest to smallest and delete everything below your chosen cut-off gamma value.

9. Once this is done delete the two inserted rows leaving no gaps in the data and sort by depth from smallest to largest.

10. Assemble all the shale data for each interval in an Excel worksheet called shale summary. There should be shale data for the entire well within it. Any gaps or rows with missing numbers should be removed and then the data should be sorted by depth from smallest to largest.

2.3 Graph Creation

The goal of this work was to produce velocity-density cross plots similar to the figure (Fig. 3.1.1) in Tingay et al. (2011). The plots were then used to investigate the type(s) of mechanisms involved in the production of overpressure in wells across the Scotian Basin. The plots were made using the drafting software Grapher ™. Appropriate axes were chosen. The Y-axis thus became the axis for Velocity (km/s 0 - 7) and X-axis the axis for Density (kg/m^3 1000 - 3500).

For both axes, large ticks were set to 0.10 inches and the smaller ticks were set to 0.05 inches. Depending on where the depth in each well in the data started, two or three plots were made. Each plot had its own color: pink was the shallowest, followed by purple, and red was the deepest. Data were plotted as small circles. In early plots they were 0.05 inches in diameter but

in later plots 0.01 inch circles were used. Various graph plots were created for each well and they are briefly described below.

Graph #1 (Fig. 2.3.1) had pink dots representing 0 to 2000 m, purple dots represented 2000 m to top of overpressure (if there was any), and red dots represented top of overpressure to total depth. This produced an overall trend for each well. Graph #2 (Fig. 2.3.2) used separations every 500 m with a different color for each interval. This allowed each interval to clearly stand out and a greater amount of detail was possible unlike Graph #1. Graph #2 used 0.01 inch rather than 0.05 inch circles. Every graph was saved as a gif and also as an emf that could be later used with CorelDraw ™. Graph #3 (Fig. 2.3.3) was the same as graph two but saw the addition of a trend line that represented the velocity-density data from individual wells. The X-axis changed to 1500-3000 kg/m^3 and the Y-axis changed to 1-5 km/s. Graph #4 (Fig. 2.3.4) took out the data above the top of overpressure from graph three and only focused on what occurred below; it also included the trend line. In some of the shale summaries there were density data that all had the same value, for example 2000. They produced a row of dots. These erroneous data were deleted.

During this project, there was some experimentation with different colours for data from different depths and experimentation on the best way to illustrate changes in velocity and density with depth. This included replacing the data from normally compacted interval above overpressure with an exponential curve (based on mean data either from multiple near-by wells or only the well in question). This allowed the data patterns in the overpressured interval to be presented more clearly (see section 2.7).

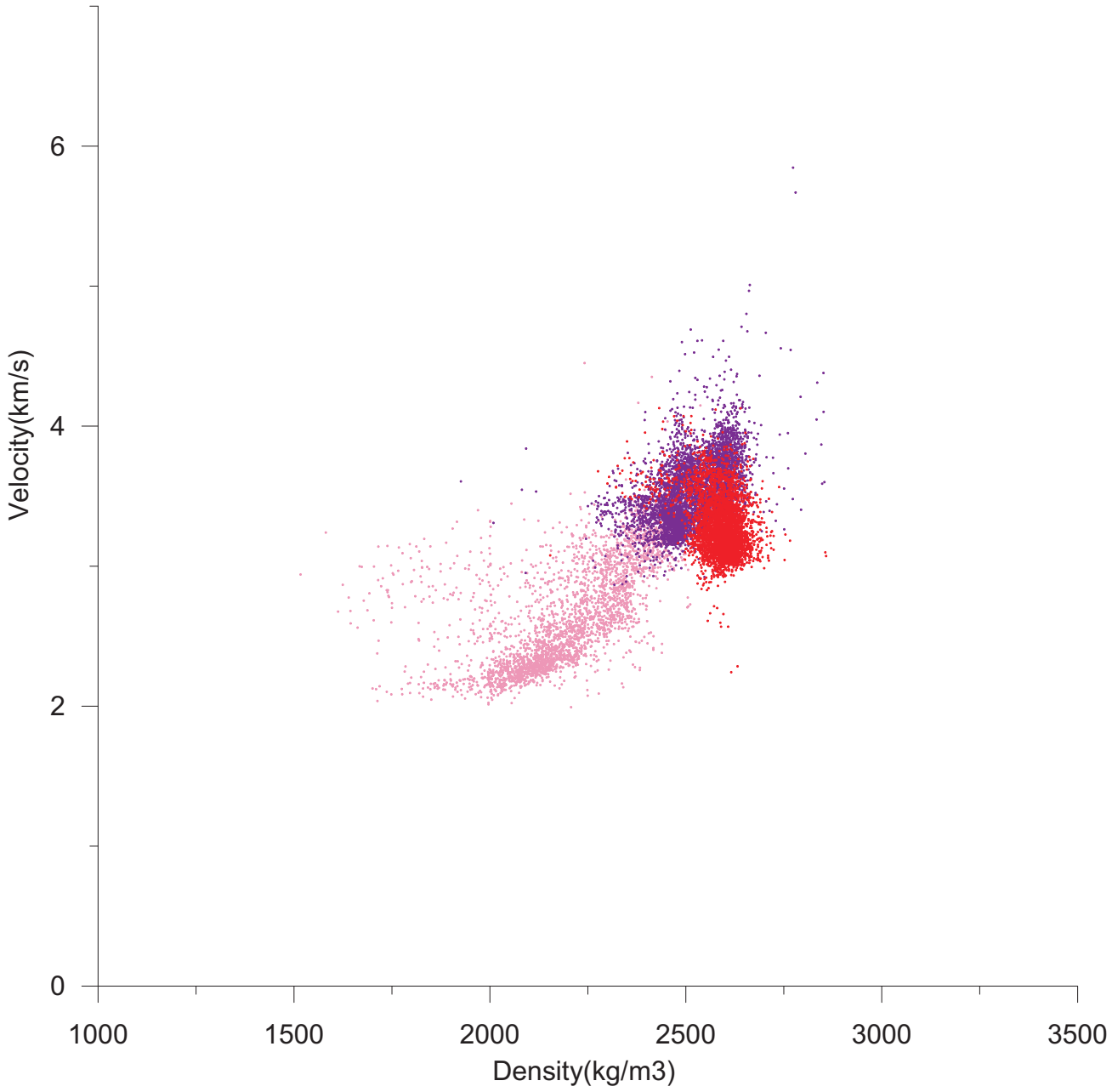

Figure 2.3.1 Graph #1 of a velocity vs. density plot.

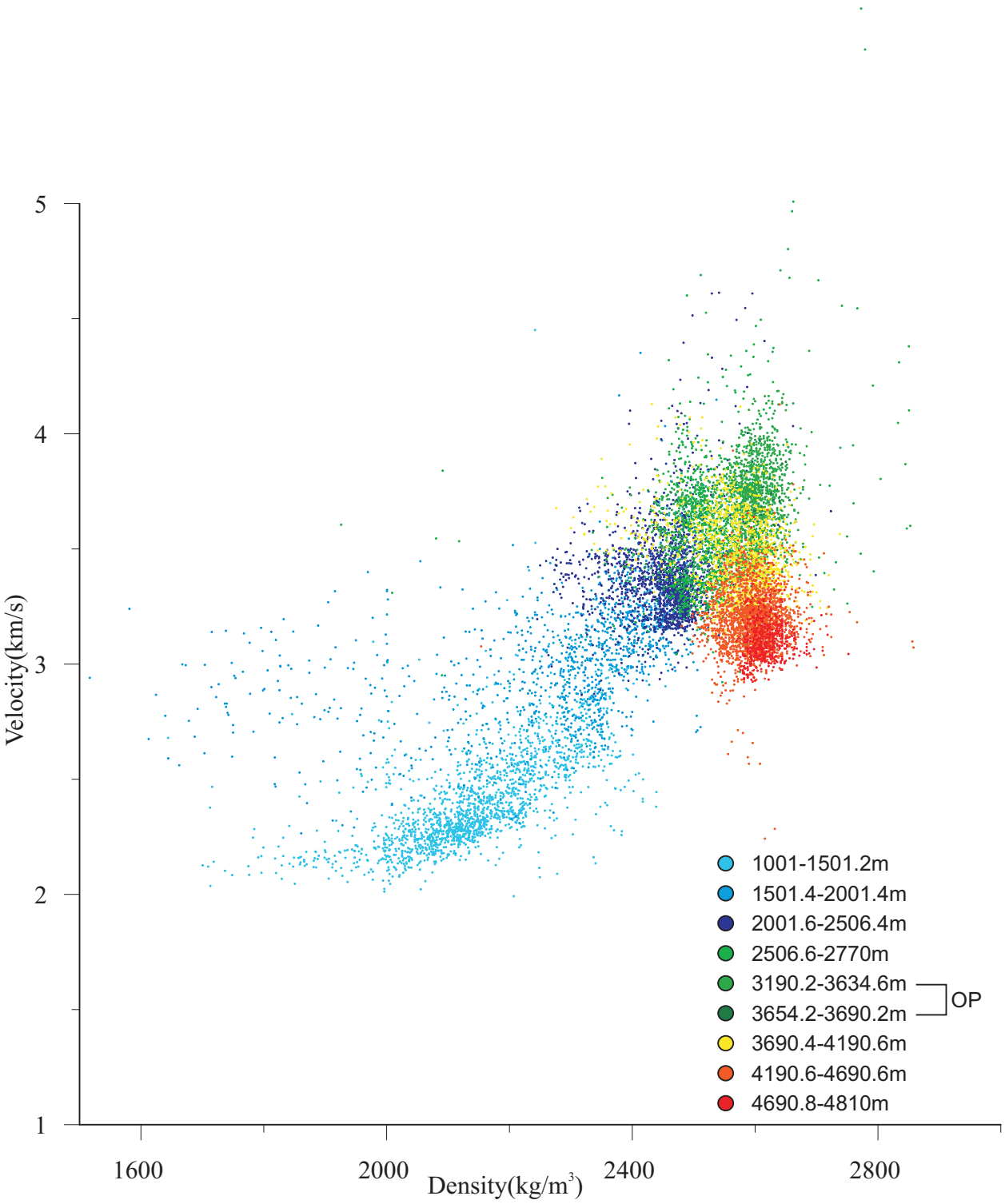

Figure 2.3.2 Graph #2 of a velocity vs. density plot.

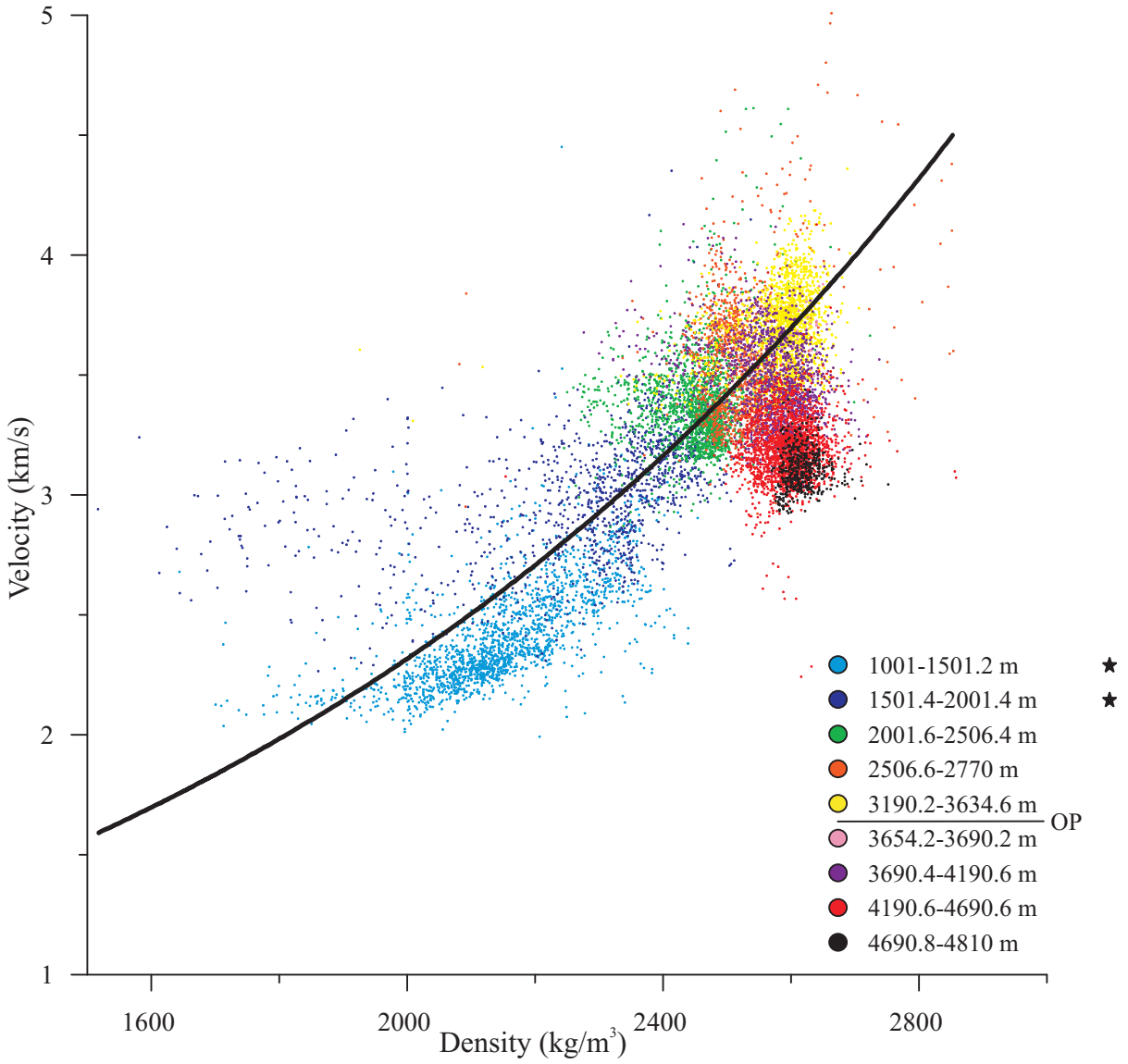

Figure 2.3.3 Graph #3 of a velocity vs. density plot.

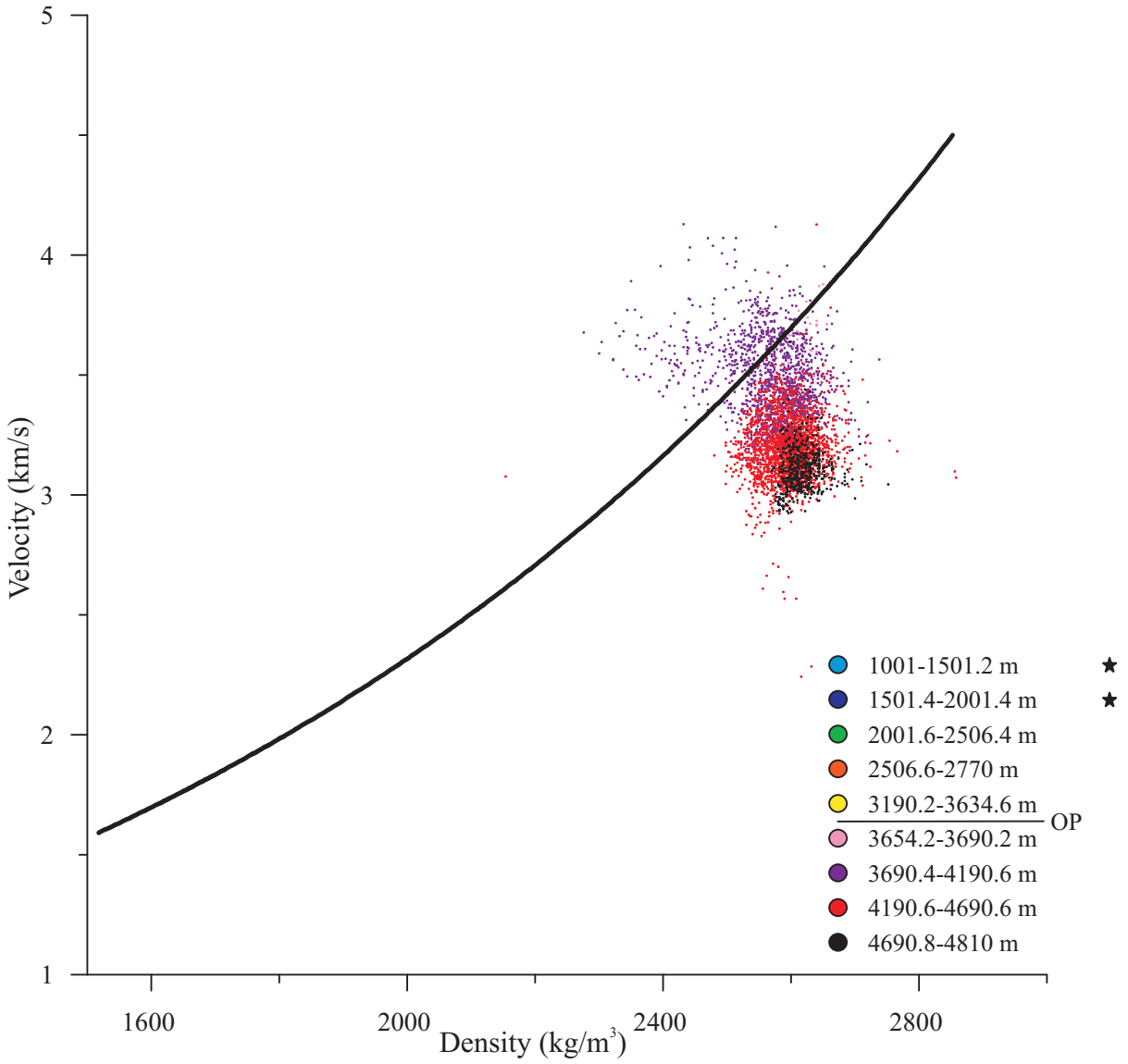

Figure 2.3.4 Graph #4 of a velocity vs. density plot.

2.4 Depth vs. Gamma

Plots of depth vs. gamma were necessary to identify the background gamma value for shale, discussed above. For most wells, the plot routine in NRCAN Basin database was used to produce depth vs. gamma plots. As necessary, plots were also created using Grapher™, from Excel data tables. This was done when no NRCAN Basin database plot was available, or when a particular interval needed to be viewed at a larger scale (e.g. South Griffin and Louisbourg) in order to determine where to sample for shale in cuttings.

2.5 500 m Separation

Since the first two versions of the velocity vs. density graphs only had 2-3 colors, it was unclear where the overpressure started on the graph and how velocity and density varied with depth. The overall shape of the graph was clear, but its relationship to depth was not well illustrated. So, we decided that every 500 m would mark a color change, hopefully allowing us to see more clearly the variations with depth. In addition, the color was changed at the top of overpressure.

Into a new Excel sheet 3 columns were added: Well, Row, and Depth. I originally started with the lowest depth from each respective shale summary and added 500 m to it and continued to the end of the hole. Then I found the corresponding rows and put them in the row column. For example, 1001-1501.2 m corresponds to rows 1-1808 for Alma F-67. The procedure was repeated in increments of 500 m. If the depth of the top of overpressure occurred within the 500 m interval, I would go from the top depth to the depth of the top of overpressure, and then from the top of overpressure to 500 m below the top depth. For example, start at 1000 m and go to 1500 m, top of overpressure is at 1300 m. I would go from 1000 m to 1300 m as one interval

then 1300 m to 1500 m as another. This was done for each well in order to make version #3 graphs with different colors to show how the graph responded at each depth interval.

2.6 CorelDRAW™

CorelDRAW™ allowed us to import Grapher™ files and make necessary additions and adjustments. The ability to put different information in the graph into different layers that could be turned off or locked was the main advantage of CorelDRAW™. When we wanted to compare two graphs you could easily turn a layer off or switch between pages and see similarities or differences. It also allowed focusing on selected sections of graphs. You could turn off a layer to only see the loading curve or dots below overpressure.

I used a CorelDRAW™ template that was set up with sensible default values for line weight, font size, duplicate distance and supernudge distance. I had copied and pasted the figure showing mechanisms of overpressure generation from the paper of Tingay et al. (2013). Then recreated the figure using CorelDRAW™ and put it into the iStandard.cdt template.

Once all of the second versions of the graphs were completed in Grapher™ they were imported into the iStandard template. As explained above, it was difficult to interpret variation with depth in this plot. That is why 500 m separation and different colors were important and a version three graph was needed.

Each Graph #3 plot was imported from Grapher™ onto the iStandard template. A legend was made with small rectangles that corresponded to the colors and their associated depths. An overpressure label was placed inside curved brackets beside the interval at which the

overpressure occurred. If it was not within an interval a square bracket was used to indicate overpressure was between two intervals. This legend style was kept the same for some wells but then later changed to small circles so the legend would not take up so much space.

Some graphs had dots that were far outside the axes, which caused problems when printing. Any dot that was >6 km s^{-1} velocity or >3000 kg m^{-3} density was deleted. Exponential trend lines were fitted to the data above the top of overpressure for individual wells in Excel (see next section below). The trend lines allowed us to turn off the colors above the top of overpressure, so we could see clearly what was happening below overpressure. I opened up three new layers. I put the graph in layer 2 and changed its scale to match the graph made in Grapher™. I aligned the trend lines axes for the trend line plot with the axes for the Grapher™ plot. Layer 2 was turned off in order to see only the curve. I found the curve segments and grouped them together and put them into layer 3. Next I took the dots below and including the top of overpressure and put them into layer 4. I turned on layer 4 to show the distribution of dots below overpressure. The colors at different depths below the top of overpressure were changed in order to tell them apart. Pink was shallowest followed by purple, red, and black. Thus graph #4 was created. Previous clay samples from Strathdee (2012) were indicated at the appropriate depth in the legend. A small black star is used to indicate sidepack samples and a large black circle is used to indicate < 2 micron samples.

2.7 Trend Line

The exponential trend line was created to summarize the change of density vs. velocity with increasing depth, i.e. to show the normal loading curve. In order to create trend lines the data

needed to be sorted. Density and 1000/velocity (columns C and E) data were taken from the shale summary worksheet and only points above overpressure were used for each well that had overpressure. If the well did not have overpressure then all of the data were used. The data were put into an Excel sheet. Data were selected in Excel and a marked scatter plot was inserted. I took off markers in order to just show the trend line and not individual points. In the Excel plot with the trend line, I made sure there were no markers, so that only the curve was brought over. I then copied the graph and clicked paste special and chose Picture (enhanced metafile).

Early in this study, trend lines used data from wells that were grouped together. The wells were grouped based on geographical location and stratigraphic similarity. Certain wells within the group skewed the data, which caused some trend lines to not fit all the graphs within the group. Therefore, an exponential trend line was created the same way as above but for each well individually. The axes were changed to match the axes used in Grapher™ and CorelDRAW™, i.e. X axis (velocity) 1-5 km s^{-1} and Y axis (density) 1500-3000 kg m^{-3}.

2.8 X-Ray Diffraction Preparation of < 2 µm clay fraction

X-Ray diffraction (XRD) is a quantitative way to determine the type of clay minerals in shale samples. For the X-ray diffraction analysis of selected representative samples from the studied wells the less than 2 µm fraction was separated from 8 core and 18 cuttings samples and slides were made from these fractions. To obtain the < 2 µm fraction the samples were crushed using a pestle and mortar and the resulting rock powder was put through a 250 µm sieve and a 63 µm sieve. Rock powder less than 63 µm was collected and suspended for 24 hours in a 1000 ml graduated cylinder using a 0.25% Calgon solution. The suspended particles were collected and

further separated by flocculating the sample using 1 ml of 0.5 mol calcium chloride and centrifuging until the < 2 μm fraction was separated. A 5% zincite standard was added to the < 2μm sample and then centrifuged again. The water was drawn off and the resulting product was preferentially smeared onto a diffraction slide and left to dry.

The < 2 μm slides were analyzed by a Siemens Kristaloflex diffractometer using Co Kα radiation. Samples were scanned from 2°-70° 2θ. Ethylene glycol was added to the samples whereby they were kept in a vacuumed chamber for 24 hours and run one at a time to reduce glycol evaporation. Glycolated samples were scanned from 2°-17° 2θ in order to identify smectites and mixed layer clays.

Diffractograms produced from the diffractometer were evaluated using Siemens Evaluation Software (diffractplus EVA). There were two diffractograms produced for the 26 samples, one raw (black) and one glycolated (grey). Clay minerals were identified and their peaks were measured using the diffractplus EVA software.

Chapter 3.0: Data presentation of velocity-density plots

3.1 Introduction

Sonic and density log data in overpressured shales have been previously used to create crossplots. They have been proposed to help distinguish between different overpressure mechanisms, notably between various fluid expansion or transfer mechanisms (Hoesni 2004, Lahann and Swarbrick 2011, O'Connor et al., 2011, Tingay et al., 2013). O'Connor et al., (2011) stated that conventional porosity-based pore pressure analysis using sonic/seismic velocity and resistivity data to measure porosity retention, underestimates the overpressure effect of these secondary mechanisms (fluid expansion, cementation) and therefore velocity-density cross plots will help understand these secondary mechanisms.

Velocity-density plots for each well were classified into ten types (Fig. 3.1.1) according to the variation of velocity and density with increasing depth, within the overpressured zone. The interpretations of the significance of different velocity-density trends by various authors (Hoesni 2004, Lahann and Swarbrick 2011, O'Connor et al., 2011, Tingay et al., 2013) were used as a guide in developing our classification and interpreting the likely mechanisms of overpressure generation. Each mechanism was specified as a certain type and will be referred to as such throughout this chapter.

Type 1 shows a pattern of velocity vs. density that follows a normal loading curve of increasing velocity and density with increasing depth and is found in rocks that are normally pressurized.

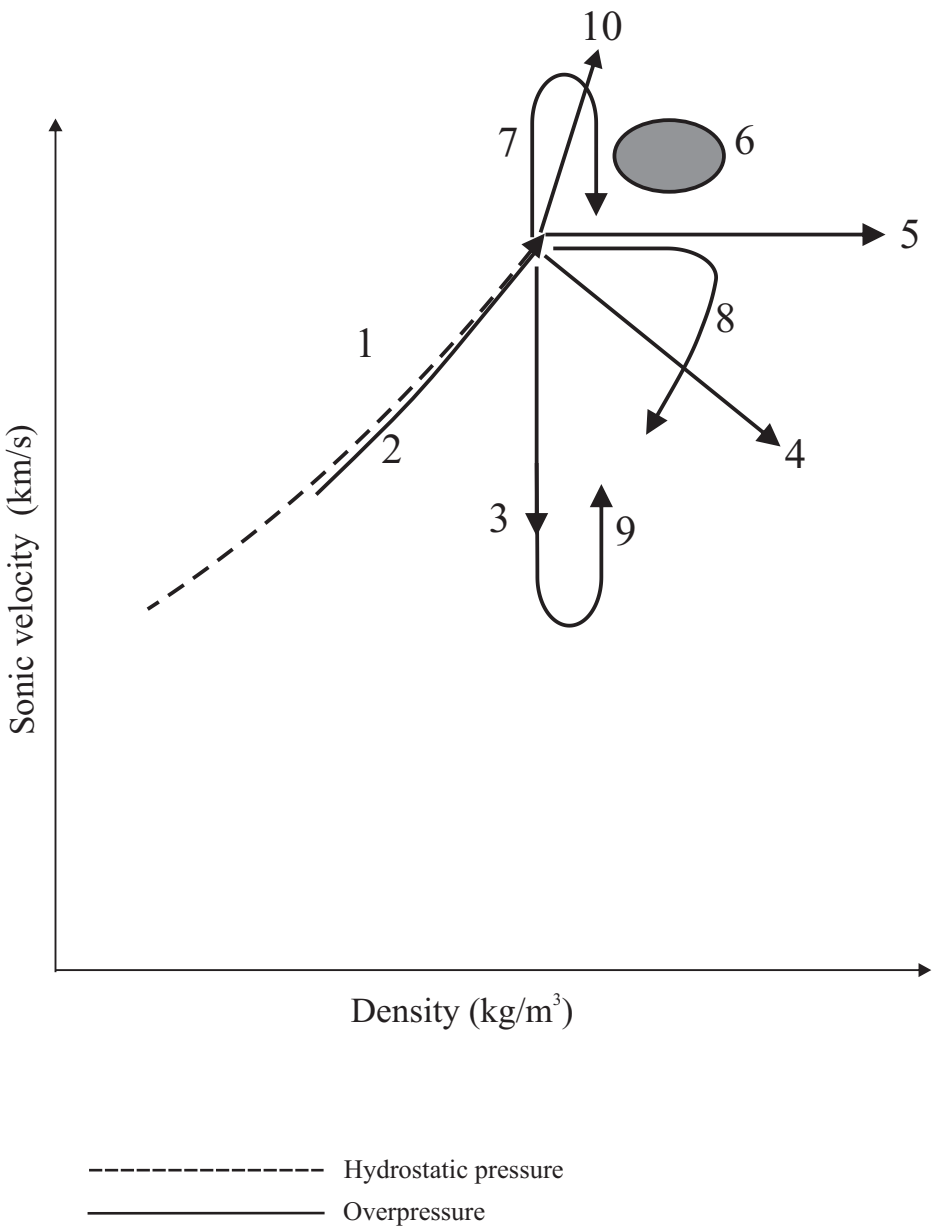

Figure 3.1.1 Types of velocity-density pattern observed in wells with overpressure. Type 1 is found at depths above overpressure. Types 2-5 are modified from Hoesni (2004) and Tingay et al. (2013). Types 6-10 are added from this study.

Type 2 shows a similar pattern to type 1, but includes rocks that are overpressured both above and within the overpressured zone. Such a pattern was interpreted O'Connor et al., (2011) as indicating disequilibrium compaction along the loading curve in overpressured rocks.

Type 3 shows a normal loading curve of increasing velocity and density with increasing depth, to a maximum near the top of overpressure. Below that, velocity decreases with little change in density. Such a pattern was interpreted by O'Connor et al., (2011) as resulting from fluid expansion, usually caused by gas generation.

Type 4 shows a normal loading curve to near the top of overpressure, followed by a decrease in velocity with an increase in density within the overpressured zone. It is interpreted as a hybrid between types 3 and 5, or may be the result of load transfer O'Connor et al., (2011).

Type 5 shows a normal loading curve to near the top of overpressure, followed by increasing density with little change in velocity with increasing depth in overpressured sediment. Such a pattern is indicative of clay diagenesis or chemical compaction O'Connor et al., (2011).

Type 6 shows a normal loading curve to near the top of overpressure, but within the overpressured sediment the pattern of velocity vs. density shows unresolved scatter, with no clear pattern with increasing depth.

Type 7 shows a normal loading curve to near the top of overpressure whereby it follows a pattern of increasing velocity with no change in density followed by decrease in velocity with no change in density.

Type 8 shows a normal loading curve to near the top of overpressure followed by an increase in density with little change in velocity until a certain point in the graph where then there is a decrease in velocity with little change in density.

Type 9 shows a similar pattern to type 7, only reversed. It shows a normal loading curve to near the top of overpressure whereby it decreases in velocity with no change in density followed by an increase in velocity with no change in density.

Type 10 shows a normal loading curve to near the top of overpressure where both density and velocity increase and finally a cluster forms.

This section of the report will describe for each well the different velocity vs. depth plots that were prepared. I will describe the patterns revealed by the plots and possible trends The character of the loading curve will also be described, including the degree of scatter from the best-fit curve, and will be compared with other wells.

3.2 Chebucto K-90

Chebucto K-90 was chosen to be the first "test" well because there was recorded overpressure, it is rich in shale (particularly within the overpressured zone), and has a lot of useable log data. The well is located in the central part of Sable Sub-Basin but more southern. It discovered gas and condensate. Overpressures starts at ~4180 m and reaches to about half way between hydrostatic and lithostatic at the base of the well at 5235 m.

Graph #2 (Fig. 3.2.1) follows up to the top of overpressure a normal loading curve of increasing velocity and density with increasing depth in overpressured rocks. Graph #3

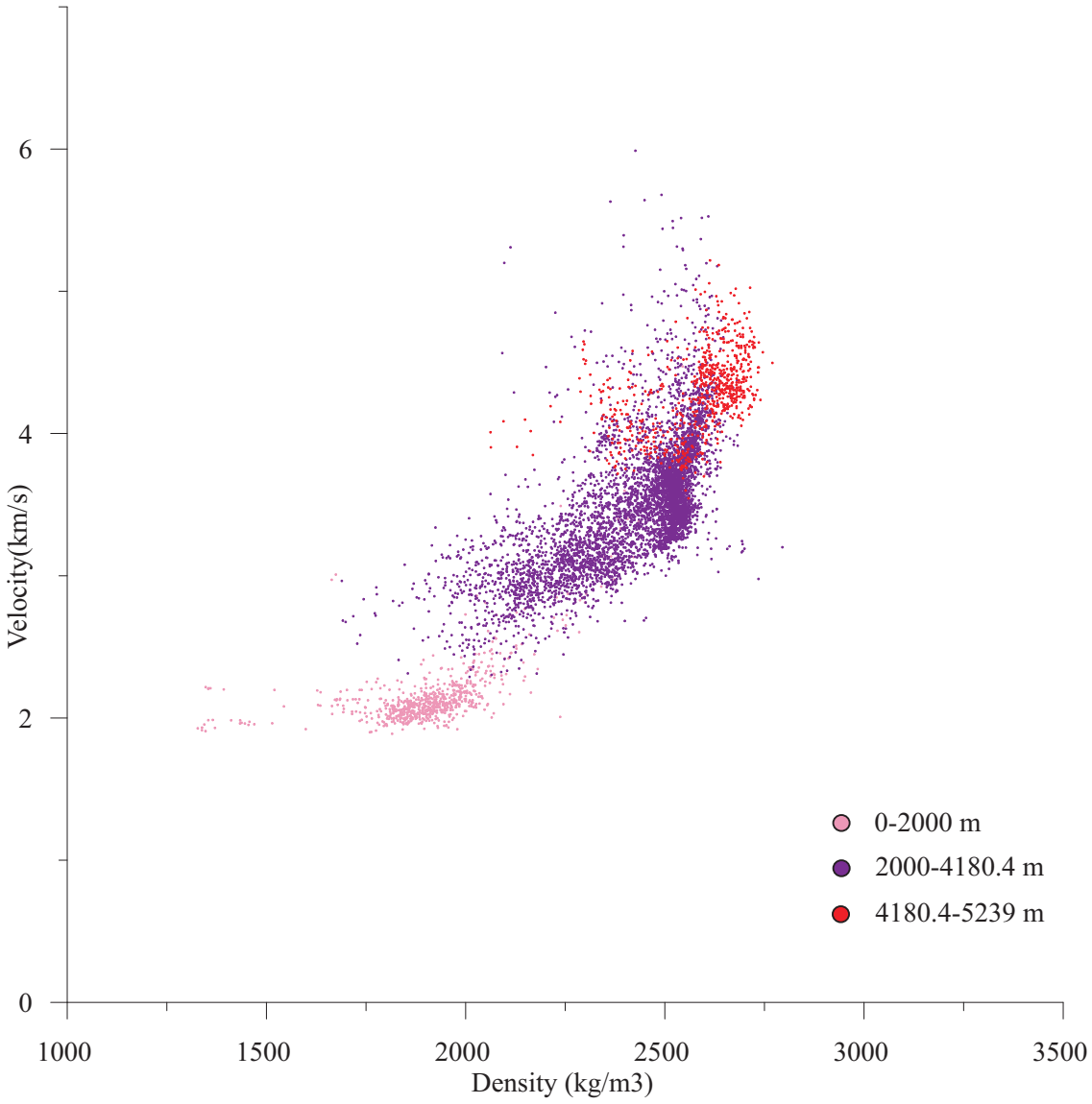

Figure 3.2.1 Graph #2 of a velocity vs. density plot for Chebucto K-90

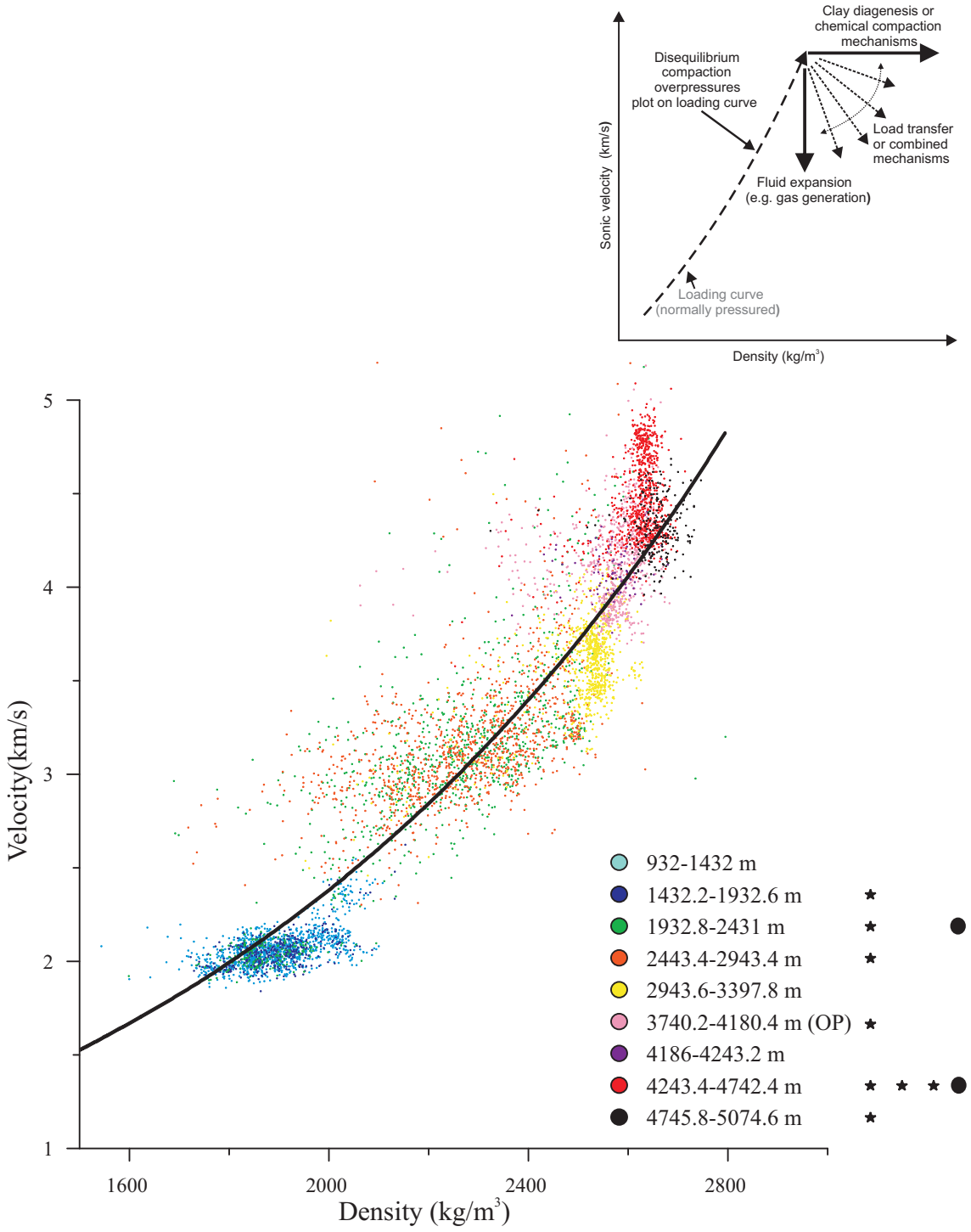

Figure 3.2.2 Graph #3 of a velocity vs. density plot for Chebucto K-90. In this and all subsequent similar figures, a mean exponential trend line has been calculated for all data points of the studied well. Stars in the legend indicate depths with a sidepack clay mineral analysis, whereas solid dots indicate depths with < 2µm clay mineral analysis. In all figures of Graph #3 and #4 the diagram in the inset is modified from Hoesni, 2004; and Tingay et al., 2013.

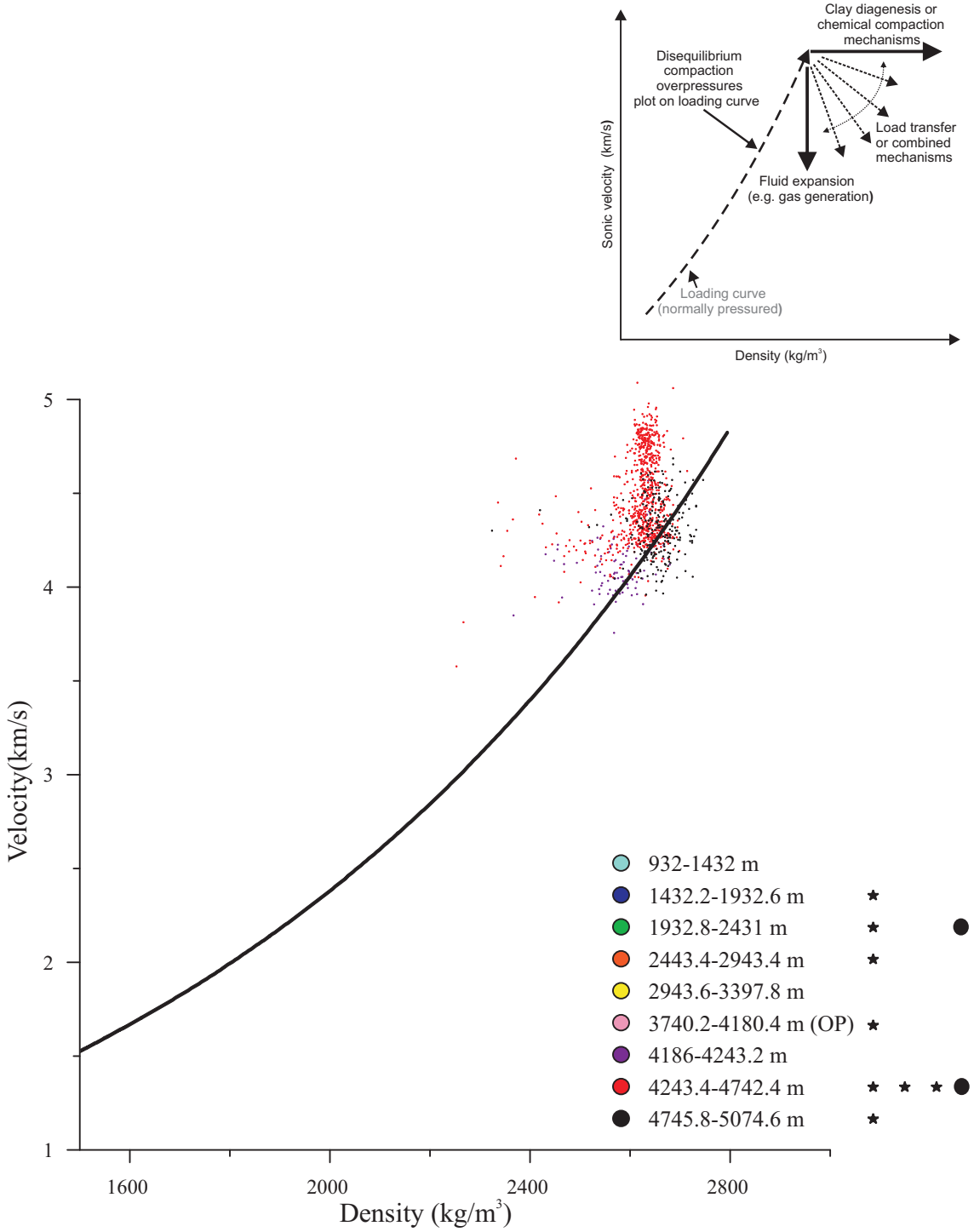

Figure 3.2.2 Graph #3 of a velocity vs. density plot for Chebucto K-90. In this and all subsequent similar figures, a mean exponential trend line has been calculated for all data points of the studied well. Stars in the legend indicate depths with a sidepack clay mineral analysis, whereas solid dots indicate depths with < 2µm clay mineral analysis. In all figures of Graph #3 and #4 the diagram in the inset is modified from Hoesni, 2004; and Tingay et al., 2013.

(Fig. 3.2.2) used a 10 API unit higher cut-off value for selecting log data as representing shale, to reduce the influence of silty shale, but showed no significant difference in pattern. In Graph #4 (Fig. 3.2.3), data from above the top of overpressure are replaced by an exponential trend line calculated from velocity and density data of the well. Graphs #2 and #3 show the same pattern but graph #3 has more data points because of the higher gamma cutoff. Samples within ~60 m of the top of overpressure (purple points) plot mostly close to the trend line. Samples from ~60-560 m below the top of overpressure (red points) form a vertical trend of increasing velocity. Finally samples >560 m below the top of overpressure (black points) show a vertical cluster similar to red points, but velocity values are not as high as the highest values shown by the red points, and the density values on average are slightly higher. Graph #4 thus shows a type 7 pattern (Fig. 3.1.1).

3.3 Alma F-67

Alma F-67 is located in the Western a part of the Sable Sub-Basin and like Chebucto K-90, there was a recorded overpressure. The well is rich in shale, and there is a lot of useable log data. The top of overpressure starts at ~3650 m and approaches lithostatic pressure down towards the bottom of the well (TD of 5054 m). The well discovered gas and condensate.

Graph #3 (Fig. 3.3.1) follows up to the top of overpressure a normal loading curve of increasing velocity and density with increasing depth in overpressured rocks, Data points from the overpressured interval (pink-purple-red-black) are arranged almost

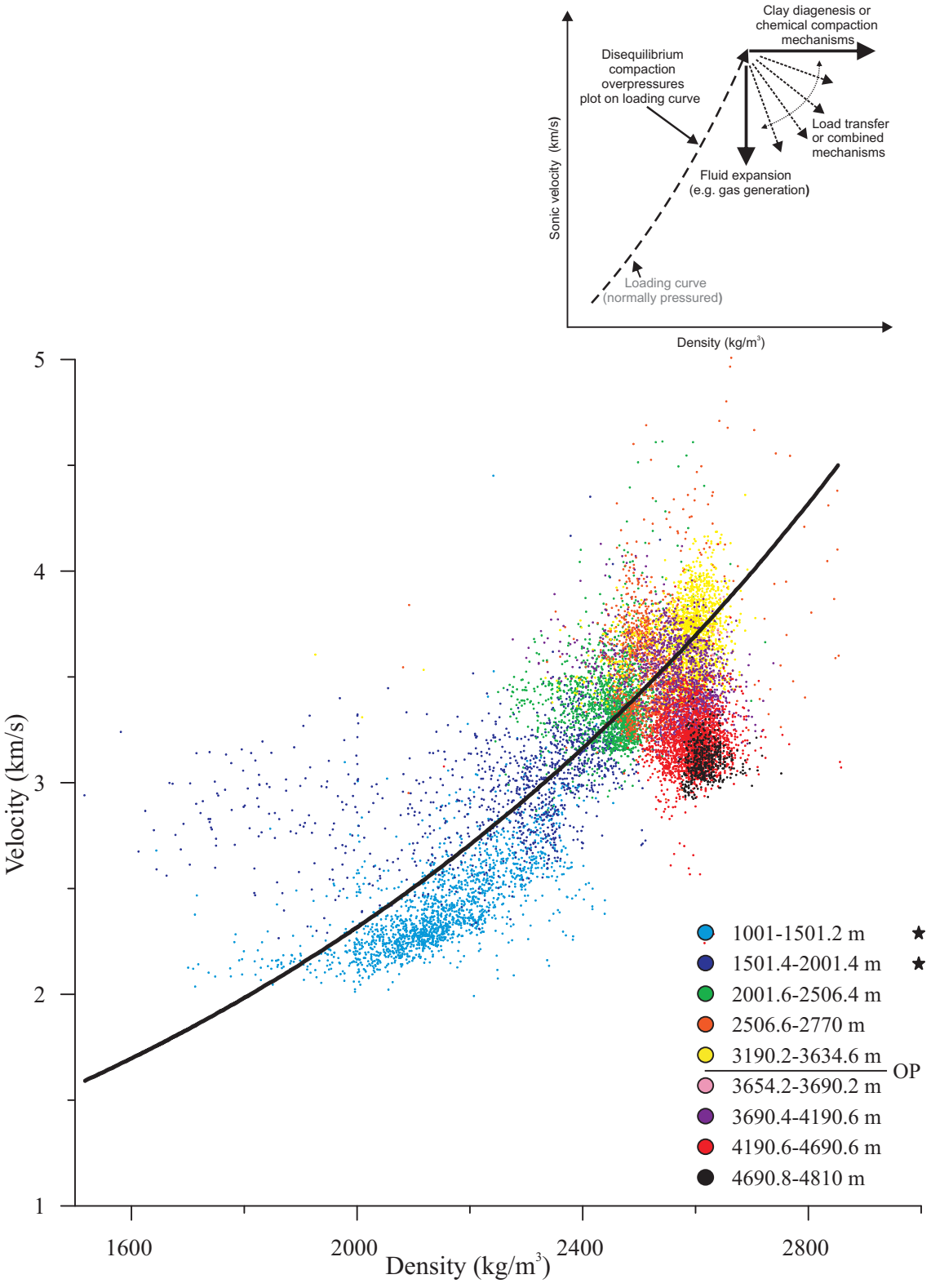

Figure 3.3.1 Graph #3 of a velocity vs. density plot for Alma F-67.

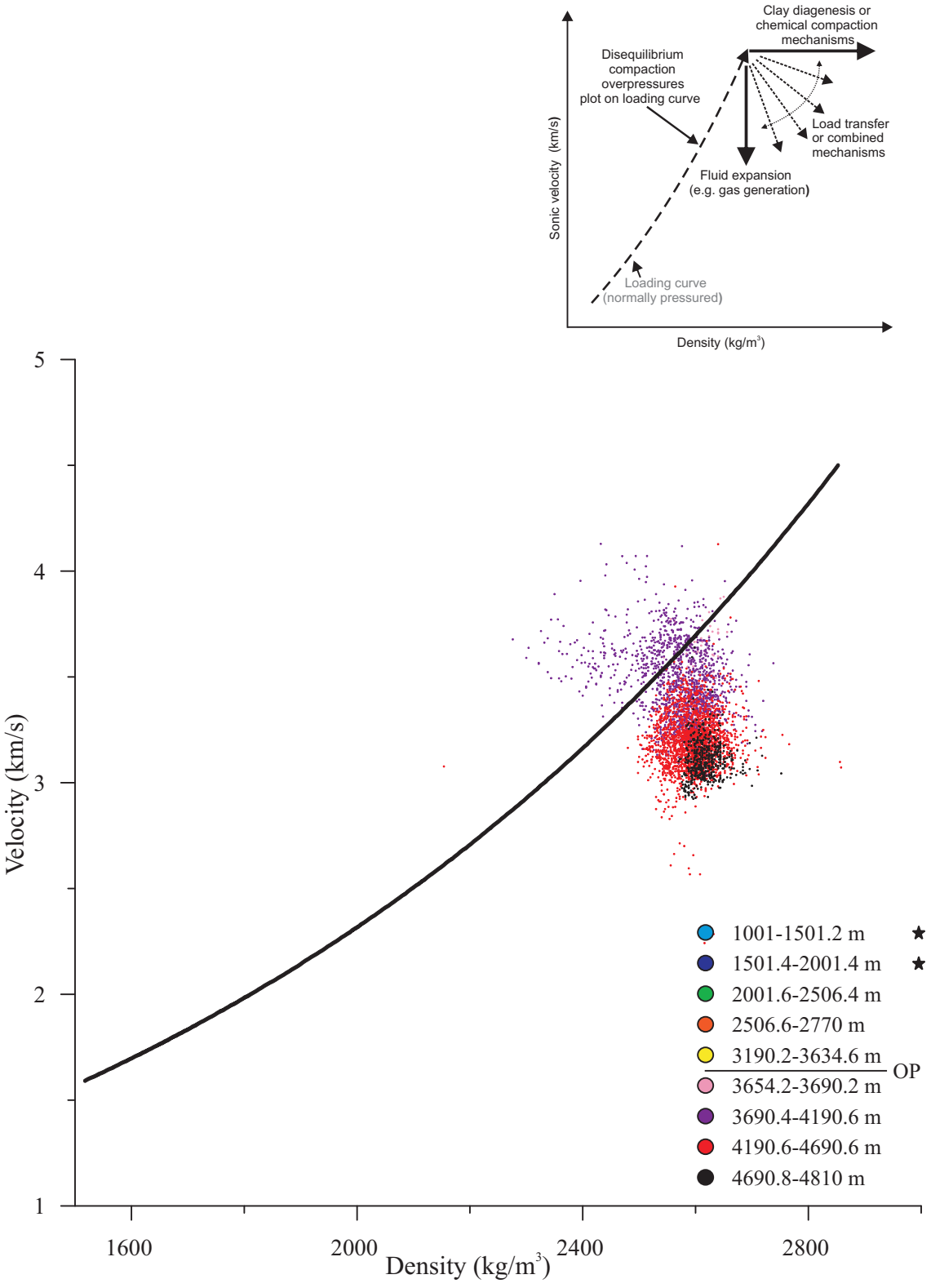

Figure 3.3.2 Graph #4 of a velocity vs. density plot for Alma F-67.

vertically. This is similar to a type 3 pattern that shows a normal loading curve of increasing velocity and density with increasing depth, to a maximum near the top of overpressure. Below that, velocity in general decreases with little change in density.

Graph #4 (Fig. 3.3.2) illustrates the overpressure interval more clearly. Samples just below the top of overpressure (pink points) are spread out below the trend line and are partly obscured by deeper data. Samples ~40–540 m below overpressure (purple points) lie mostly below the trend line, defining an almost vertical trend. A few are also scattered above and to the left of the trend line. Samples ~540–1040 m below overpressure (red points) show a trend parallel to the purple points, but with fewer points close to the trend line. The deepest samples, ~1040–1160 m below overpressure (black points), form a small cluster at the low velocity tip of the red points, at 3 km s^{-1} and 2600 kg m^{-3}. This graph shows a type 3 pattern (Fig. 3.1.1).

3.4 Cohasset A-52

The Cohasset A-52 well overlies the Upper Jurassic carbonate bank edge at the Western end of the Sable Sub-Basin. The well discovered oil and minor amounts of gas. Cohasset A-52 did not experience overpressure. The well was drilled directionally, with a TD at 2495 m (TVD). Data were available relative to both measured depth (MD) and true vertical depth (TVD) : true vertical depth was used to create graph #3 for Cohasset A-52. Cohasset A-52 has shale interbedded with sandstone near the top of the well and towards the bottom sandstone becomes more abundant.

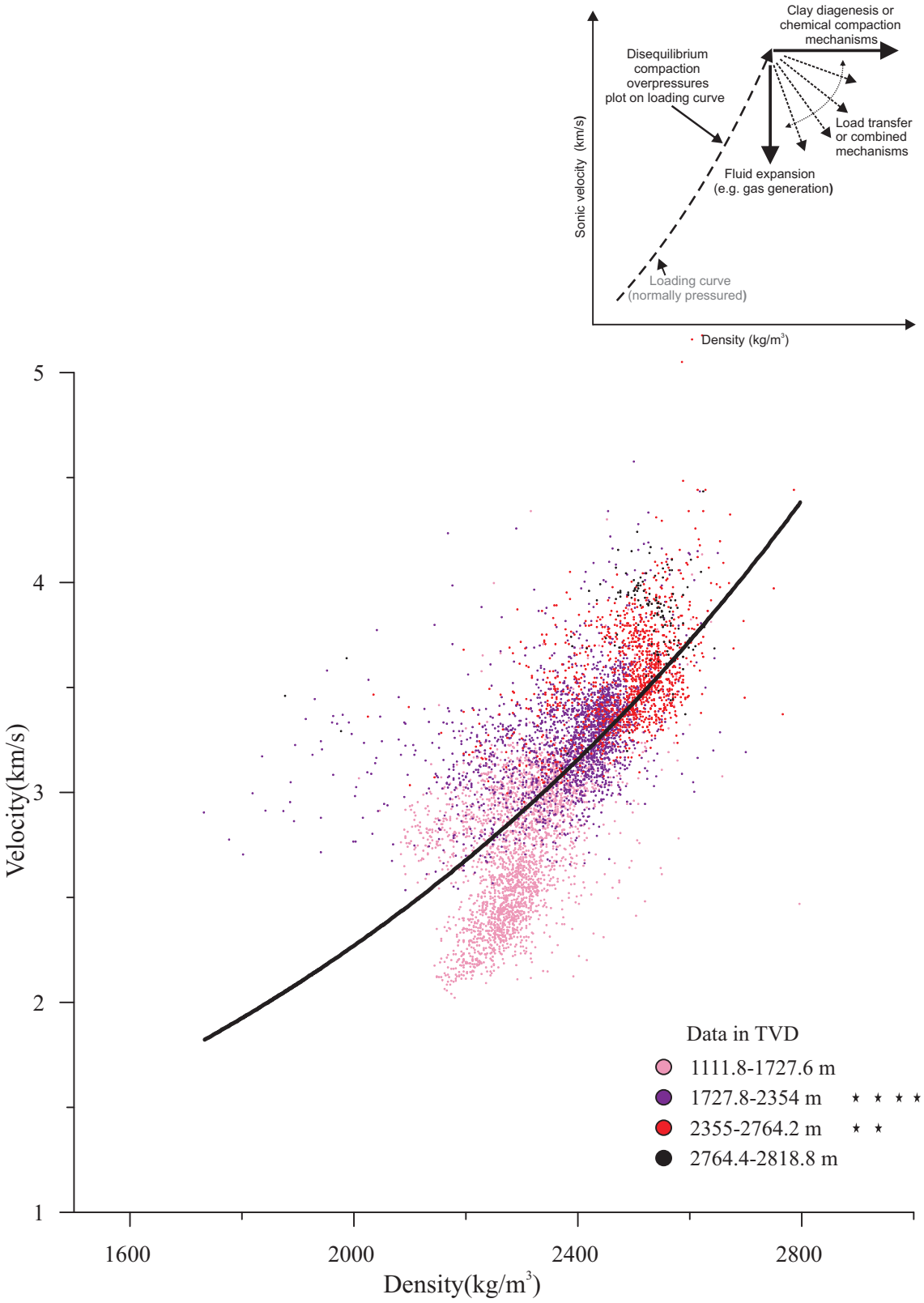

Figure 3.4.1 Graph #3 of a velocity vs. density plot for Cohasset A-52.

Graph #3 (Fig. 3.4.1) follows to the top of overpressure a normal loading curve of increasing velocity and density with increasing depth and is found in rocks that did not experience overpressure, in other words a type 1 pattern. The shallowest data points in the well differ from those in Chebucto K-90 and Alma F-67 in having relatively high density (2200 kg m^{-3}) at velocities as low as 2 km s^{-1}.

3.5 Evangeline H-98

Evangeline H-98 is located southwest of Alma F-67, at the edge of the Scotian Shelf. Overpressure starts at ~ 4023 m and goes to > 50 % between hydrostatic and lithostatic on a pressure vs. depth graph (Fig. 3.5.1). The well was drilled to a TD of 5044 m. Evangeline H-98 is very endowed with shale throughout the well. It has a recorded overpressure and the well was found to be dry.

Graph #3 (Fig. 3.5.2) shows a normal loading curve up to the top of overpressure. Graph #4 (Fig. 3.5.3) shows only a small interval (51 m) below the top of overpressure, which has 206 data points forming a small cluster both above and below the trend line. This graph was classified as type 6 pattern (Fig. 3.1.1).

3.6 Glenelg E-58

Glenelg E-58 is located in the southwest Sable Sub-Basin, between Alma F-67 and Chebucto K-90. Although the presence of overpressure was not reported either in the BASIN database or the East Coast Basin Atlas (MacLean and Wade, 1993), the depth vs.

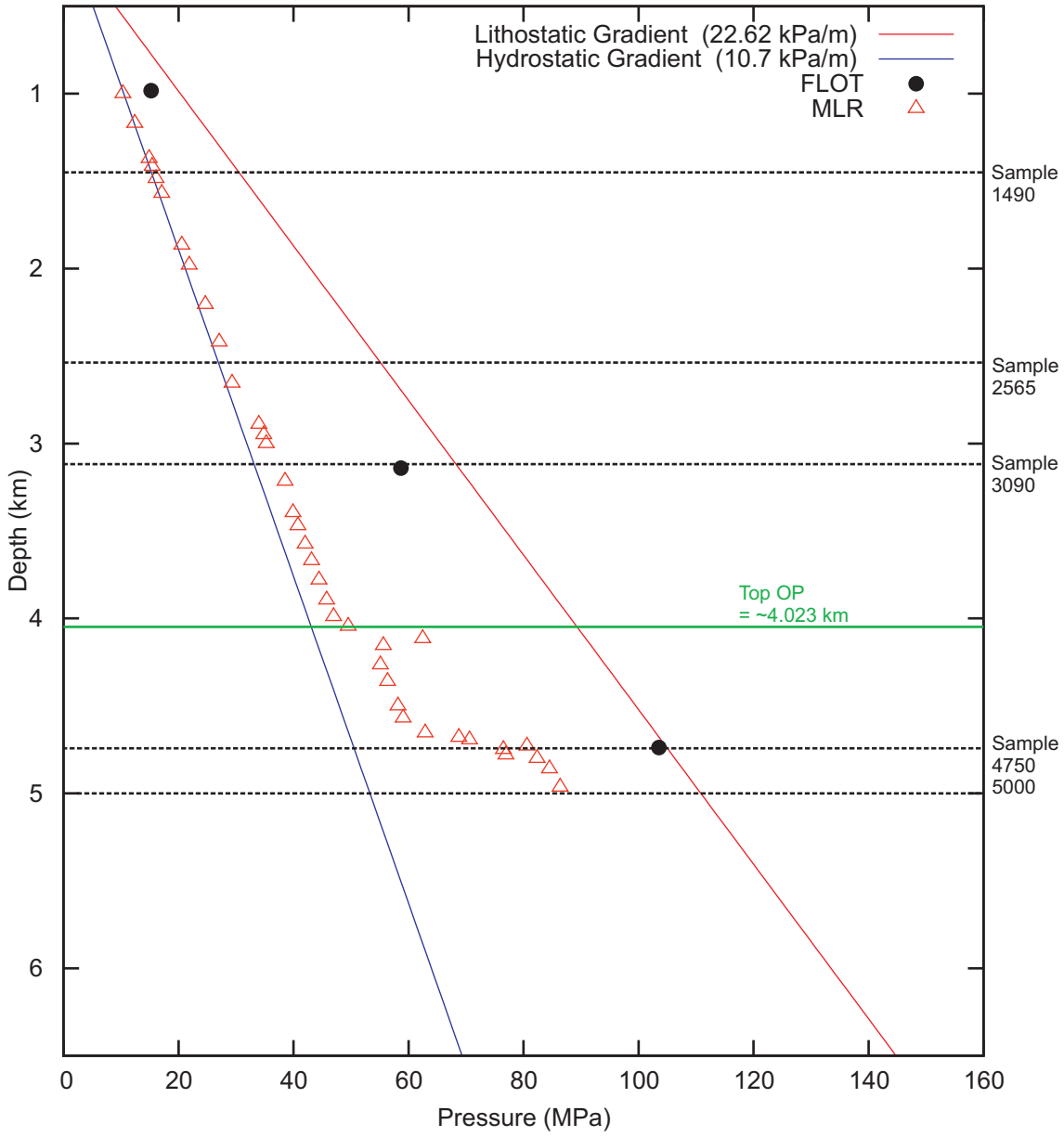

Figure 3.5.1 Depth vs. Pressure graph for Evangeline H-98 Modified from NRCAN Basin Database.

Testing types of pressure:

BDP = Breakdown Pressure
DST = Drillstem test
DMR = Drilling Mud Record
FLOT = Formation Leak-Off Test
FRP = Feedrate Pressure
MDT = Modular Formation Dynamics Tester
MLR = Mudloggers Report
PIT = Pressure Integrity Test
RFT = Repeat Formation Tester
WK = Well Kick

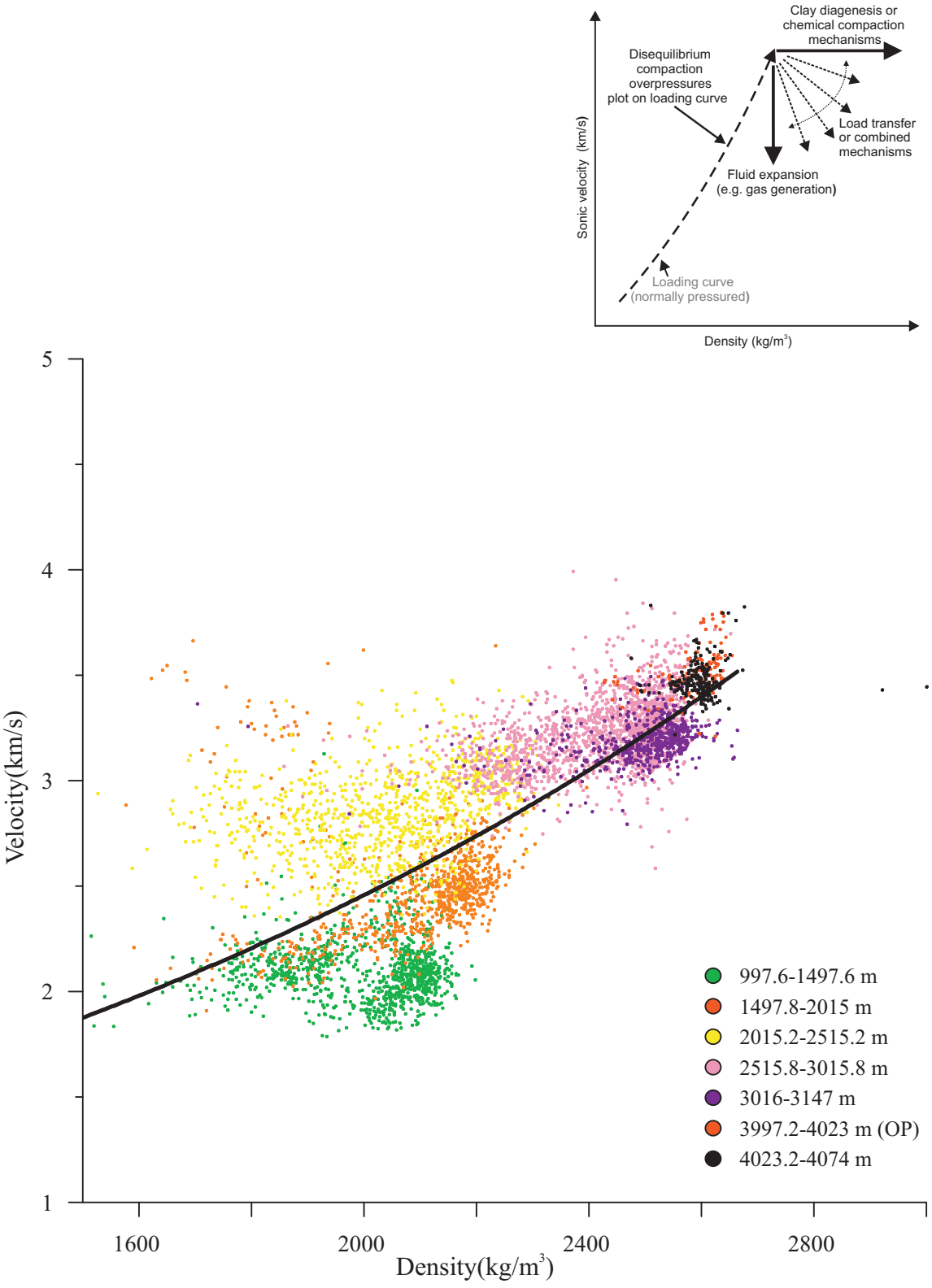

Figure 3.5.2 Graph #3 of a velocity vs. density plot for Evangeline H-98.

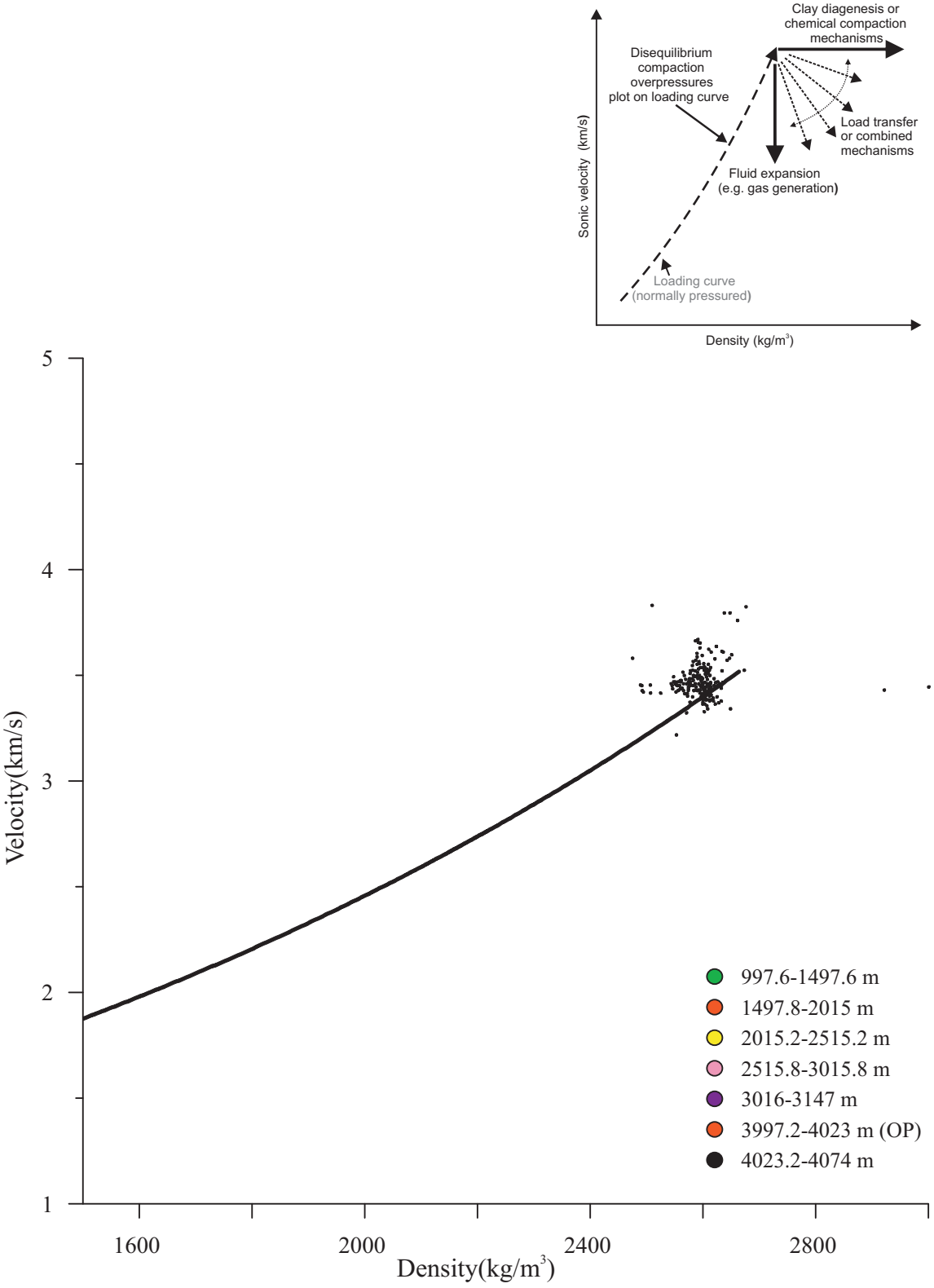

Figure 3.5.3 Graph #4 of a velocity vs. density plot for Evangeline H-98.

pressure graph from BASIN showed Glenelg E-58 indeed did have overpressure below 3693 m (Fig. 3.6.1). The well was drilled to a TD of 4154 m and discovered gas and condensates.

Graph #3 (Fig. 3.6.2) shows a normal loading curve of increasing velocity and density with increasing depth, to a maximum near the top of overpressure. Below that, velocity decreases with little change in density. Graph #4 (Fig. 3.6.3) shows samples over a ~388 m overpressured interval (black points) that form a vertical cluster lying on the trend line, with points above and below. The data show a type 2 pattern (Fig. 3.1.1), which reflects a normal loading curve of increasing velocity and density with increasing depth.

3.7 Kegeshook G-67

Kegeshook G-67 is located in the western Sable Sub-Basin, to the northeast of Cohasset A-52. It was drilled to a depth of 3540 m and no overpressure was encountered, as is evident from the depth vs. pressure data from BASIN database (Fig. 3.7.1). The well was found to be dry. Below 3115 m, the well penetrates upper Jurassic limestones: none of these are included in the plots.

Graph #3 (Fig. 3.7.2) shows a pattern of velocity vs. density that follows a normal loading curve of increasing velocity and density with increasing depth and is found in rocks that are normally pressurized and thus resembles type 1 pattern (Fig. 3.1.1). The graph resembles Cohasset A-52, with that the shallowest data are relatively dense and have a velocity of ~2.1 km s^{-1}.

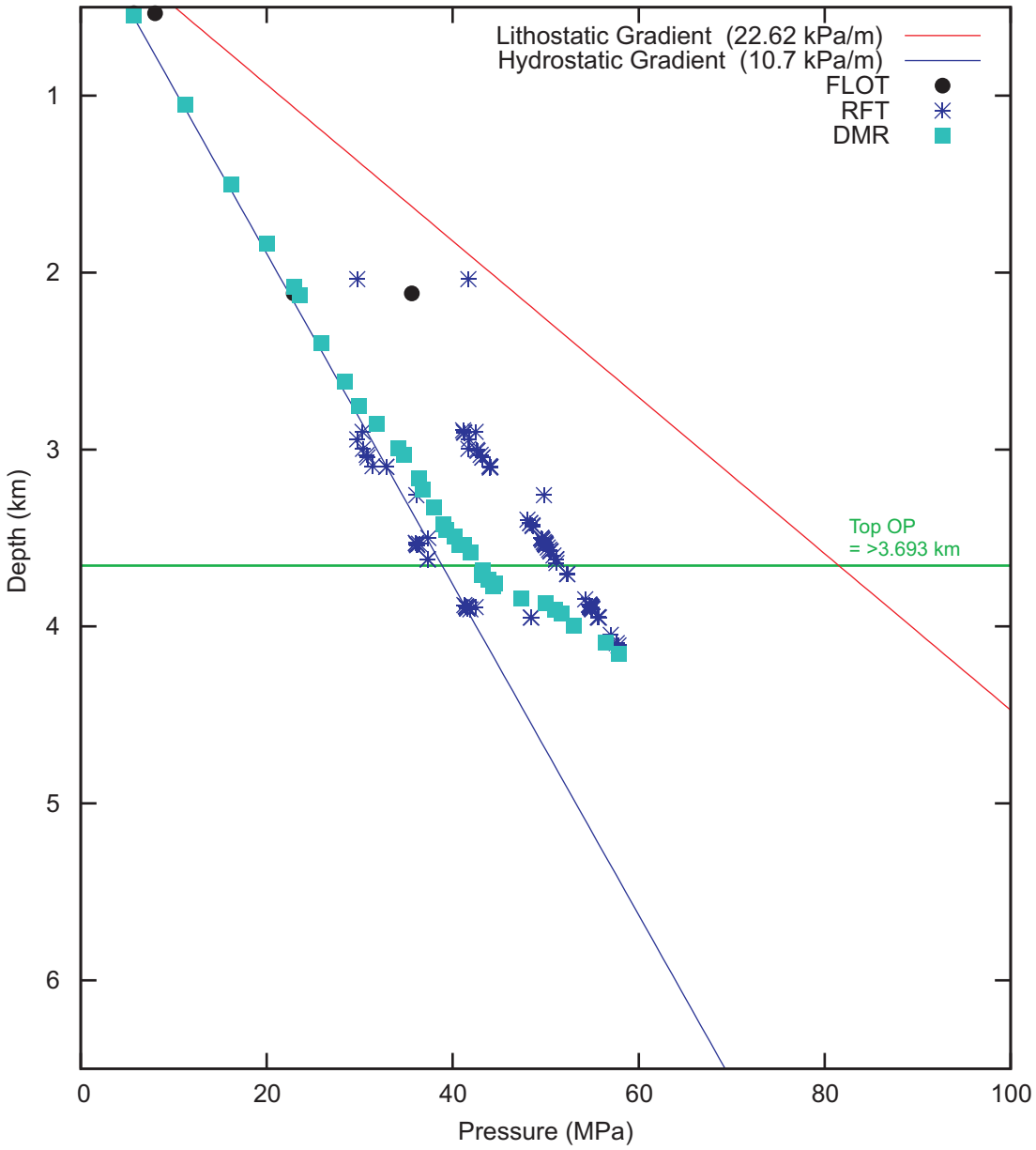

Figure 3.6.1 Depth vs. Pressure graph for Glenelg E-58 modified from NRCAN Basin Database.

Testing types of pressure:

BDP = Breakdown Pressure
DST = Drillstem test
DMR = Drilling Mud Record
FLOT = Formation Leak-Off Test
FRP = Feedrate Pressure
MDT = Modular Formation Dynamics Tester
MLR = Mudloggers Report
PIT = Pressure Integrity Test
RFT = Repeat Formation Tester
WK = Well Kick

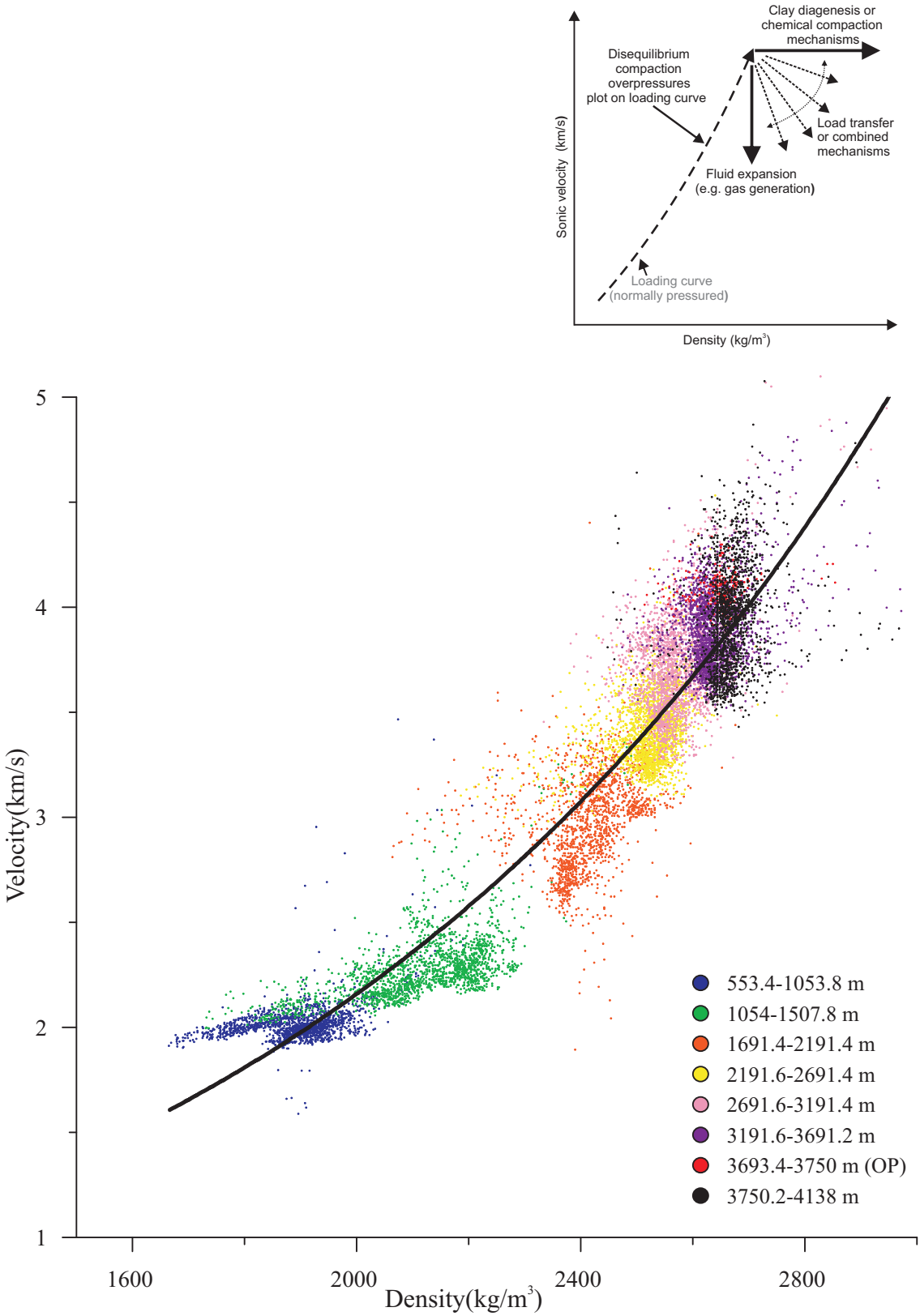

Figure 3.6.2 Graph #3 of a velocity vs. density plot for Glenelg E-58.

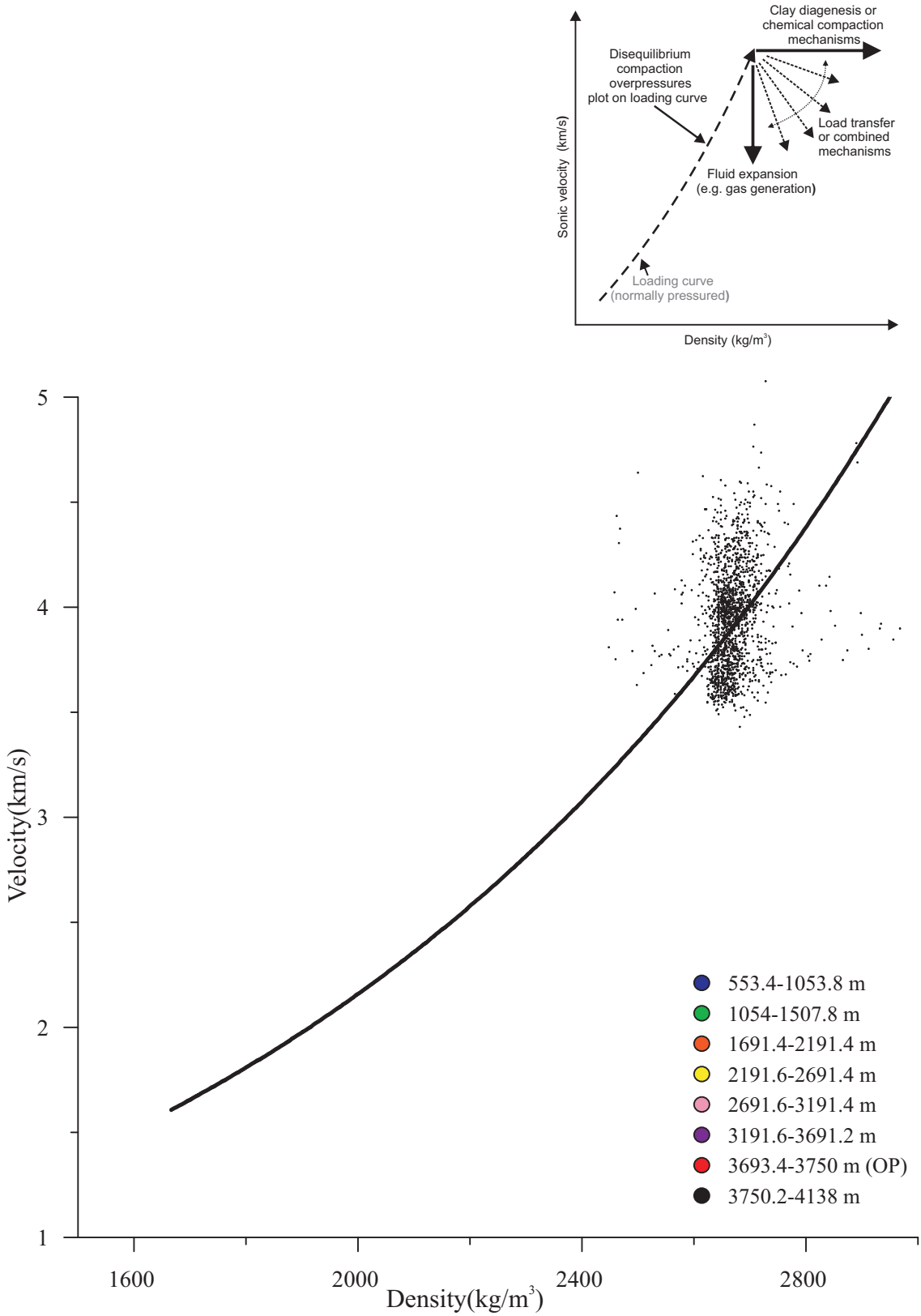

Figure 3.6.3 Graph #4 of a velocity vs. density plot for Glenelg E-58.

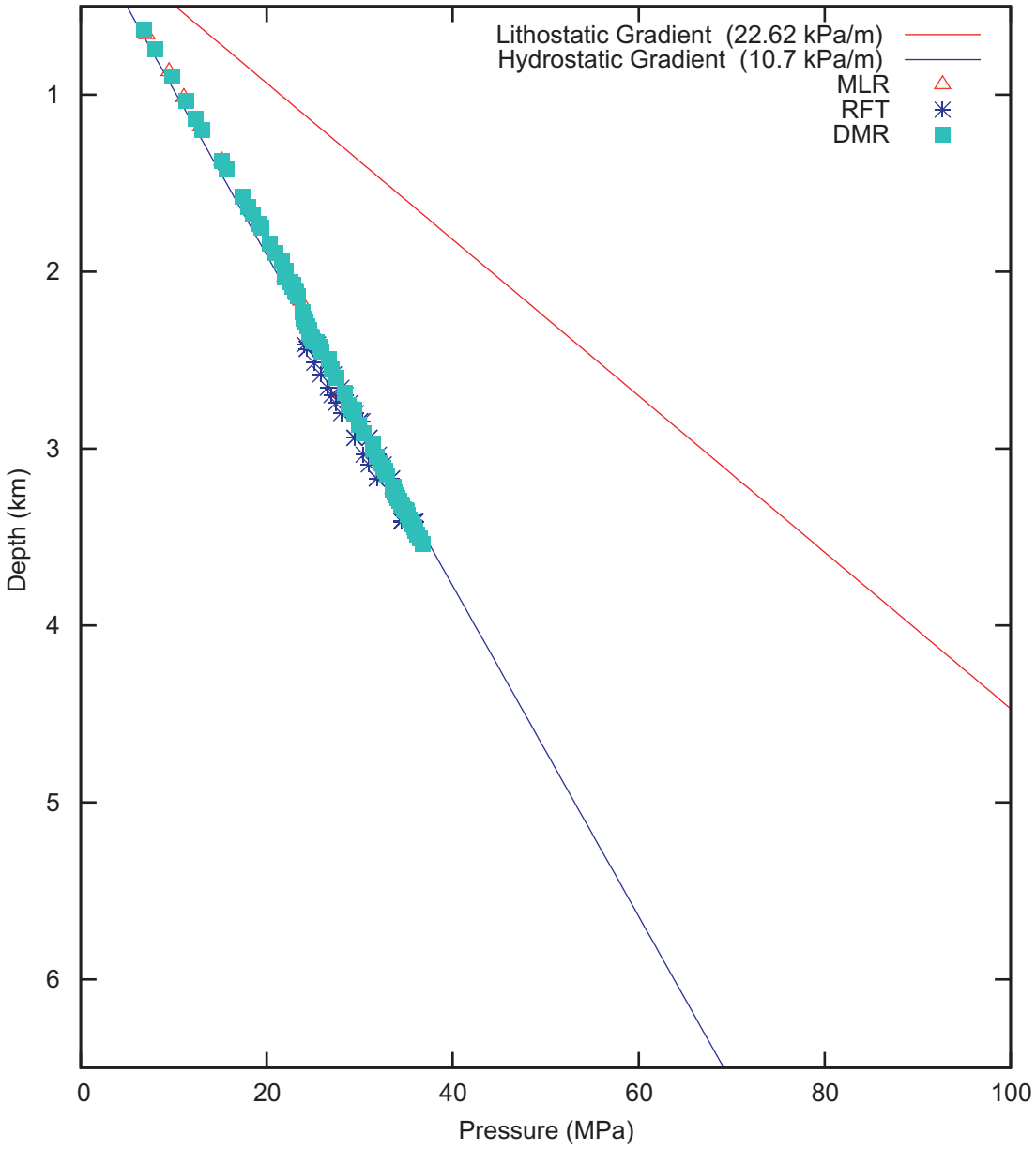

Figure 3.7.1 Depth vs. Pressure graph for Kegeshook G-67 modified from NRCAN Basin Database.

Testing types of pressure:

BDP = Breakdown Pressure
DST = Drillstem test
DMR = Drilling Mud Record
FLOT = Formation Leak-Off Test
FRP = Feedrate Pressure
MDT = Modular Formation Dynamics Tester
MLR = Mudloggers Report
PIT = Pressure Integrity Test
RFT = Repeat Formation Tester
WK = Well Kick

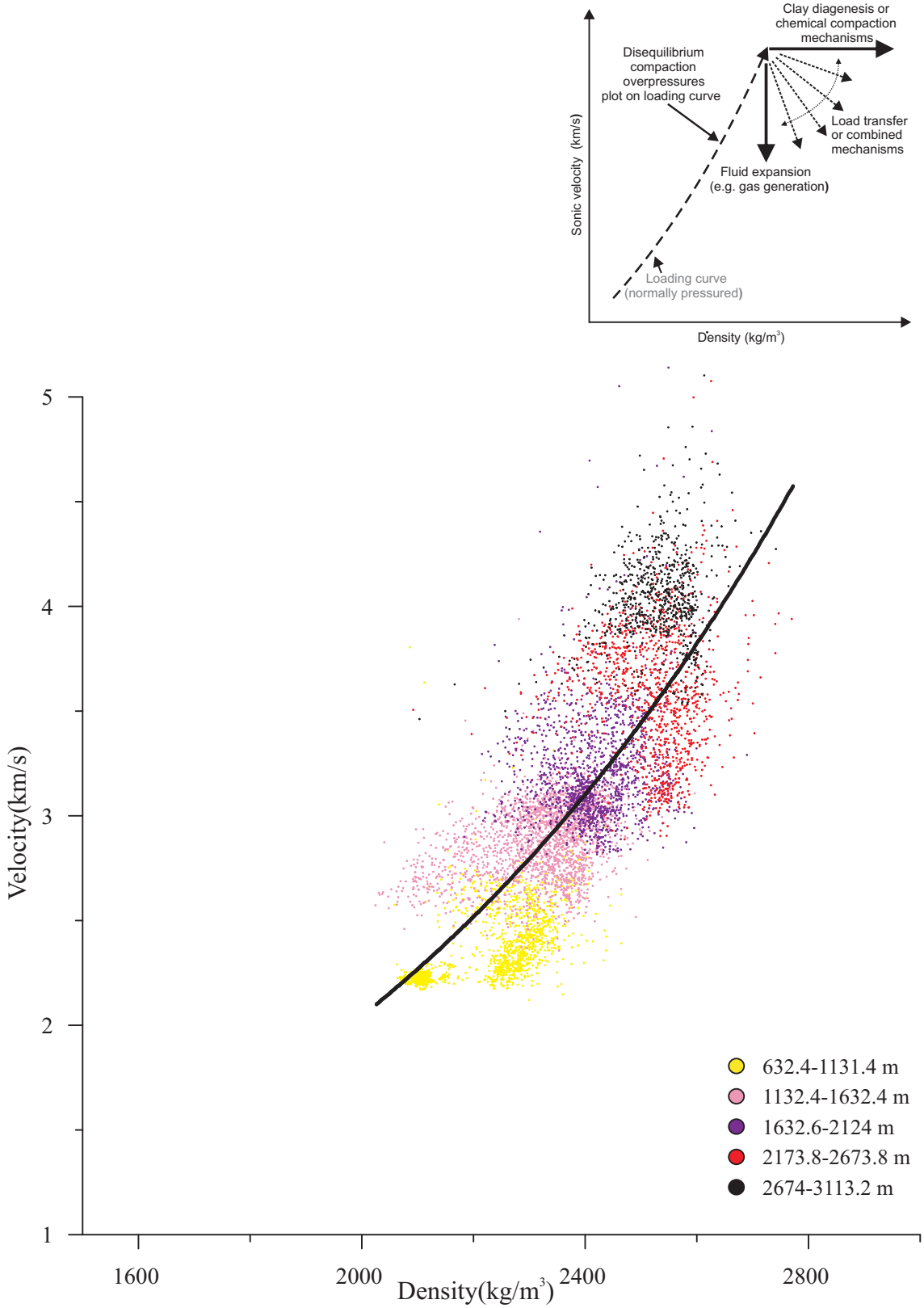

Figure 3.7.2 Graph #3 of a velocity vs. density plot for Kegeshook G-67.

3.8 Louisbourg J-47

Louisbourg J-47 is in the Abenaki Sub-Basin, located next to South Griffin J-13. Overpressure starts at ~4520 m and was drilled to a TD of 6043 m. Pressure vs. depth graphs from the BASIN database (Fig. 3.8.1) show points vey close to the lithostatic gradient, indicating a large overpressure. The well discovered gas. Louisbourg J-47 does not have abundant shale like other wells. There is abundant sandstone and the top of overpressure occurs within a limestone interval.

Graph #3 (Fig. 3.8.2) shows a pattern of velocity vs. depth like type 3, which shows a normal loading curve of increasing velocity and density with increasing depth, to a maximum near the top of overpressure. Graph #4 (Fig. 3.8.3) shows an increase in density followed by a gradual decrease in density and velocity. This represents a type 8 pattern (Fig. 3.1.1). The few samples to ~35.6 m below overpressure (pink points) are mainly spread out above the trend line. Samples ~35.6–676 m below overpressure (purple points) form a cluster around the upper end of the trend line. Samples from ~676–1176 m below overpressure (red points) form a vertical cluster, mostly below the trend line, but shifted to the left of the purple points, i.e. representing lower density. The samples ~1176–1540.6 m below overpressure (black points) form a similar vertical cluster, but with even lower density. The upper part of the overpressured section has calcareous shale interbedded with limestone, whereas the lower part has shale interbedded with sandstone. It is the limestone-rich interval, shown in the purple dots, that has the highest density and velocity.

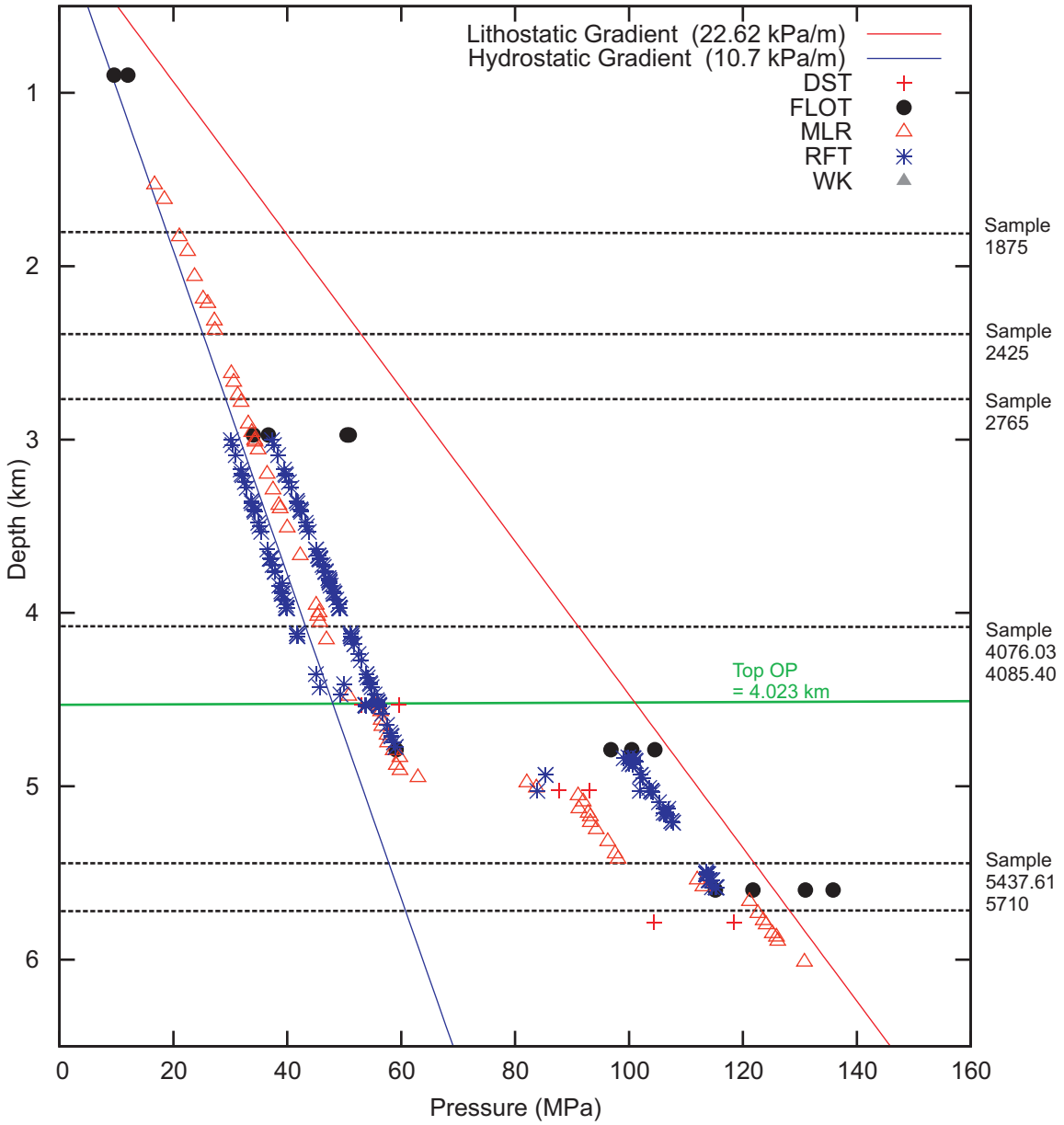

Figure 3.8.1 Depth vs. Pressure Graph for Louisbourg J-47 modified from NRCAN Basin Database.

Testing types of pressure:

BDP = Breakdown Pressure
DST = Drillstem test
DMR = Drilling Mud Record
FLOT = Formation Leak-Off Test
FRP = Feedrate Pressure
MDT = Modular Formation Dynamics Tester
MLR = Mudloggers Report
PIT = Pressure Integrity Test
RFT = Repeat Formation Tester
WK = Well Kick

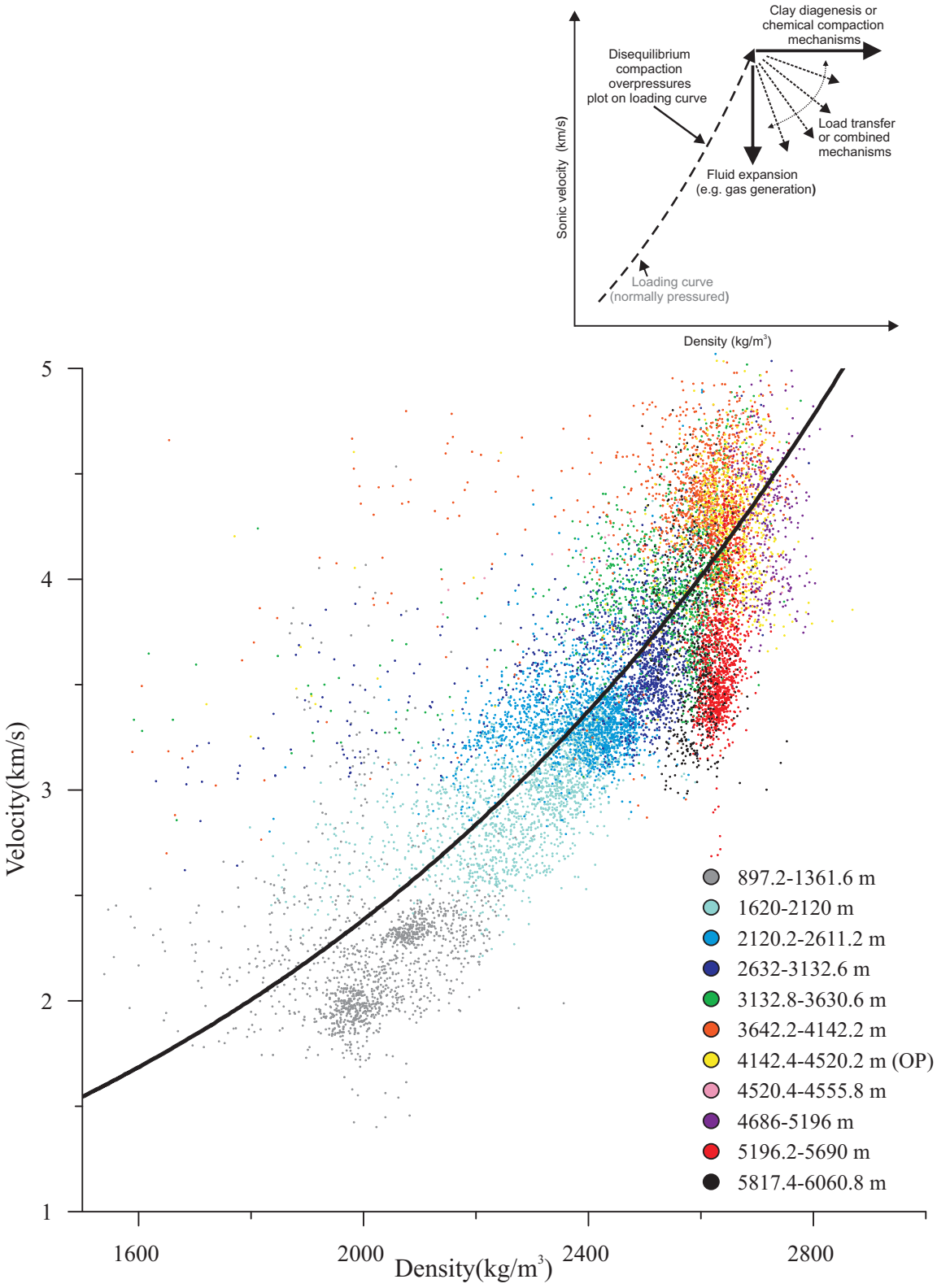

Figure 3.8.2 Graph #3 of a velocity vs. density plot for Louisbourg J-47.

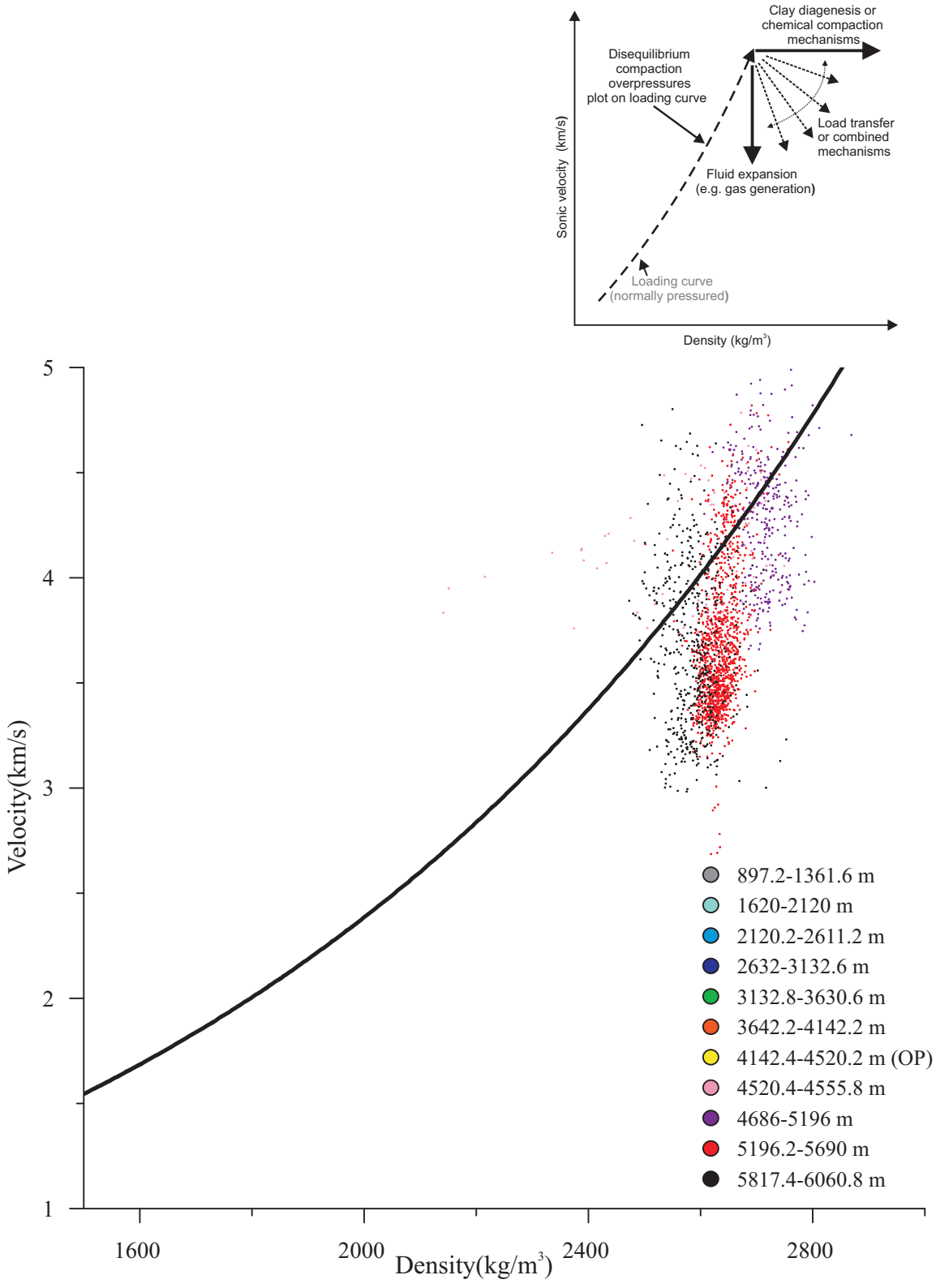

Figure 3.8.3 Graph #4 of a velocity vs. density plot for Louisbourg J-47.

3.9 Mohican I-100

Mohican I-100 is close to the shelf edge in the southwestern part of the Scotian Basin that penetrates to Argo Formation salt at 4365 m. The well was drilled to a TD of 4394 m. There is abundant shale above ~2400 m and below that there is limestone and minor dolostone. It was a dry well.

Pressure data from the BASIN database shows moderate overpressure (about 30% of excess lithostatic over hydrostatic) from 1500–2200 m, corresponding to the Shortland Shale unit (Fig. 3.9.1). The underlying Mississauga Formation and deeper strata have normal (hydrostatic) pressure. Similar patterns in other wells on the outermost shelf and slope suggest that this observation is not due to faulty data collection. Moheida P-15 and Glooscap C-63, both have slight but distinct overpressure in the same stratigraphic interval, over normally pressured Mississauga Formation. In the Shelburne G-29 well on the Scotian Slope, the Shortland Shale unit is marked by an unconformity, but the overlying Dawson Canyon Formation is moderately overpressured, dropping to only slight overpressure in the underlying Mississauga Formation.

Graph #3 (Fig. 3.9.2) looked very sparse with a concentration of points at the bottom of the graph and many gaps throughout. The overall shape of the graph shows a pattern of velocity vs. density that follows a normal loading curve of increasing velocity and density with increasing depth and is found in rocks that are overpressured. The trend line similar to that of Cohasset and Kegeshook. However, the data below ~2450 kg/m^3 mostly lie above the trend line, with high velocities corresponding to intervals of shale

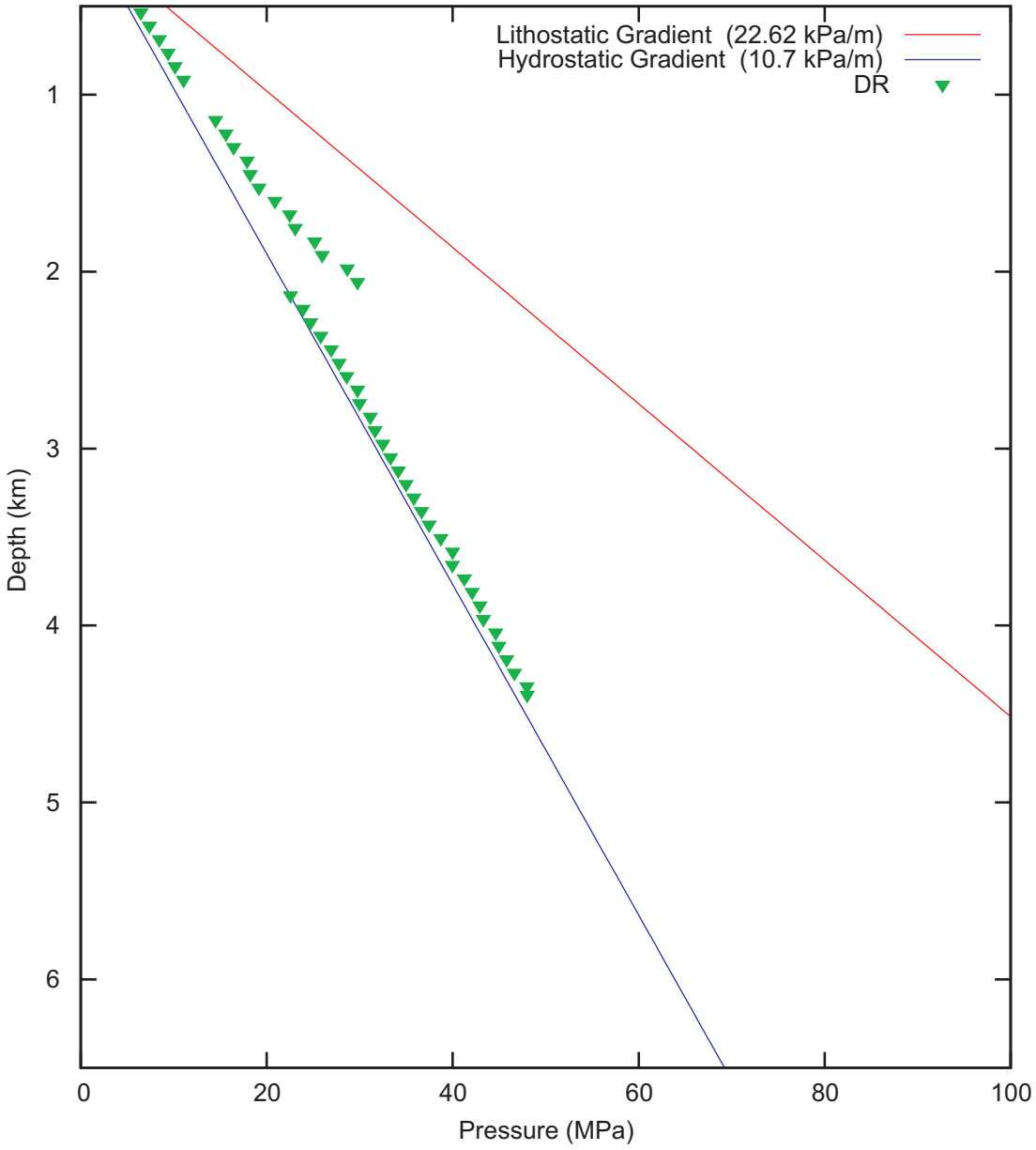

Figure 3.9.1 Depth vs. Pressure graph for Mohican I-100 modified from NRCAN Basin Database.

Testing types of pressure:

BDP = Breakdown Pressure
DST = Drillstem test
DMR = Drilling Mud Record
FLOT = Formation Leak-Off Test
FRP = Feedrate Pressure
MDT = Modular Formation Dynamics Tester
MLR = Mudloggers Report
PIT = Pressure Integrity Test
RFT = Repeat Formation Tester
WK = Well Kick

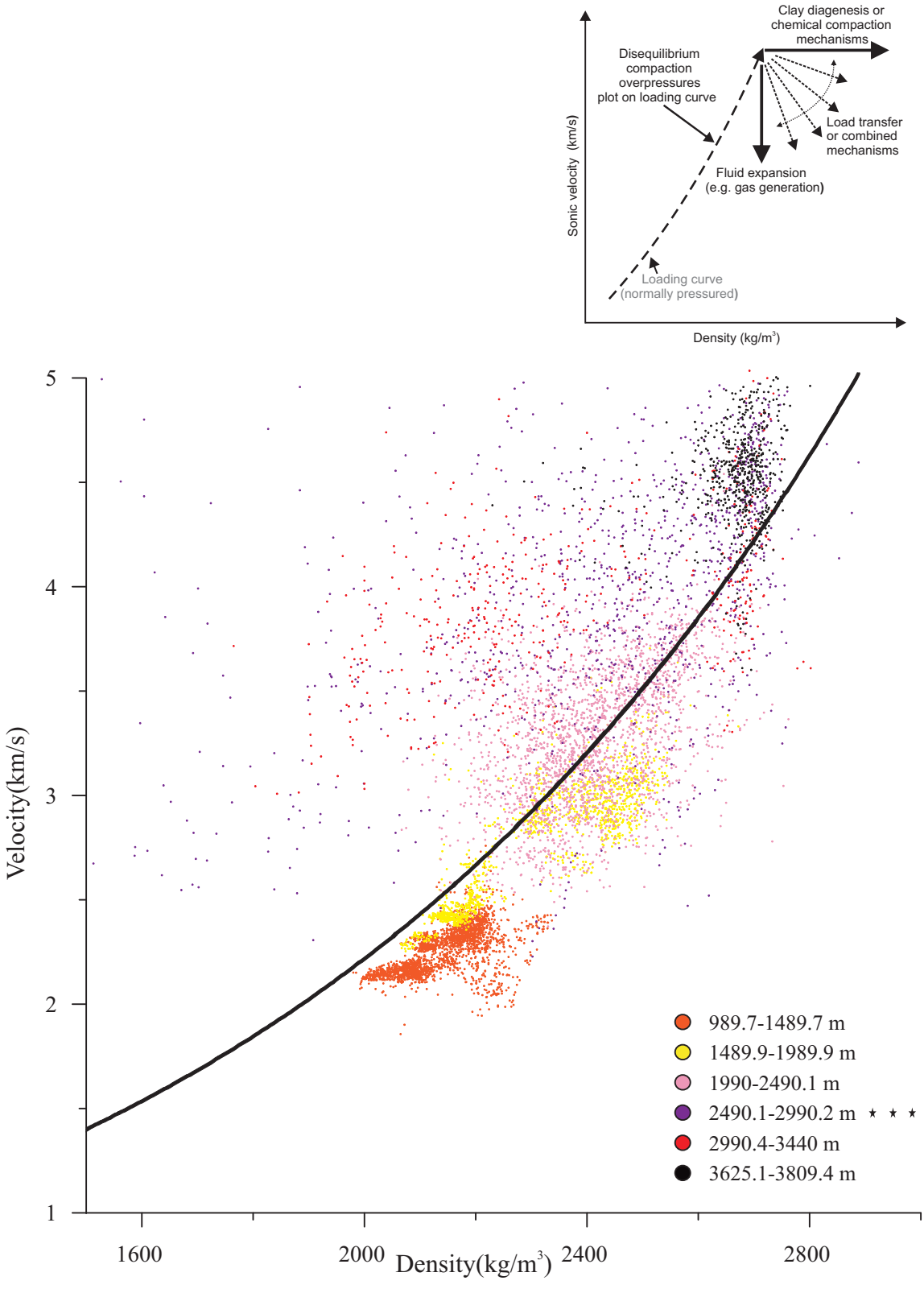

Figure 3.9.2 Graph #3 of a velocity vs. density plot for Mohican I-100.

interbedded with limestones and dolostones. The graph thus reflects a type 2 pattern (Fig. 3.1.1).

3.10 North Banquereau I-13

North Banquereau I-13 is located near Louisbourg J-47, with a TD of 5188 m near the top of the limestones that are more prominent in the deeper parts of Louisbourg. It's overpressure starts at ~4350 m. The well was found to be dry.

Graph #3 (Fig. 3.10.1) follows a pattern of increasing velocity and density to the top of overpressure. Graph #4 (Fig. 3.10.2) shows a trend line that is similar to Evangeline and Mohican. The overall shape of the graph above the top of overpressure can be classified as a type 2 pattern (Fig. 3.1.1). Below the top of overpressure, velocity decreases with little change in density. Samples ~240 m below overpressure (purple points) start below the trend line with some scattered above it. Samples ~240–741 m below overpressure (red points) are mostly above the curve in somewhat of a vertical cluster with many points spread out to the left and right of the trend line. There are thin beds of limestone interbedded with shales at ~4900 m corresponding to higher velocity and density red points. Samples in the bottom 100 m of the well (black points) show scatter in velocity similar to the overlying strata (red points), except for the lack of high-density samples. The graph is classified as a type 10 pattern (Fig. 3.1.1).

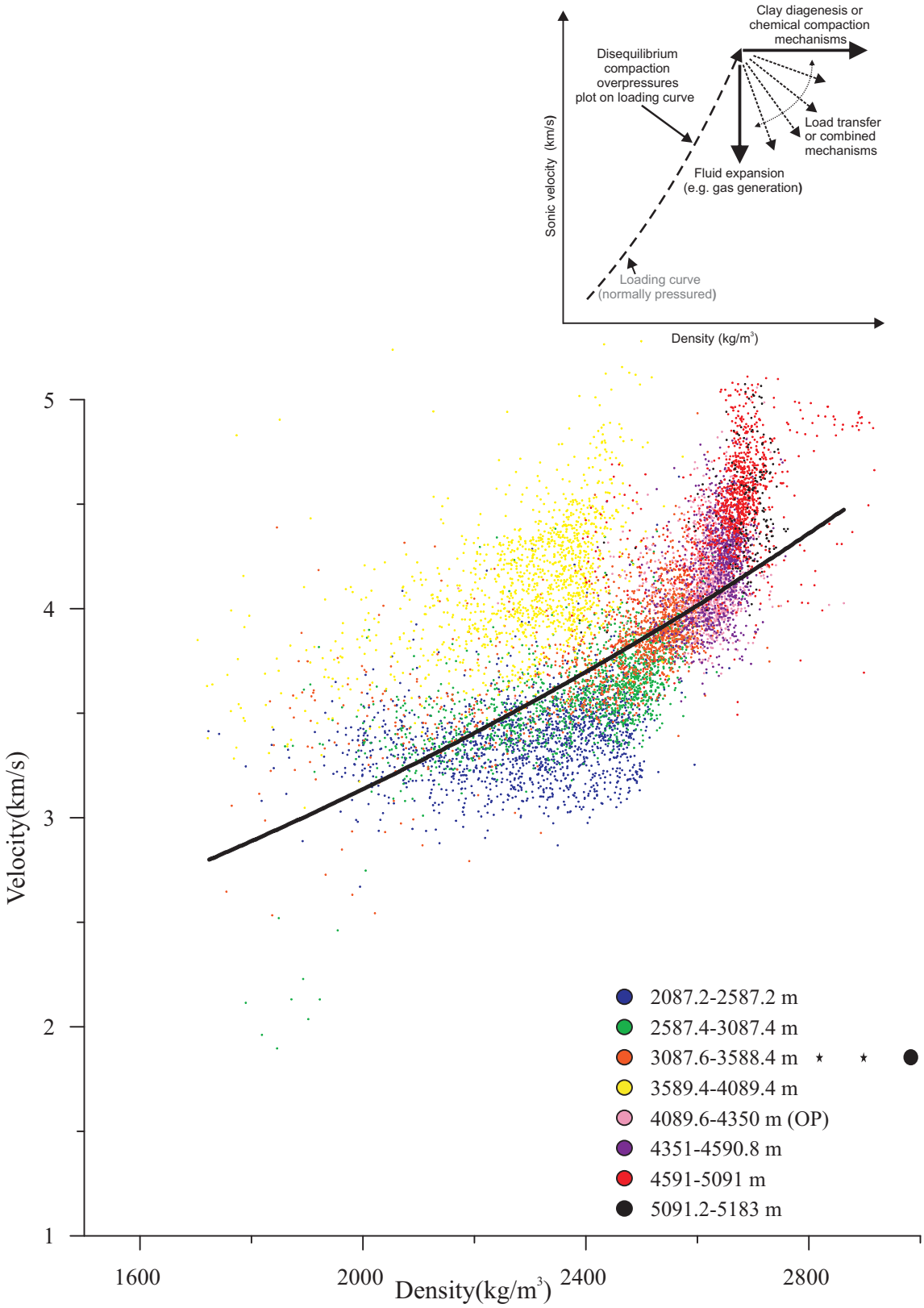

Figure 3.10.1 Graph #3 of a velocity vs. density plot for North Banquereau I-13.

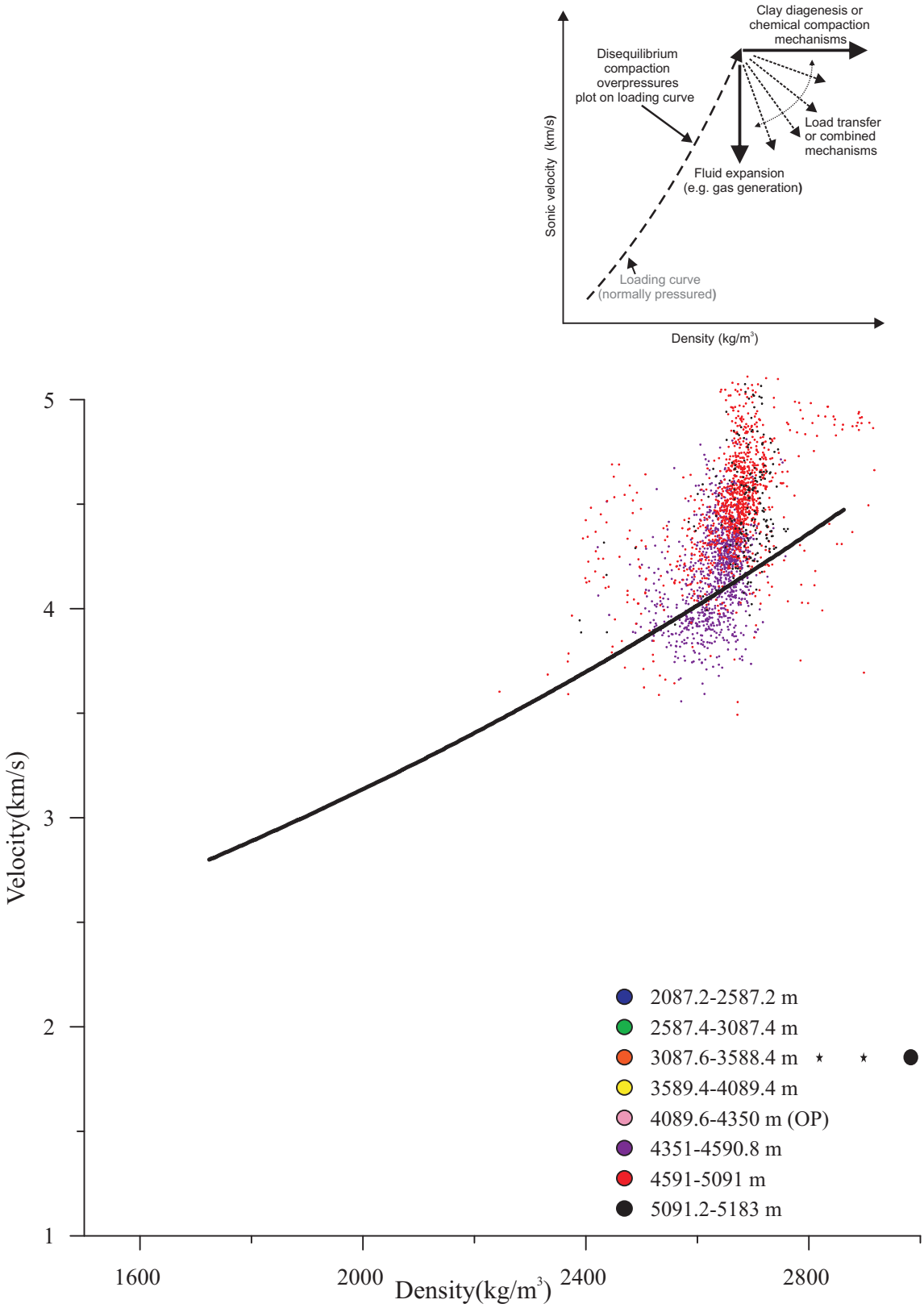

Figure 3.10.2 Graph #4 of a velocity vs. density plot for North Banquereau I-13.

3.11 Peskowesk A-99

Peskowesk A-99 is located in the eastern Scotian Basin inboard from Louisbourg J-47 and North Banquereau I-13. There was no observable overpressure. It has a TD of 4003 m and was found to be dry. The East Coast Basin Atlas (MacLean and Wade, 1993) indicates Peskowesk A-99 has minor amounts of shale interbeded with more prominent sandstone.

Graph #3 (Fig. 3.11.1) shows a trend line that almost perfectly bisects the velocity and density points. It thus shows a type 1 pattern (Fig. 3.1.1), which increases in velocity and density with depth, following a normal loading curve.

3.12 Sable Island C-67

The Sable Island C-67 well is located in the middle of Sable Island, in the centre of the Sable Sub-Basin, almost equidistant between the Venture and Thebaud fields. Overpressure starts at ~4388.8 m until the bottom of the well at TD of 4604 m. The well discovered oil and gas. The East Coast Basin Atlas (MacLean and Wade, 1993) shows that Sable C-67 is predominantly sandstone with minor beds of shale throughout.

Graph #3 (Fig. 3.12.1) follows an “S” shaped pattern that acts as the normal loading curve to the top of overpressure. Graph #4 (Fig. 3.12.2) shows that data to ~207 m below the top of overpressure (black points) form an ovoid cluster extending from higher velocity but lower density to lower velocity but higher density, centered just below the trend line. This well has similarities to type 4 pattern (Fig. 3.1.1), which shows a

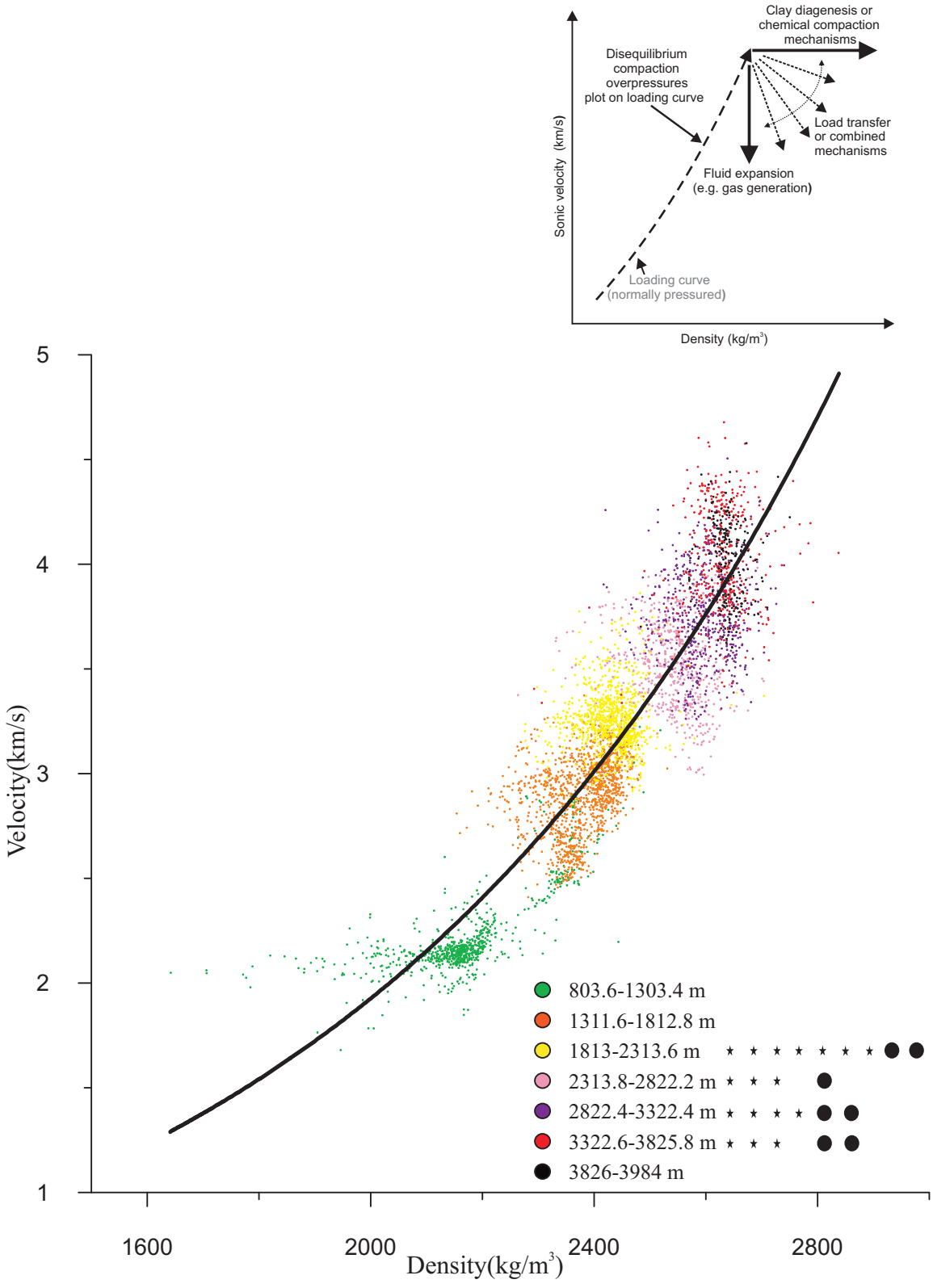

Figure 3.11.1 Graph #3 of a velocity vs. density plot for Peskowesk A-99.

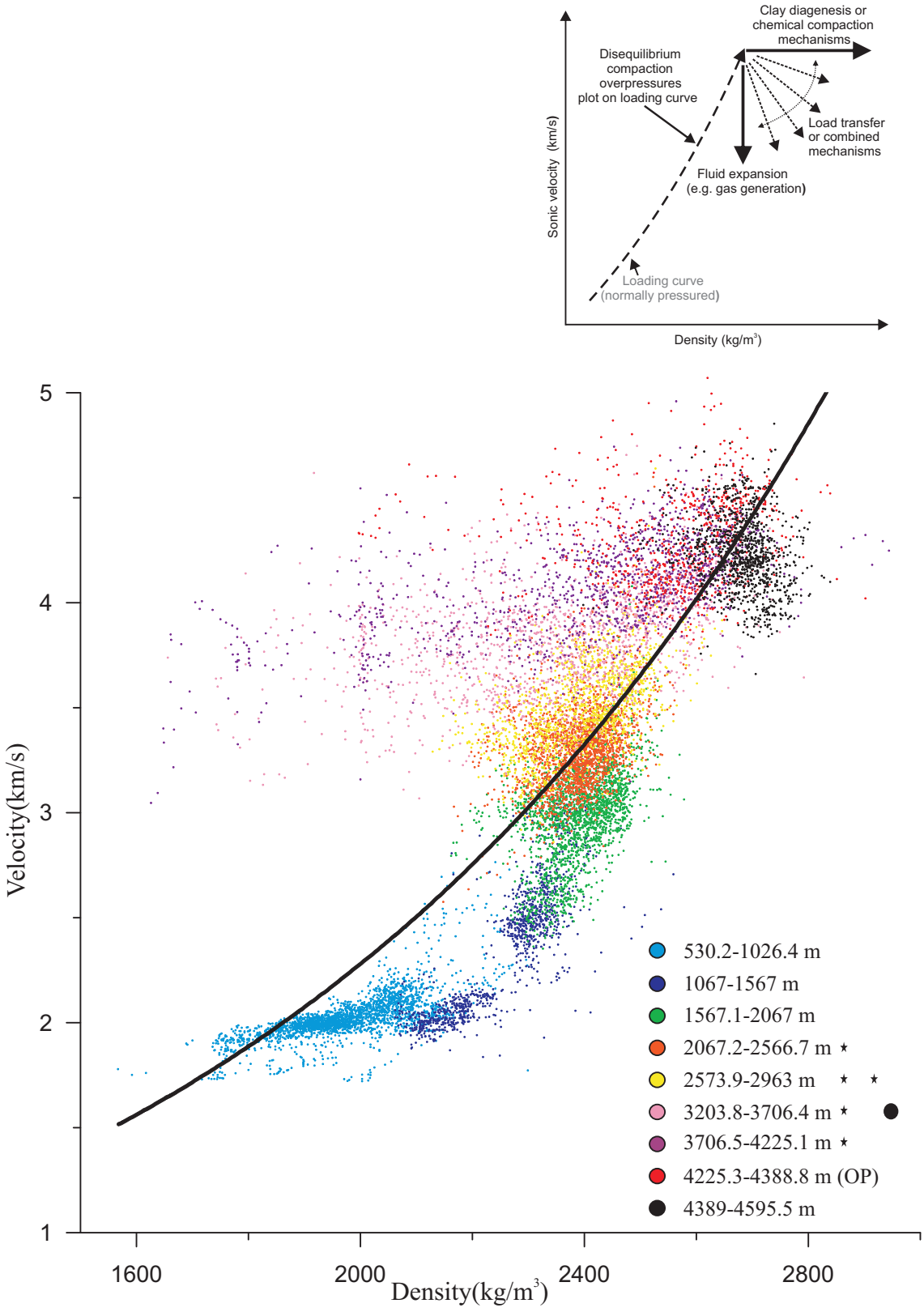

Figure 3.12.1 Graph #3 of a velocity vs. density plot for Sable Island C-67.

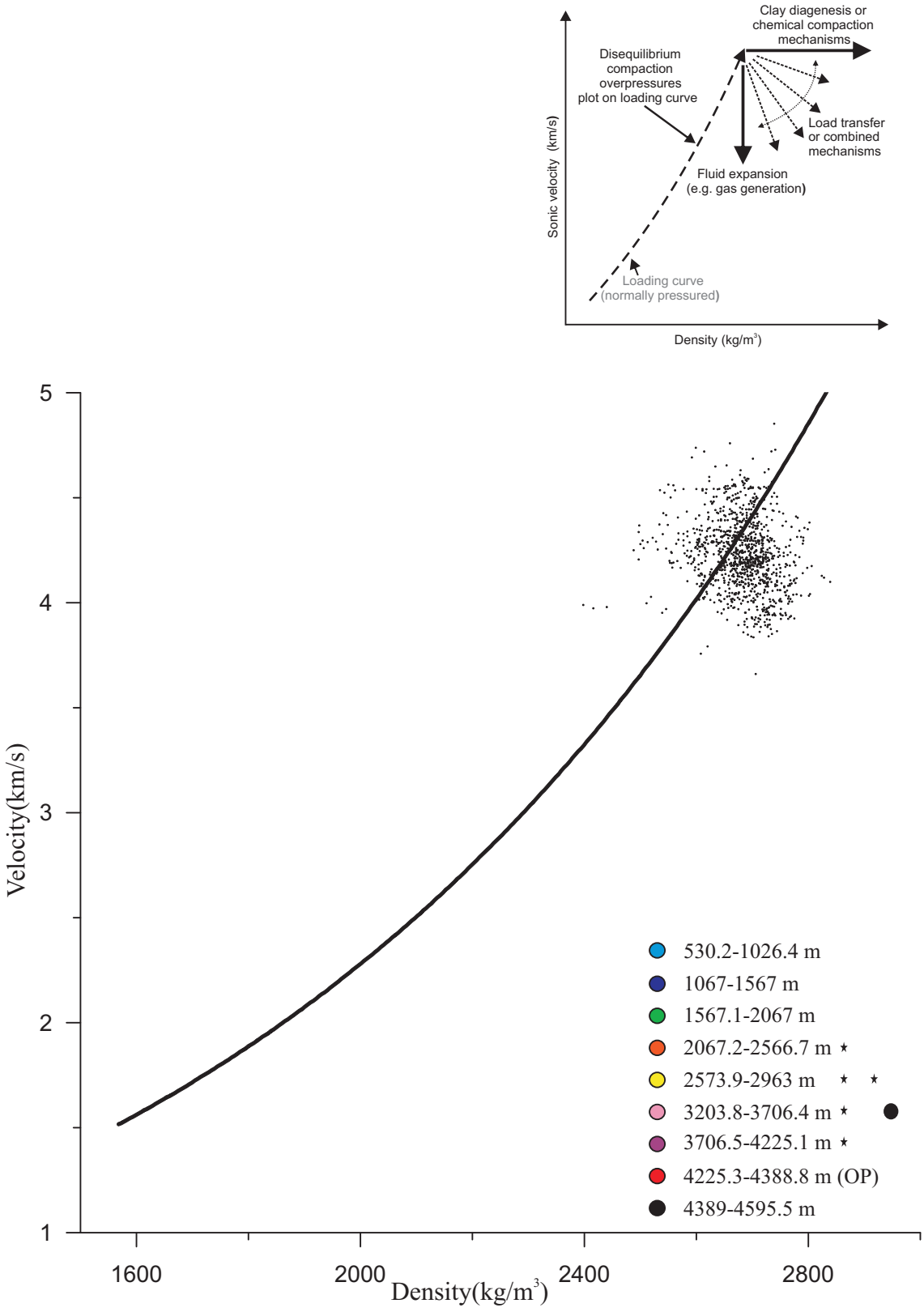

Figure 3.12.2 Graph #4 of a velocity vs. density plot for Sable Island C-67.

normal loading curve to near the top of overpressure, followed by a decrease in velocity with an increase in density.

3.13 South Desbarres O-76

South Desbarres O-76 is located 20 km north of Sable Island C-67 in the middle of the Sable Sub-Basin. Overpressure starts at ~4570 m until a TD of 6039 m. The East Coast Basin Atlas (MacLean and Wade, 1993) shows that there is a limestone layer immediately above the top of overpressure, which occurs within shale. The depth vs. pressure graph (Fig. 3.13.1) shows the points very close to the lithostatic gradient indicating a large overpressure. The well was dry.

Graph #3 (Fig. 3.13.2) follows a pattern of increasing velocity and density to the top of overpressure. Graph #4 (Fig. 3.13.3) shows that samples to ~255 m below overpressure (purple points) are mostly below the trend line and follow a vertical pattern. Samples ~255–960 m below overpressure (red points) also show a vertical pattern stacked upon the purple points, but extending to lower velocity. Samples ~960–1456 m below overpressure (black points) again follow a vertical pattern overlapping the red points but have a higher mean velocity than the red points, with some plotting above the trend line. Although this resembles a type 3 pattern, it differs in that the deepest samples show an increasing, rather than a decreasing, trend of velocity and thus classified as a type 9 pattern (Fig. 3.1.1).

A plot of velocity and gamma against depth (Fig. 3.13.4) generally shows higher velocity for lower gamma values, which are presumably related to higher silt content.

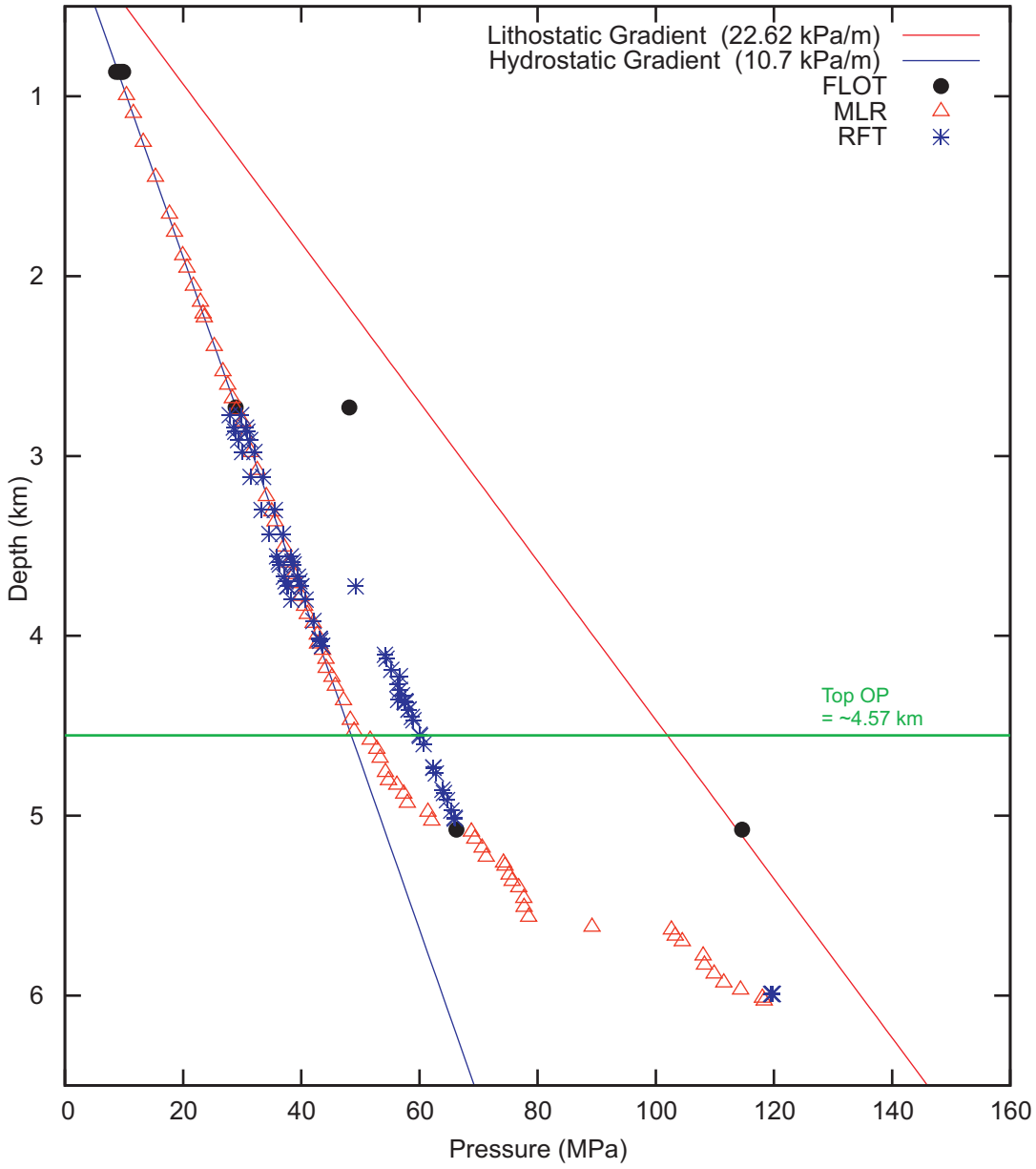

Figure 3.13.1 Depth vs. Pressure graph for South Desbarres O-76 modified from NRCAN Basin Database.

Testing types of pressure:

BDP = Breakdown Pressure
DST = Drillstem test
DMR = Drilling Mud Record
FLOT = Formation Leak-Off Test
FRP = Feedrate Pressure
MDT = Modular Formation Dynamics Tester
MLR = Mudloggers Report
PIT = Pressure Integrity Test
RFT = Repeat Formation Tester
WK = Well Kick

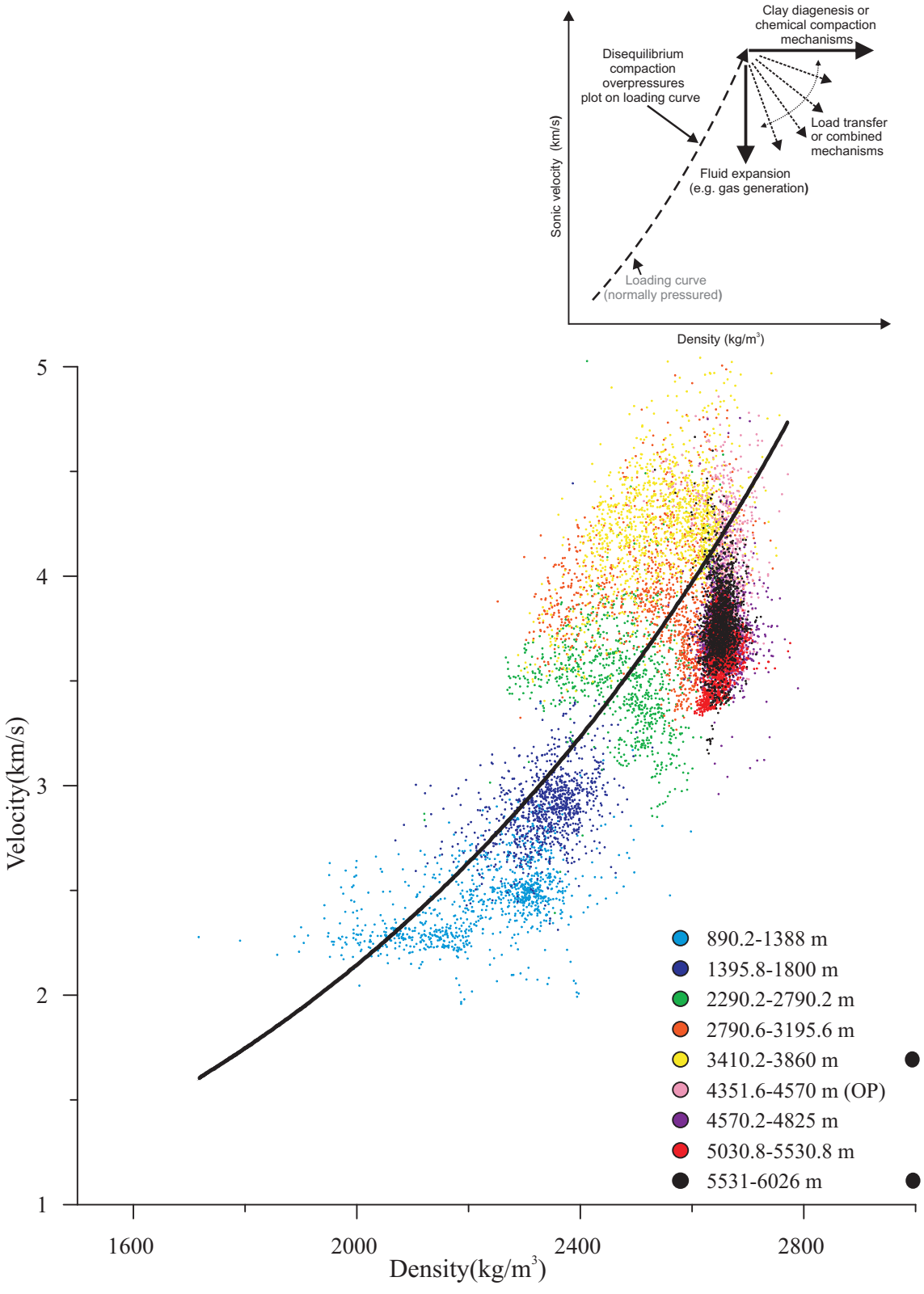

Figure 3.13.2 Graph #3 of a velocity vs. density plot for South Desbarres O-76.

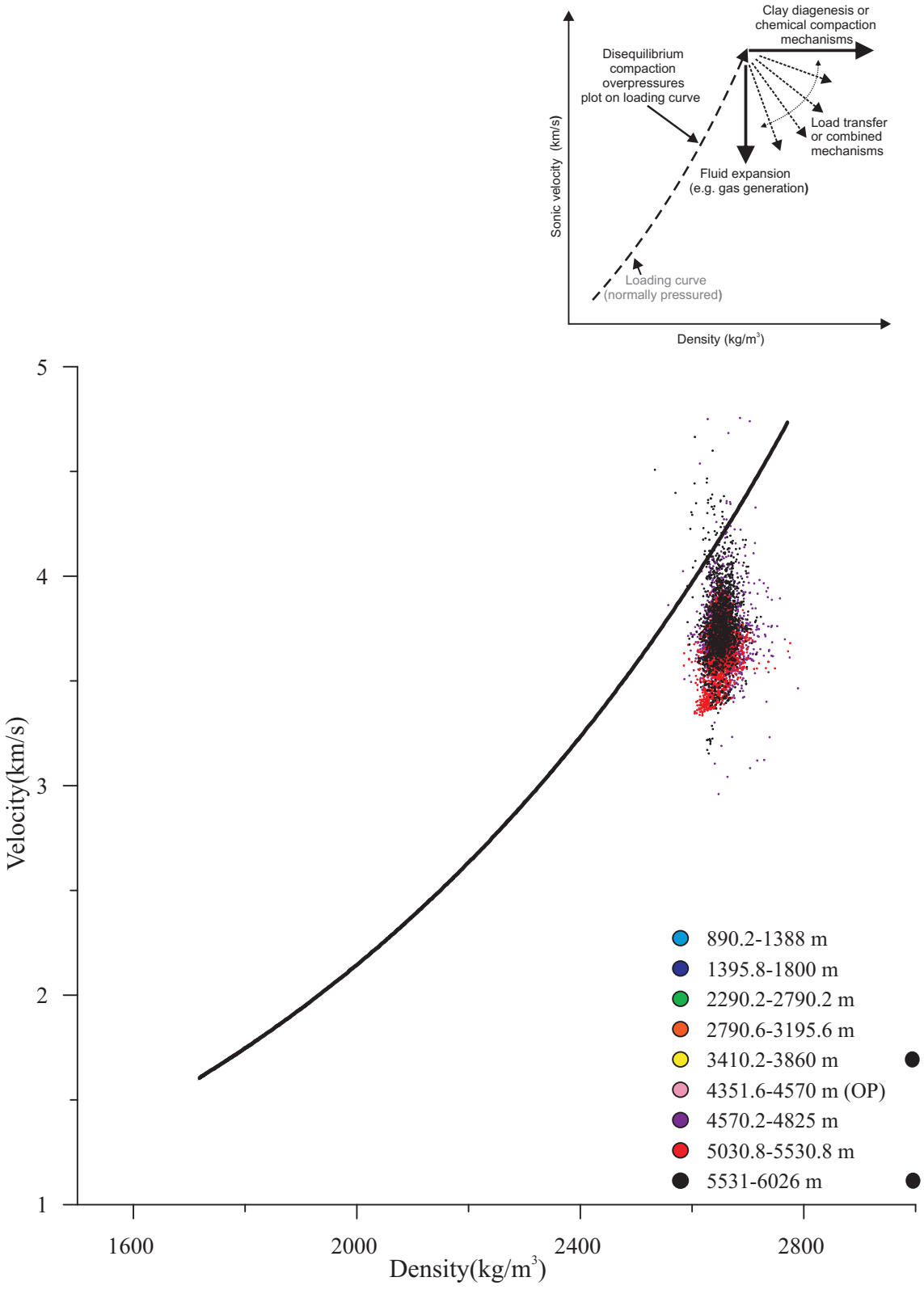

Figure 3.13.3 Graph #4 of a velocity vs. density plot for South Desbarres O-76.

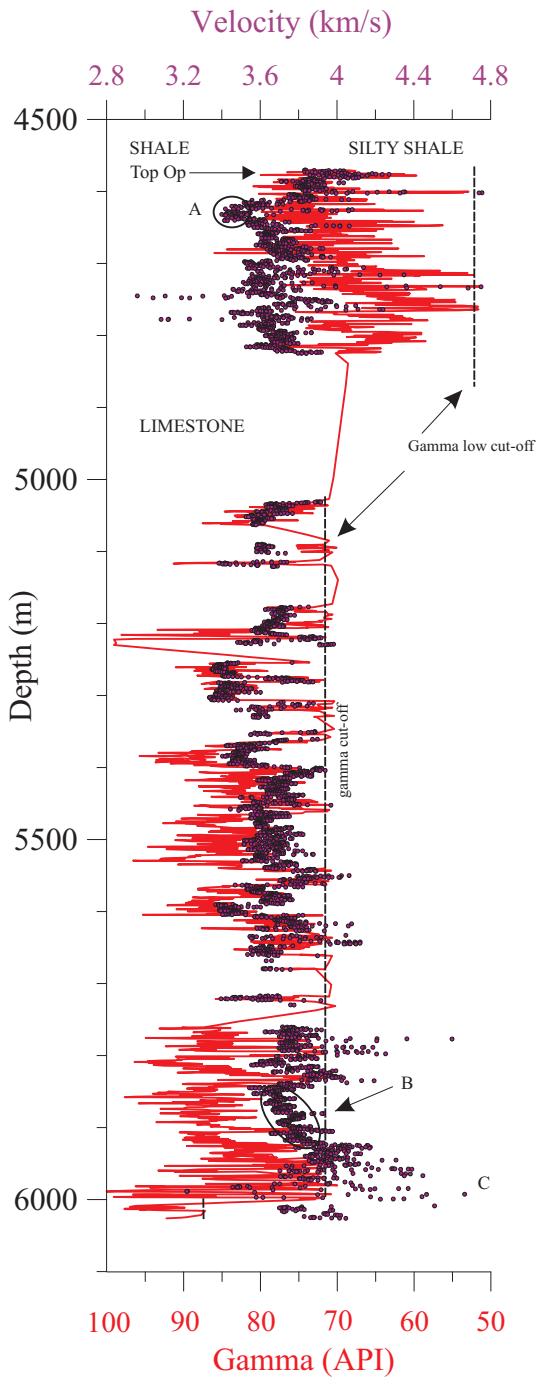

Figure 3.13.4 Changes in velocity and gamma with depth in the overpressure interval in South Desbarres O-76. Interval A has low velocity but high gamma, perhaps due to fractures. Interval B shows a progressive increase in velocity downwards with rather uniform gamma, perhaps due to cementation of fractures. C indicates the siltier basal part of the well.

However, overall, the velocity values increase with depth. From 4500-4850 m, the highest gamma sediments have velocities around 3.6 km/s. From 5000-5700 m, the highest gamma sediments have velocities from 3.6-3.7 km/s. Below 5700 m, the highest gamma sediments have velocities from 3.7-3.8 km/s. Presumably this represents a real increase in compaction with depth, although there are other explanations, e.g. greater cementation with depth. The observed increase in velocity near the base of the well (C in Fig. 3.13.4) is related to siltier lithologies. Near the top of overpressure, a low velocity zone at 4600-4640 m corresponds to high gamma (A in Fig. 3.14.4). This may be a zone in which open fractures are present. The gradual increase in velocity with no systematic change in gamma around 5900 m (B in Fig. 3.13.4) may indicate progressive cementation of fractures.

3.14 South Griffin J-13

South Griffin J-13 is 10 km southeast of Louisbourg J-47 in the eastern Scotian Basin, near the edge of the shelf. Overpressure occurs at ~5023 m and continues to a TD of 5911 m. The top of overpressure is within a limestone bed, which is also seen in Louisbourg J-47. Depth vs. pressure graph (Fig. 3.14.1) for South Griffin J-13 shows the degree of overpressure becomes greater with increasing depth, indicated by points ~30 % between hydrostatic and lithostatic gradients. The well was dry.

Graph #3 (Fig. 3.14.2) follows a normal trend line to the top of overpressure. Graph #4 (Fig. 3.14.3) shows a trend line that looks similar to Evangeline and Mohican. Samples to ~423 m below overpressure (purple points) are sparsely distributed between

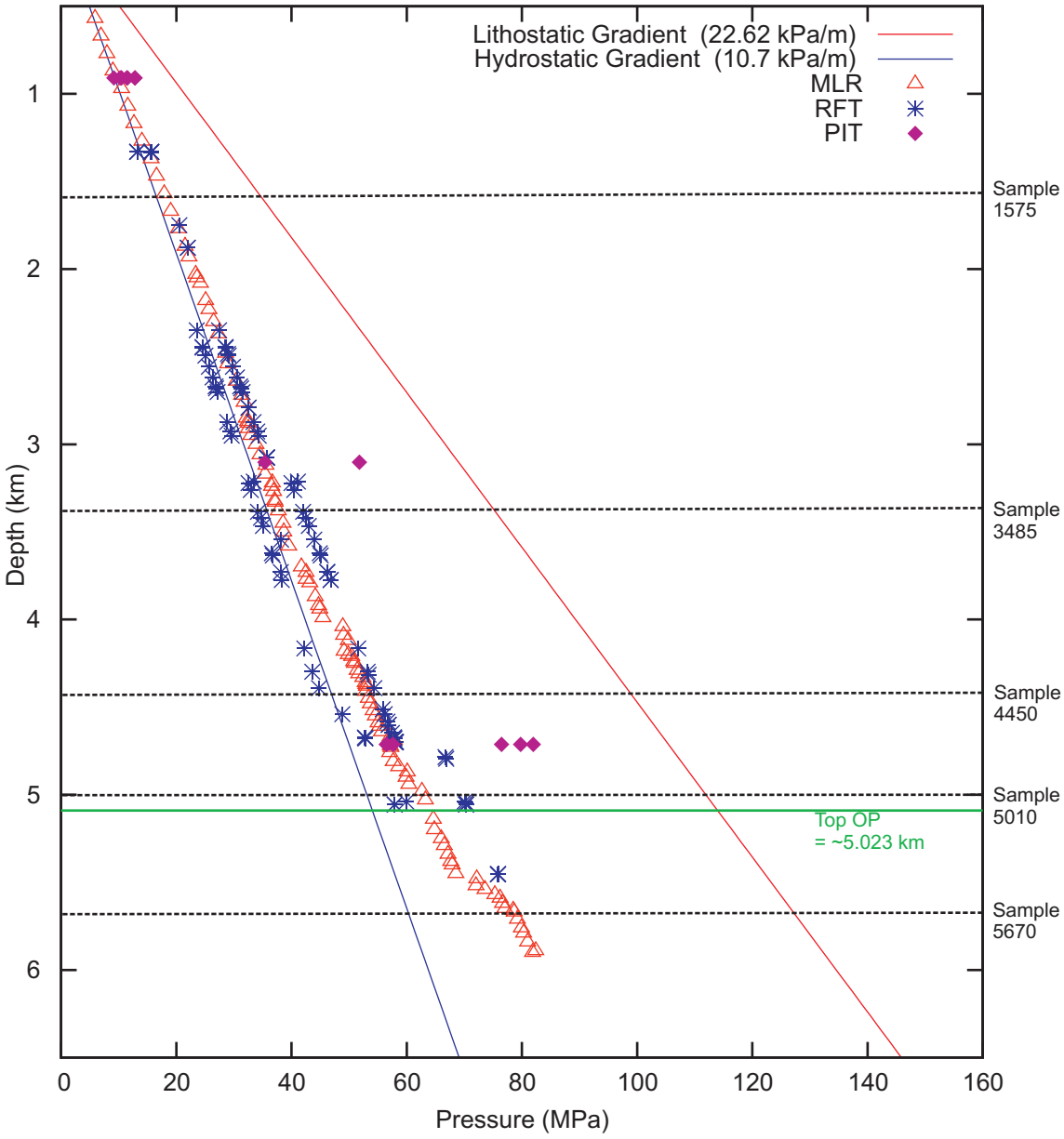

Figure 3.14.1 Depth vs. Pressure graph for South Griffin J-13 modified from NRCAN Basin Database.

Testing types of pressure:

BDP = Breakdown Pressure
DST = Drillstem test
DMR = Drilling Mud Record
FLOT = Formation Leak-Off Test
FRP = Feedrate Pressure
MDT = Modular Formation Dynamics Tester
MLR = Mudloggers Report
PIT = Pressure Integrity Test
RFT = Repeat Formation Tester
WK = Well Kick

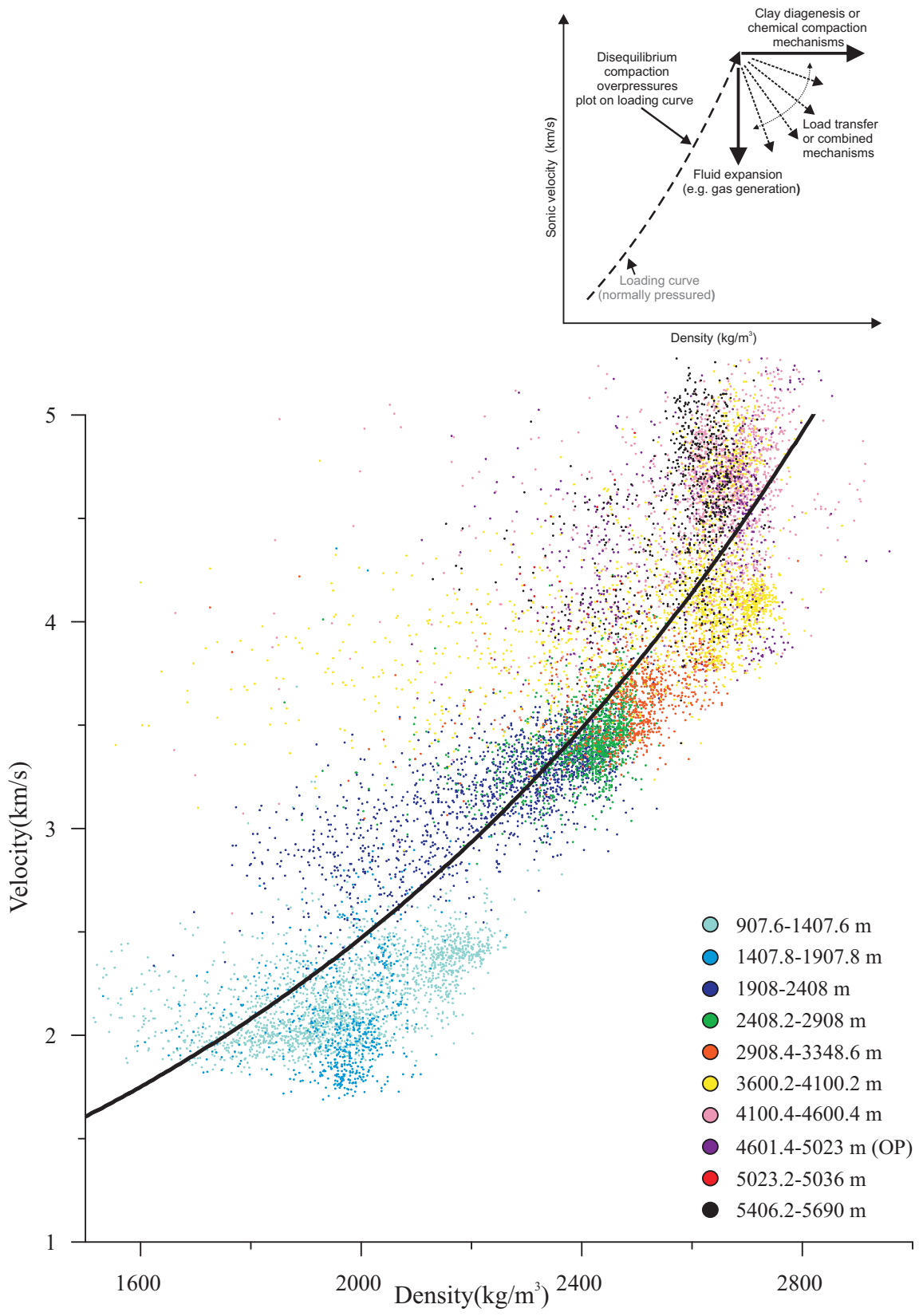

Figure 3.14.2 Graph #3 of a velocity vs. density plot for South Griffin J-13.

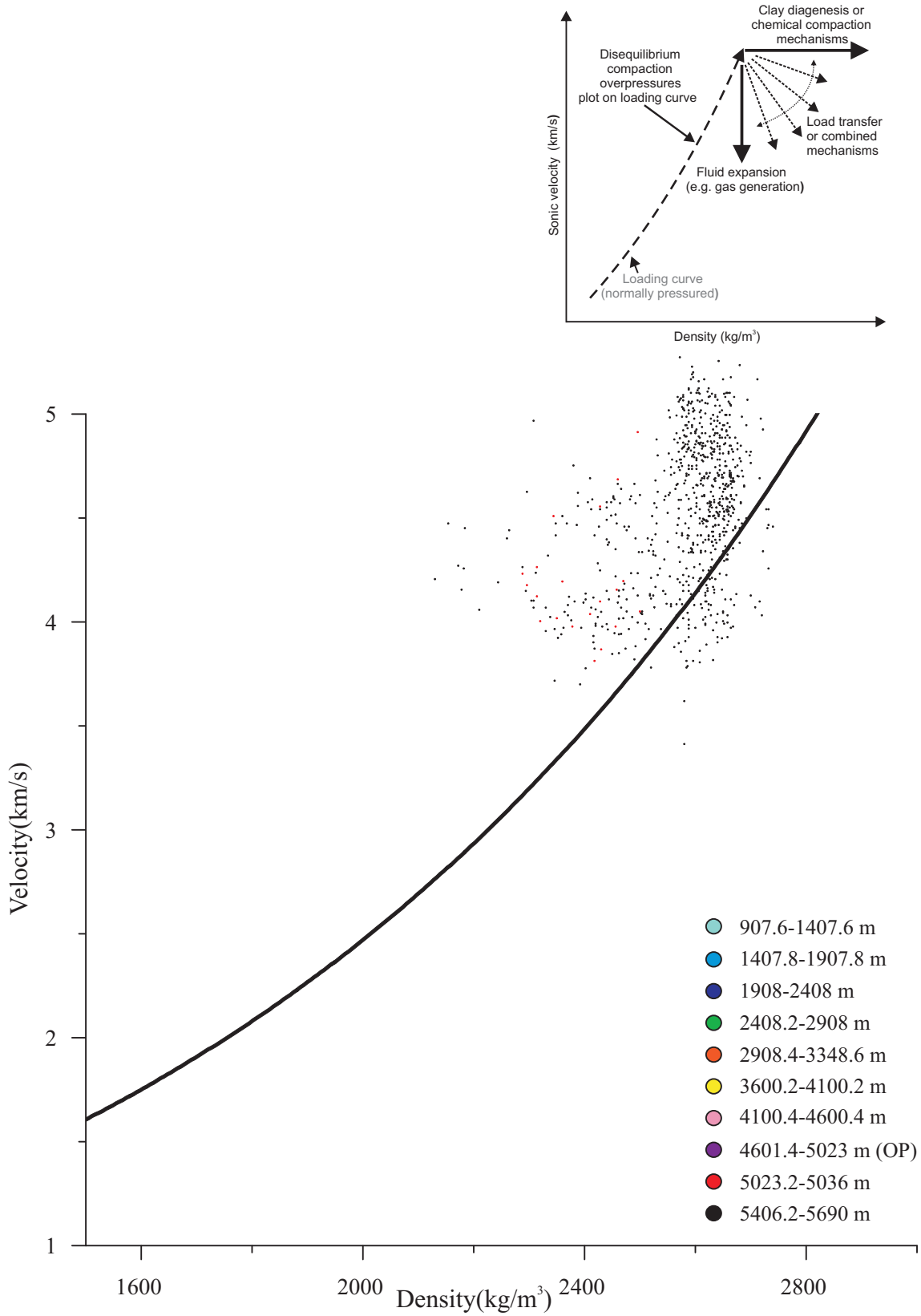

Figure 3.14.3 Graph #4 of a velocity vs. density plot for South Griffin J-13.

4-5 velocity. Samples to ~436 m below overpressure (red points) are parallel to but above the trend line and can hardly be seen because they are so few and are covered by other points. Samples ~1090 m below overpressure (black points) form an ovoid cluster near the top of the trend line. Graph #4 suggests a type 6 pattern (Fig. 3.1.1), therefore within the overpressured sediments there is no velocity vs. density pattern. The scatter does not show an observable trend with increasing depth.

3.15 Tantallon M-41

The Tantallon M-41 well was drilled on the Scotian Slope 50 km south of Louisbourg J-47, in 1516 m water depth, to a TD of 5602 m. Although it is not recorded as having overpressure in the East Coast Basin Atlas, data from the BASIN database suggest moderate overpressure below ~3800 m (Fig. 3.15.1). Tantallon M-41 is predominantly shale. The well was dry.

Graph #3 (Fig. 3.15.2) follows a normal loading curve to the top of overpressure. Graph #4 (Fig. 3.15.3) shows that samples to ~75 m-1779 m below the top of overpressure (yellow-black points) show a trend of increasing density and velocity with depth, above the trend line. Deeper samples (purple, red, and black) form overlapping vertical clusters, with the deepest samples showing the highest mean density and the velocity maximum extending above a trend line defined by the Tantallon data only. The type of pattern shown by Graph #4 is similar to that of North Banquereau (Fig. 3.10.2), and less so to Chebucto K-90 (Fig. 3.2.3). Therefore it shows a type 10 pattern (Fig. 3.1.1).

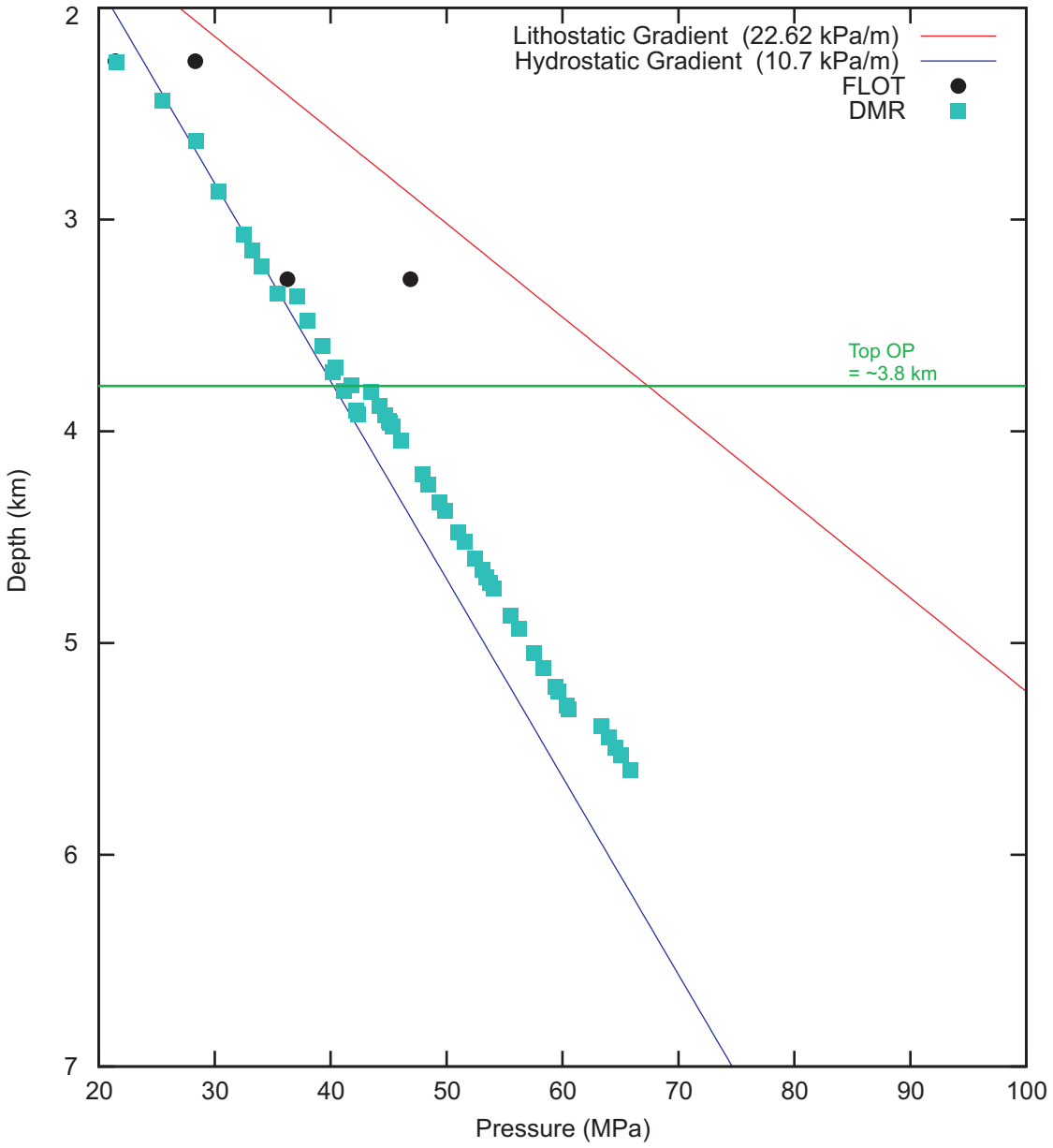

Figure 3.15.1 Depth vs. Pressure graph for Tantallon M-41 modified from NRCAN Basin Database.

Testing types of pressure:

BDP = Breakdown Pressure
DST = Drillstem test
DMR = Drilling Mud Record
FLOT = Formation Leak-Off Test
FRP = Feedrate Pressure
MDT = Modular Formation Dynamics Tester
MLR = Mudloggers Report
PIT = Pressure Integrity Test
RFT = Repeat Formation Tester
WK = Well Kick

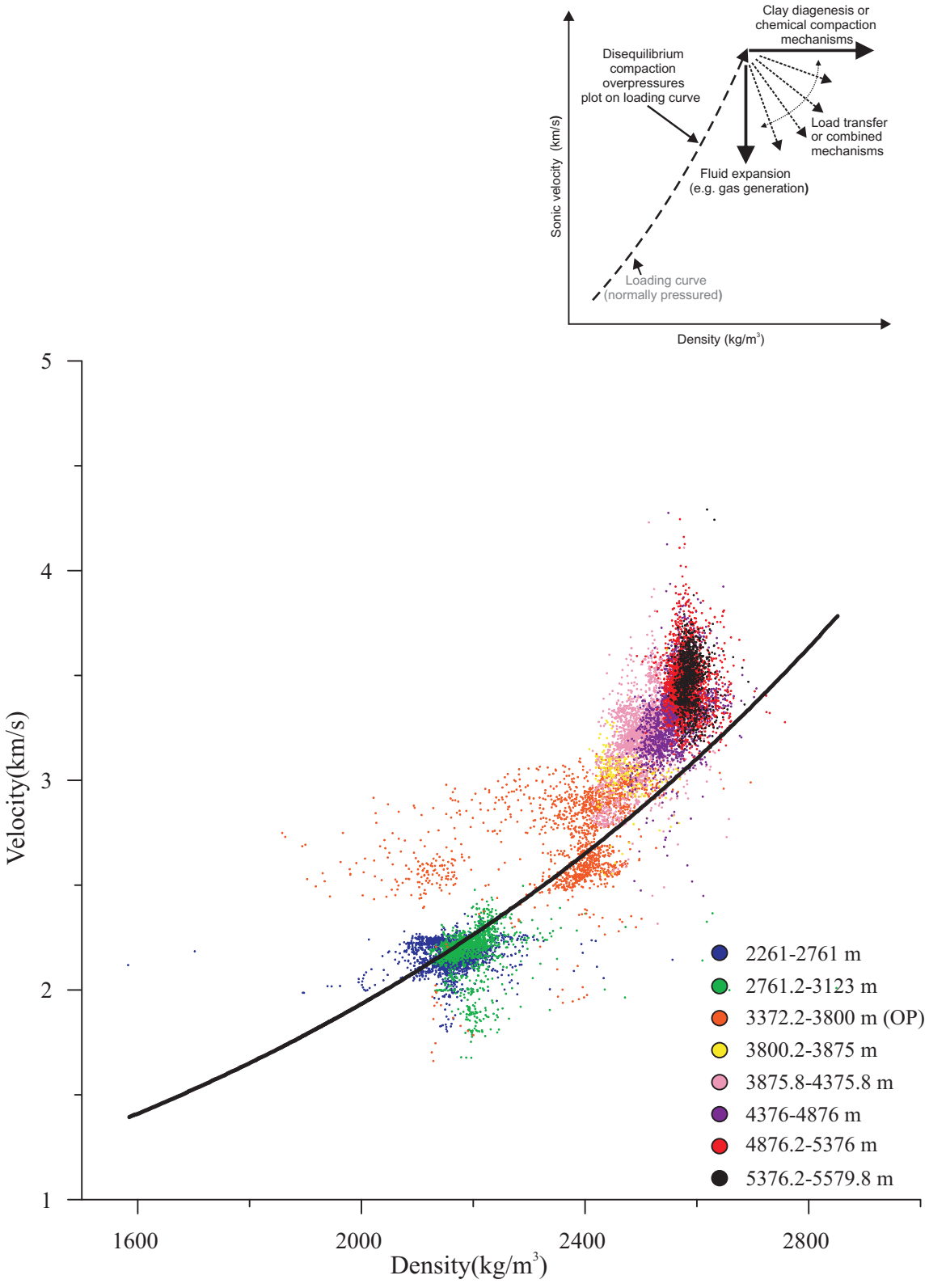

Figure 3.15.2 Graph #3 of a velocity vs. density plot for Tantallon M-41.

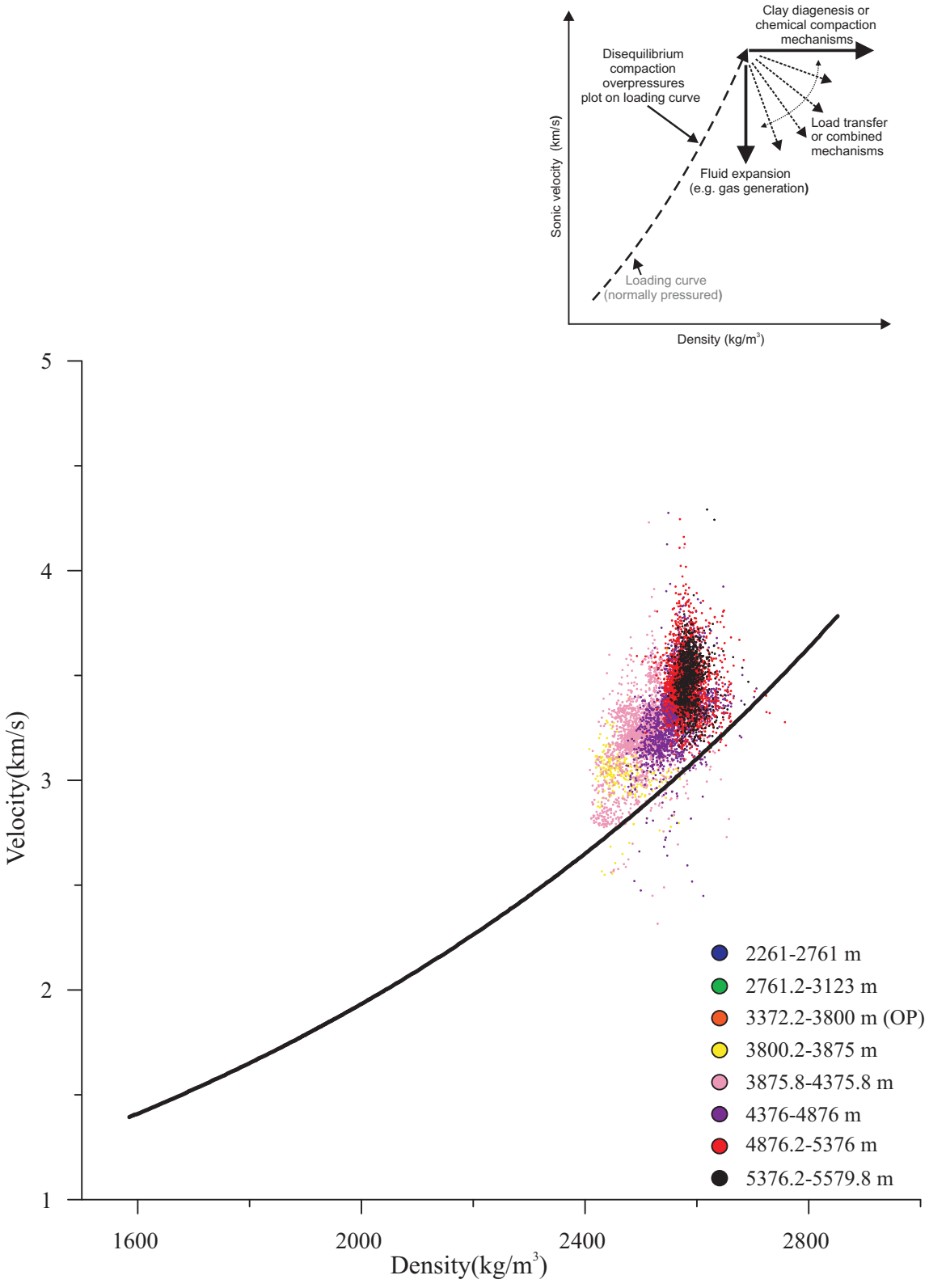

Figure 3.15.3 Graph #4 of a velocity vs. density plot for Tantallon M-41.

3.16 Thebaud C-74

Thebaud C-74 is located to the west of the Sable Sub-Basin within the Thebaud field. Overpressure starts at ~3800 m and continues until a TD of 5150 m. The graph from BASIN database (Fig. 3.16.1) shows a fairly significant overpressure because points are very close to the lithostatic gradient and some are even over it. The East Coast Basin Atlas (MacLean and Wade, 1993) indicates the top of overpressure occurs within a sandstone interval. Gas and condensates were discovered.

Graph #3 (Fig. 3.16.2) does not have a pronounced loading curve because of the lack of data, but it does show a clear trend below the top of overpressure. Graph #4 (Fig. 3.16.3) shows samples ~500 m below overpressure (red points) below the trend line oriented in a vertical cluster. The red points reach farther down than black points. Samples ~500-944.8 m below overpressure (black points) also are below the trend line, oriented in a vertical cluster, but above the red points. The graph's trend follows a type 9 pattern, which shows a normal loading curve to near the top of overpressure whereby it decreases in velocity with no change in density followed by an increase in velocity with no change in density.

3.17 Thebaud I-93

Thebaud I-93 is located within the Thebaud field, which is west of the Sable Sub-Basin. Overpressure occurs at ~3915 m and continues until a TD of 5166 m. The East Coast Basin Atlas (MacLean and Wade, 1993) shows the onset of overpressure starting below a shale bed and above a gap. BASIN database depth vs. pressure plot for this well (Fig.

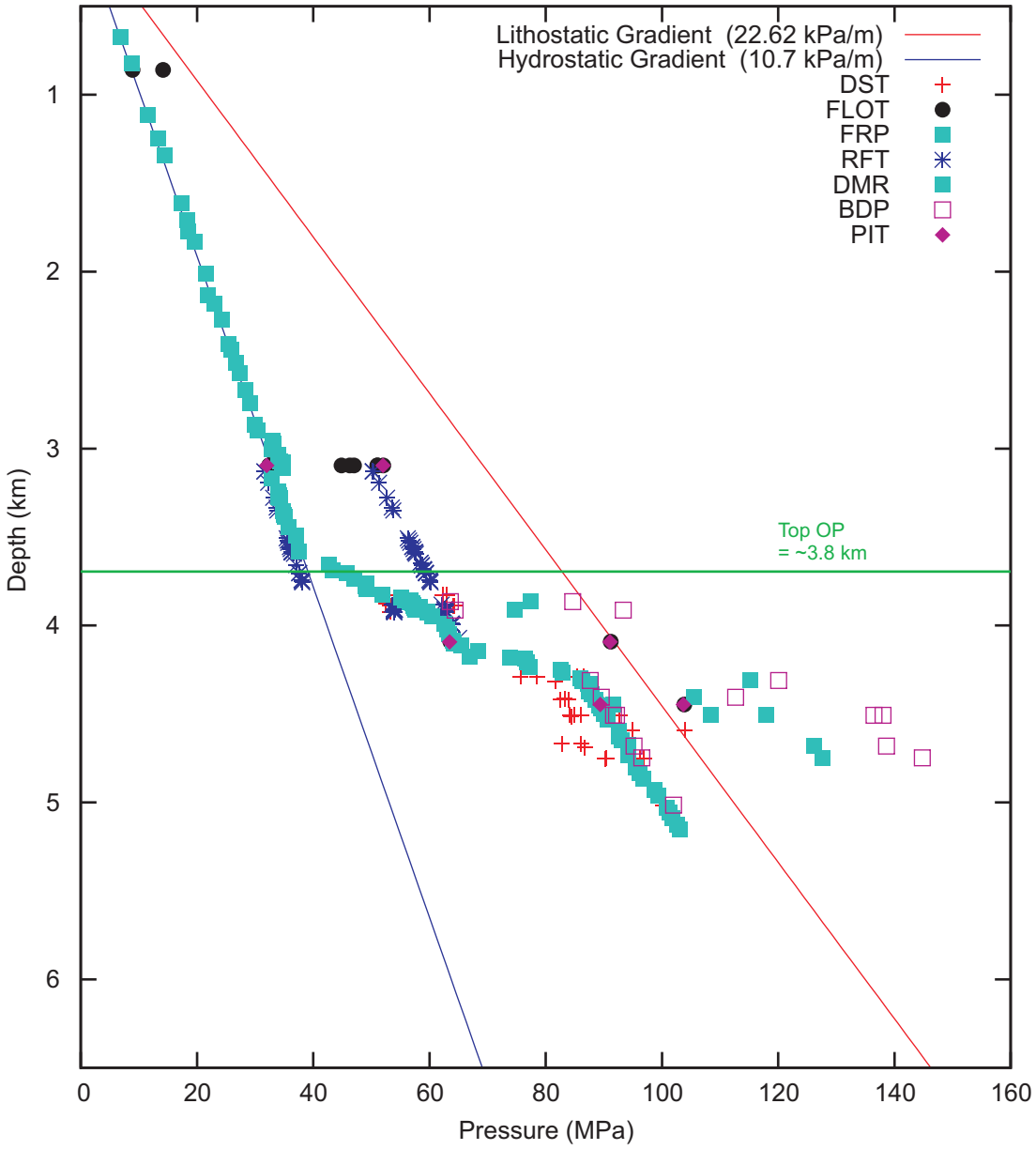

Figure 3.16.1 Depth vs. Pressure graph for Thebaud C-74 modified from NRCAN Basin Database.

Testing types of pressure:

BDP = Breakdown Pressure
DST = Drillstem test
DMR = Drilling Mud Record
FLOT = Formation Leak-Off Test
FRP = Feedrate Pressure
MDT = Modular Formation Dynamics Tester
MLR = Mudloggers Report
PIT = Pressure Integrity Test
RFT = Repeat Formation Tester
WK = Well Kick

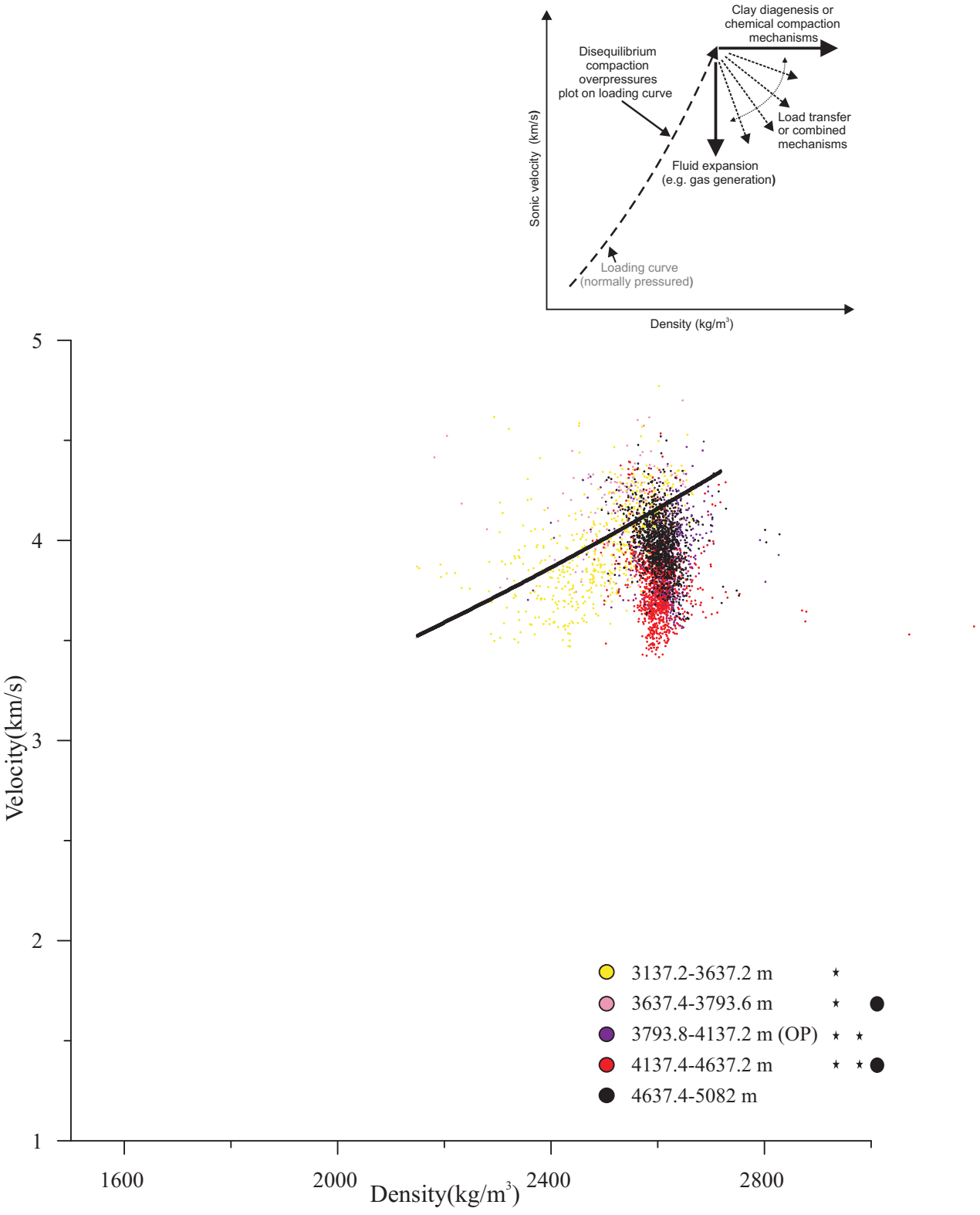

Figure 3.16.2 Graph #3 of a velocity vs. density plot for Thebaud C-74.

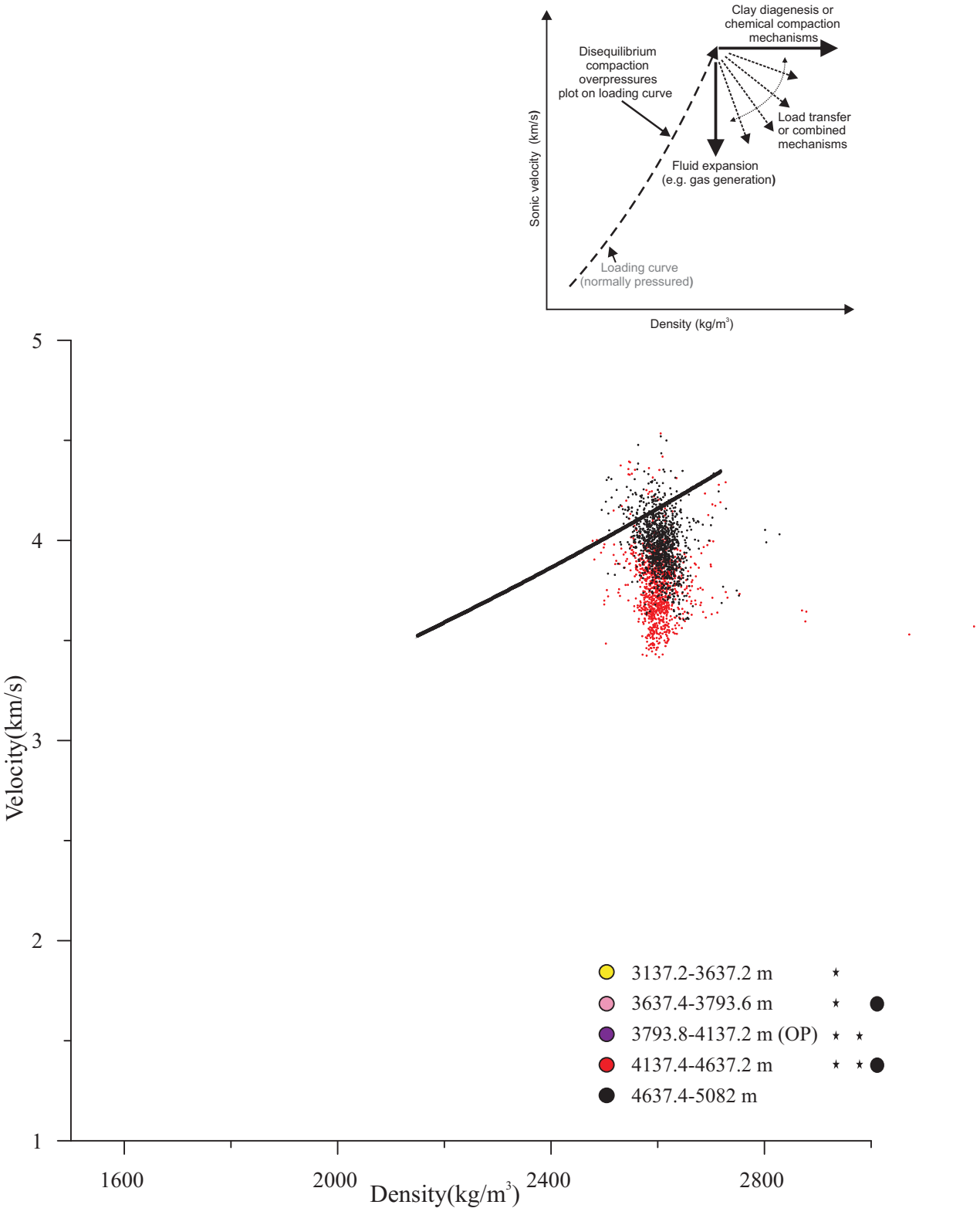

Figure 3.16.3 Graph #4 of a velocity vs. density plot for Thebaud C-74.

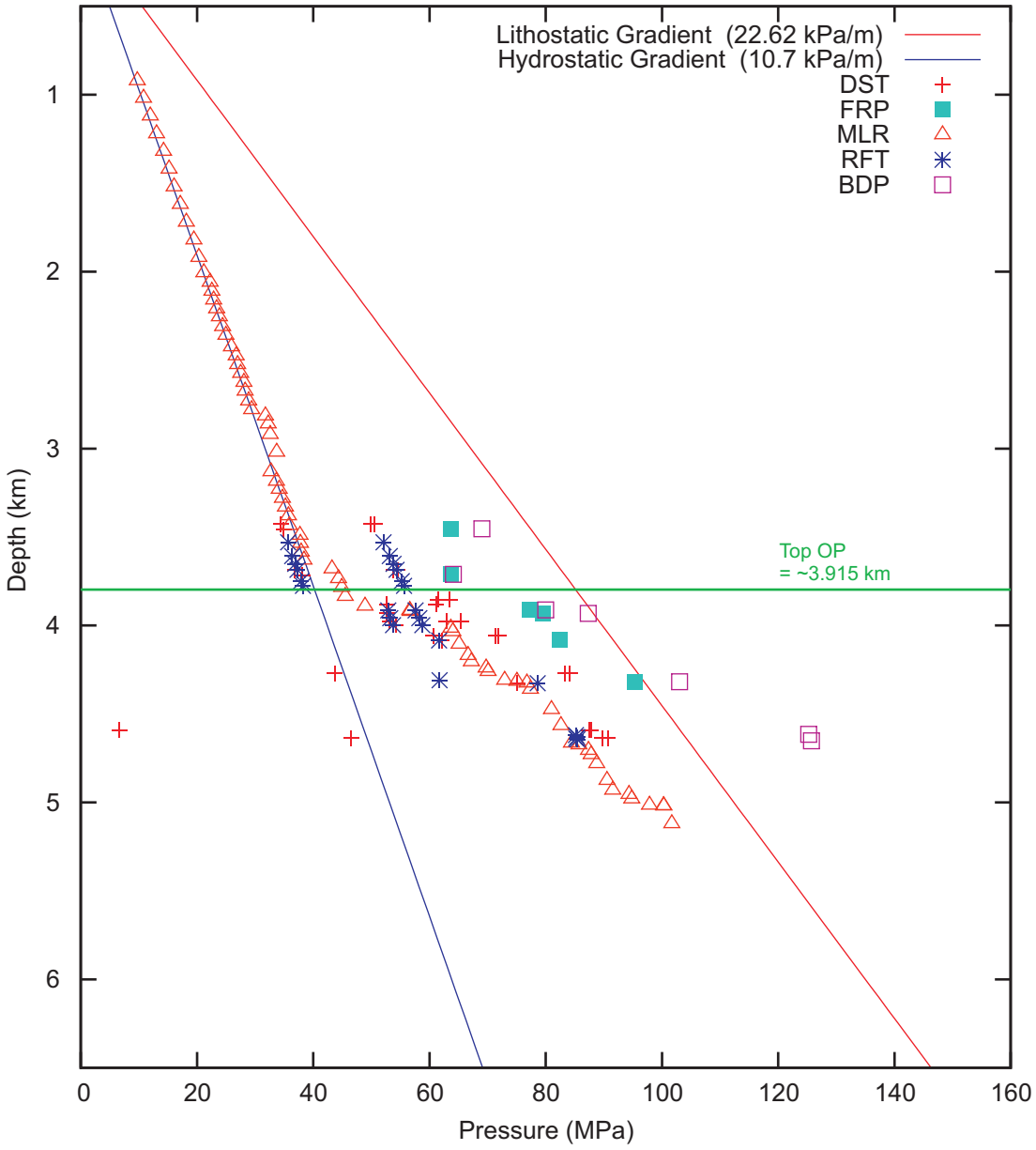

Figure 3.17.1 Depth vs. Pressure graph for Thebaud I-93 modified from NRCAN Basin Database.

Testing types of pressure:

BDP = Breakdown Pressure
DST = Drillstem test
DMR = Drilling Mud Record
FLOT = Formation Leak-Off Test
FRP = Feedrate Pressure
MDT = Modular Formation Dynamics Tester
MLR = Mudloggers Report
PIT = Pressure Integrity Test
RFT = Repeat Formation Tester
WK = Well Kick

3.17.1) shows a significant overpressure exhibited by points close to the lithostatic gradient. The well discovered gas and water.

Graph #3 (Fig. 3.17.2) shows a normal loading curve of increasing velocity and density with increasing depth, to a maximum near the top of overpressure. The velocity below the top of overpressure decreases with little change in density.

Graph #4 (Fig. 3.17.3) looks very similar to Thebaud C-74 with the exception of black points being below red points in Thebaud I-93. The majority of samples ~490 m below overpressure (red points) are oriented vertically below the trend line. Samples ~ 595-868 m below overpressure (black points) are arranged in a vertical cluster at the tip of the red points below the trend line. There is a visible trend that supports a type 3 pattern.

3.18 Thebaud I-94

Thebaud I-94 is located within the Thebaud field, which is west of the Sable Sub-Basin. Overpressure starts at ~3810 m and continues to a TD of 3962.4 m. The BASIN database plot of depth vs. pressure (Fig. 3.18.1) shows the overpressure is not as significant as Thebaud C-74 or I-93. Points reach to about 45 % between hydrostatic and lithostatic. It has a recorded overpressure and the well discovered gas and condensates.

Graph #3 (Fig. 3.18.2) looks very different from the other Thebaud graphs because it has more data above overpressure and no data below overpressure. There were no points at shallow depths above overpressure found in Thebaud C-74 or I-93, therefore

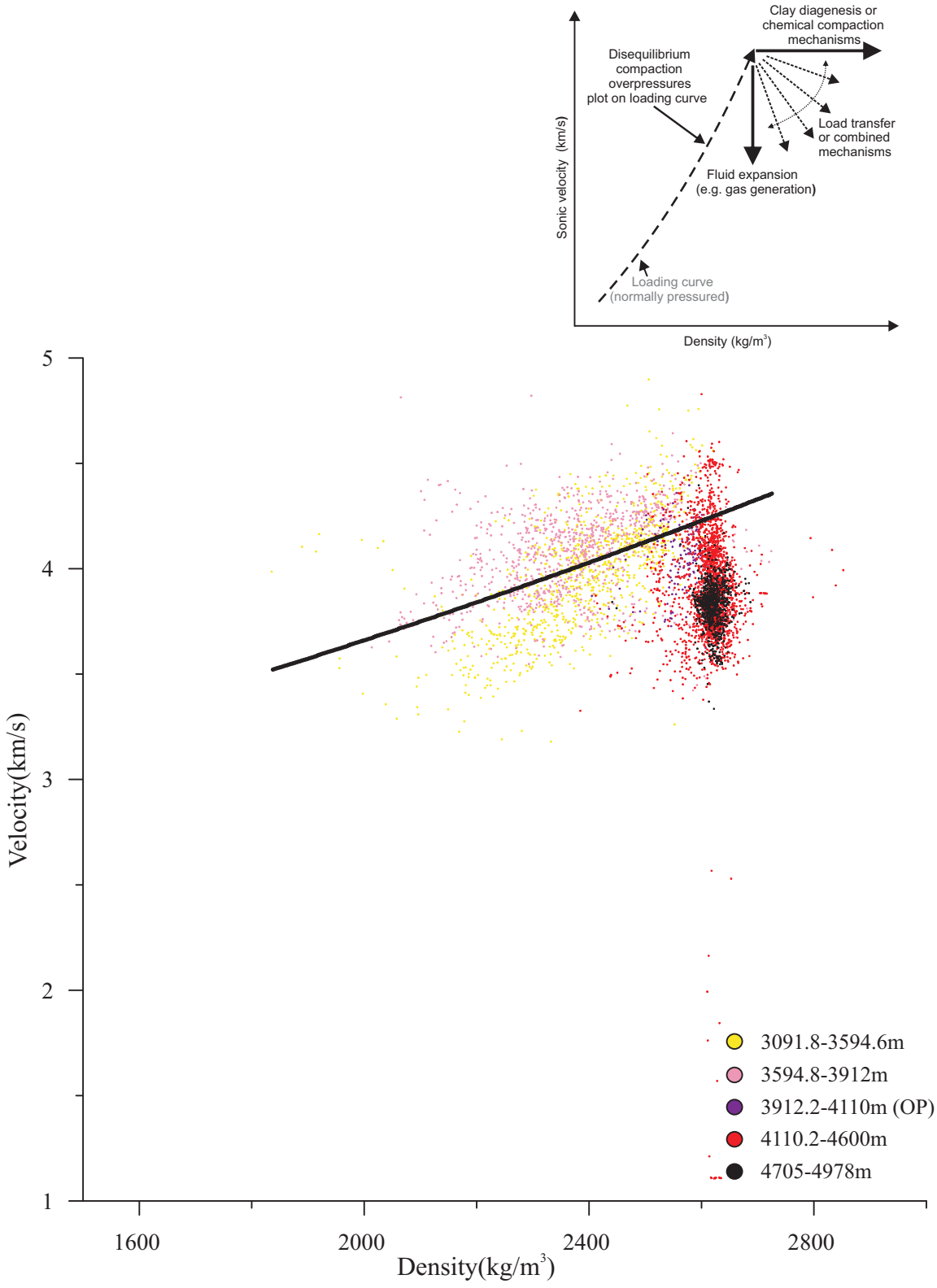

Figure 3.17.2 Graph #3 of a velocity vs. density plot for Thebaud I-93.

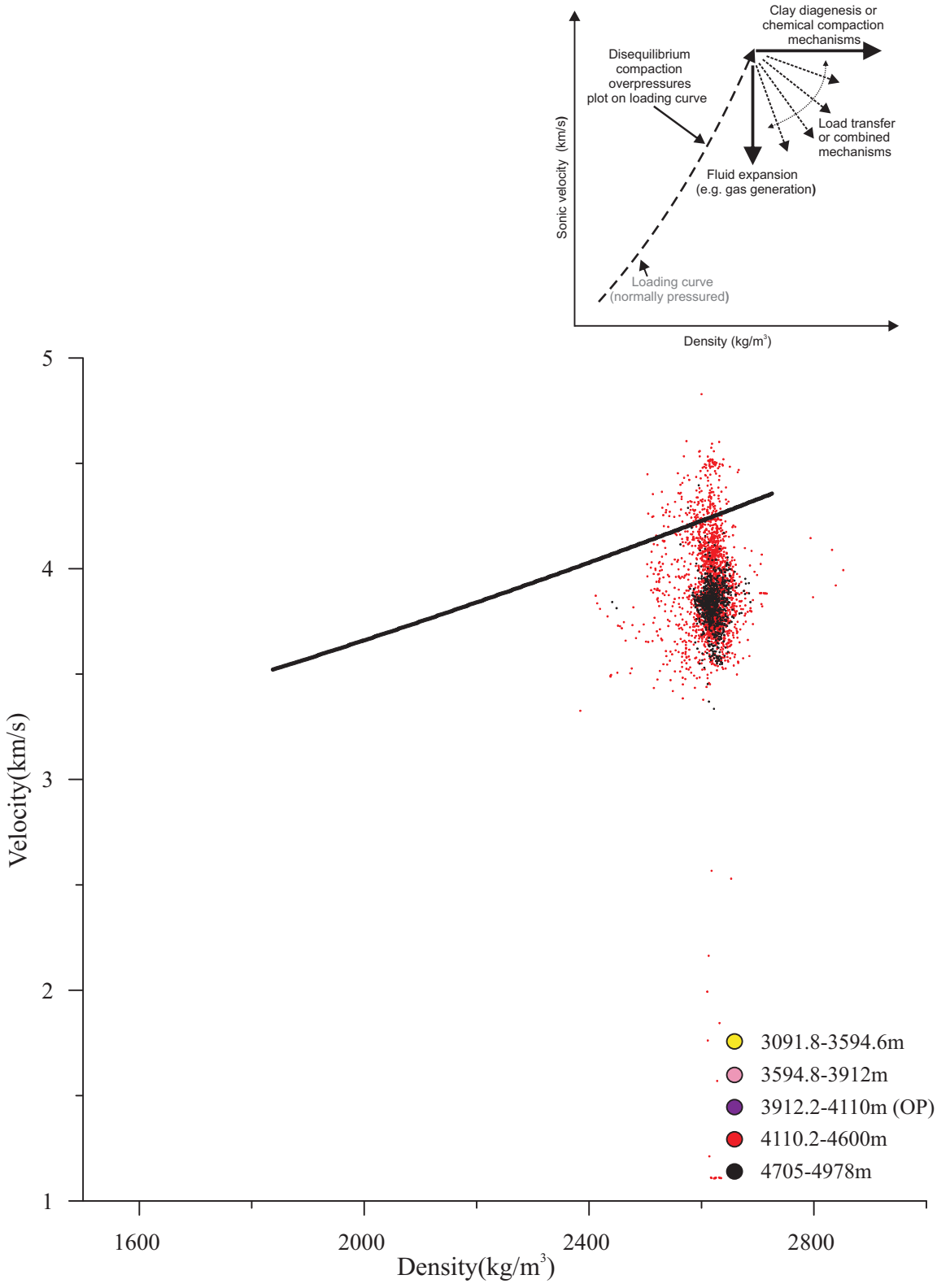

Figure 3.17.3 Graph #4 of a velocity vs. density plot for Thebaud I-93.

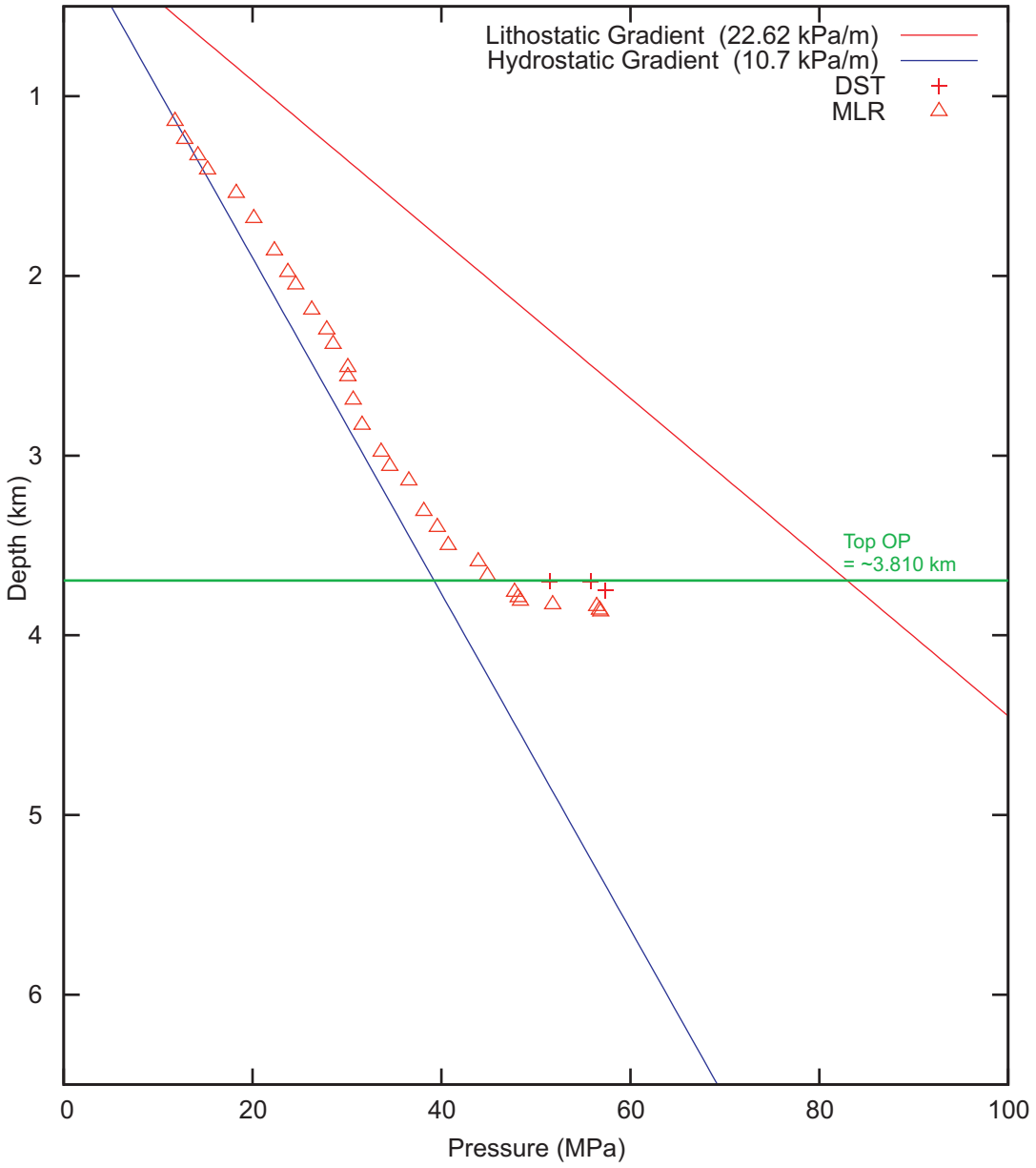

Figure 3.18.1 Depth vs. Pressure graph for Thebaud I-94 modified from NRCAN Basin Database.

Testing types of pressure:

BDP = Breakdown Pressure
DST = Drillstem test
DMR = Drilling Mud Record
FLOT = Formation Leak-Off Test
FRP = Feedrate Pressure
MDT = Modular Formation Dynamics Tester
MLR = Mudloggers Report
PIT = Pressure Integrity Test
RFT = Repeat Formation Tester
WK = Well Kick

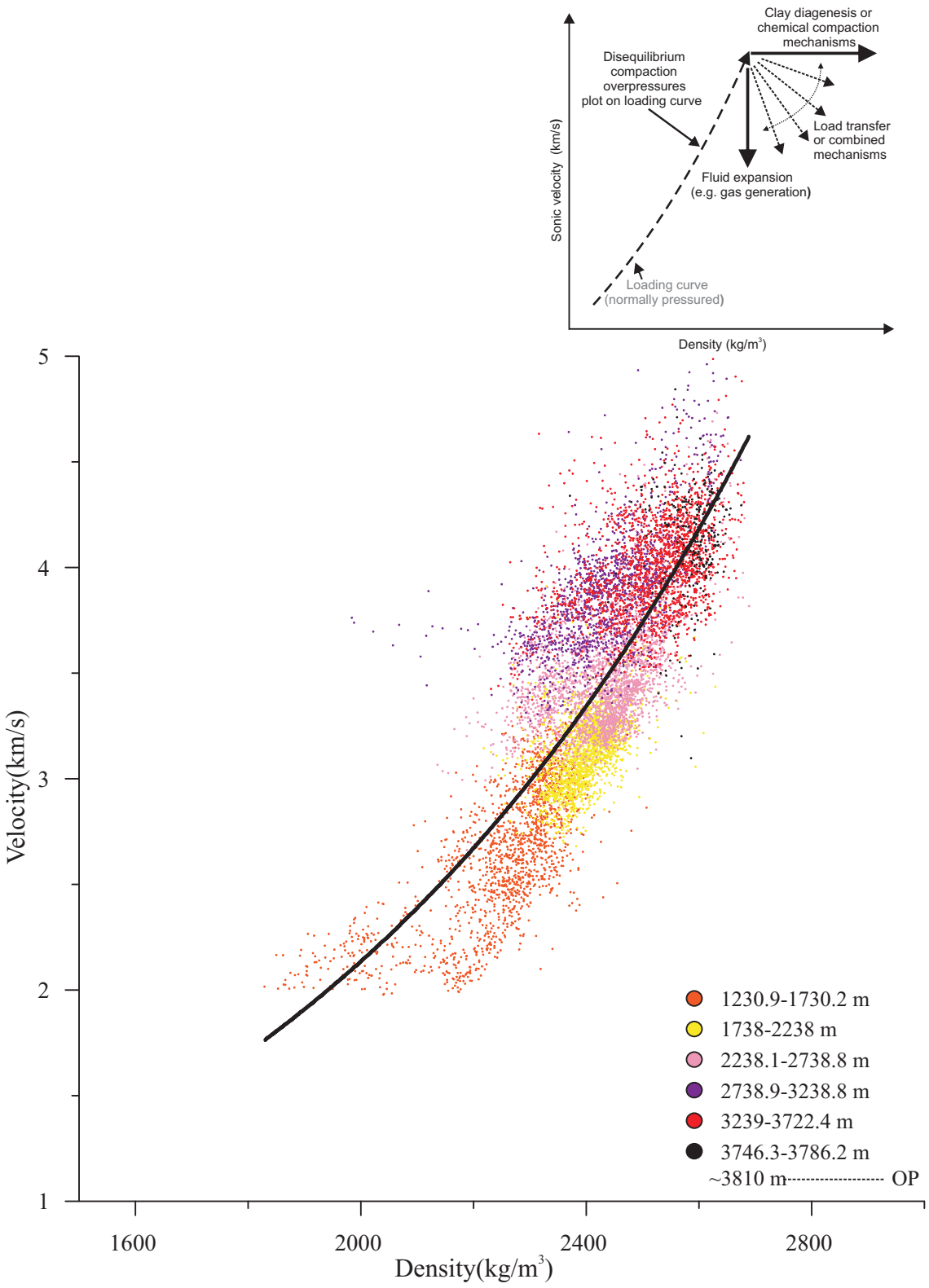

Figure 3.18.2 Graph #3 of a velocity vs. density plot for Thebaud I-94.

Thebaud I-94 acted as the loading curve or body for the other two wells. Shallower points (orange, yellow, pink) are clustered on top of each other; the same goes for the deeper points (purple, red, black). The graph moves up the trend line until it reaches its deepest part, where it just stops above the trend line. This reflects a type 2 pattern because it increases velocity and density following the loading curve, which occurs in overpressured rocks.

3.19 Venture B-43

Venture B-43 is located within the Venture field to the east of the Sable Sub-Basin. Overpressure starts at ~4450 m and continues to a TD of 5872 m, The BASIN database depth vs. pressure plot (Fig. 3.19.1) shows a large overpressure because points are very close to lithostatic. The East Coast Basin Atlas (MacLean and Wade, 1993) shows the top of overpressure occurring in a sandy-silty unit. The well has a recorded overpressure and discovered gas, condensate, and water.

Graph #3 (Fig. 3.19.2) shows a normal loading curve of increasing velocity and density with increasing depth to a maximum near the top of overpressure. Graph #4 (Fig. 3.19.3) shows samples ~7-101 m below overpressure (pink points) are few in number and sit near the top of the trend line. Samples ~101-602 m below overpressure (purple points) are in a sparse cluster below the trend line mixed with red points. Samples ~602-1103 m below overpressure (red points) sit below the graph in an almost vertical shape. The pink, purple, and red points are all clustered together making it sometimes hard to differentiate. Samples ~1103-1401 m below overpressure (black points) sit at the tip of the red points

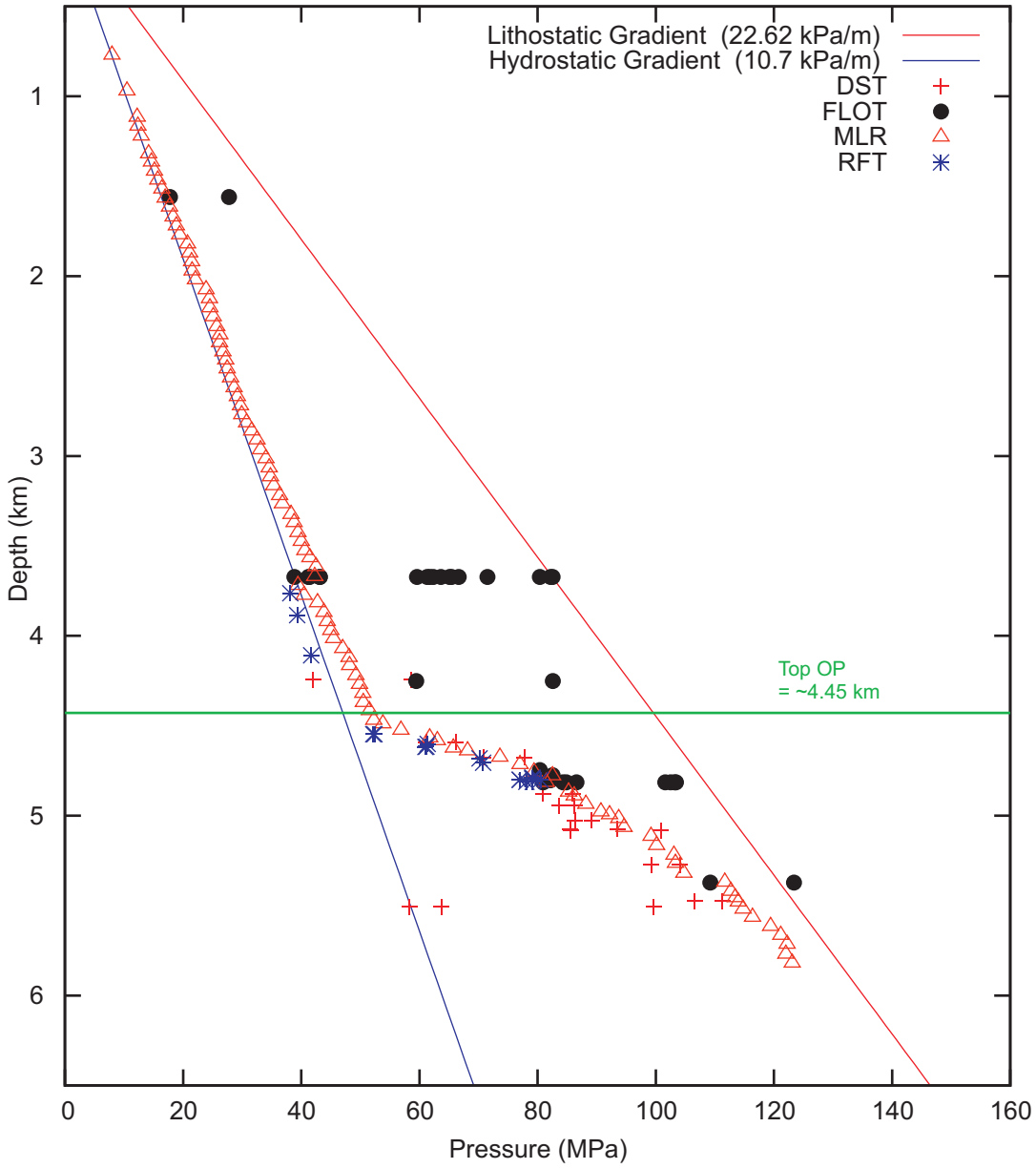

Figure 3.19.1 Depth vs. Pressure graph of Venture B-43 modified from NRCAN Basin Database.

Testing types of pressure:

BDP = Breakdown Pressure
DST = Drillstem test
DMR = Drilling Mud Record
FLOT = Formation Leak-Off Test
FRP = Feedrate Pressure
MDT = Modular Formation Dynamics Tester
MLR = Mudloggers Report
PIT = Pressure Integrity Test
RFT = Repeat Formation Tester
WK = Well Kick

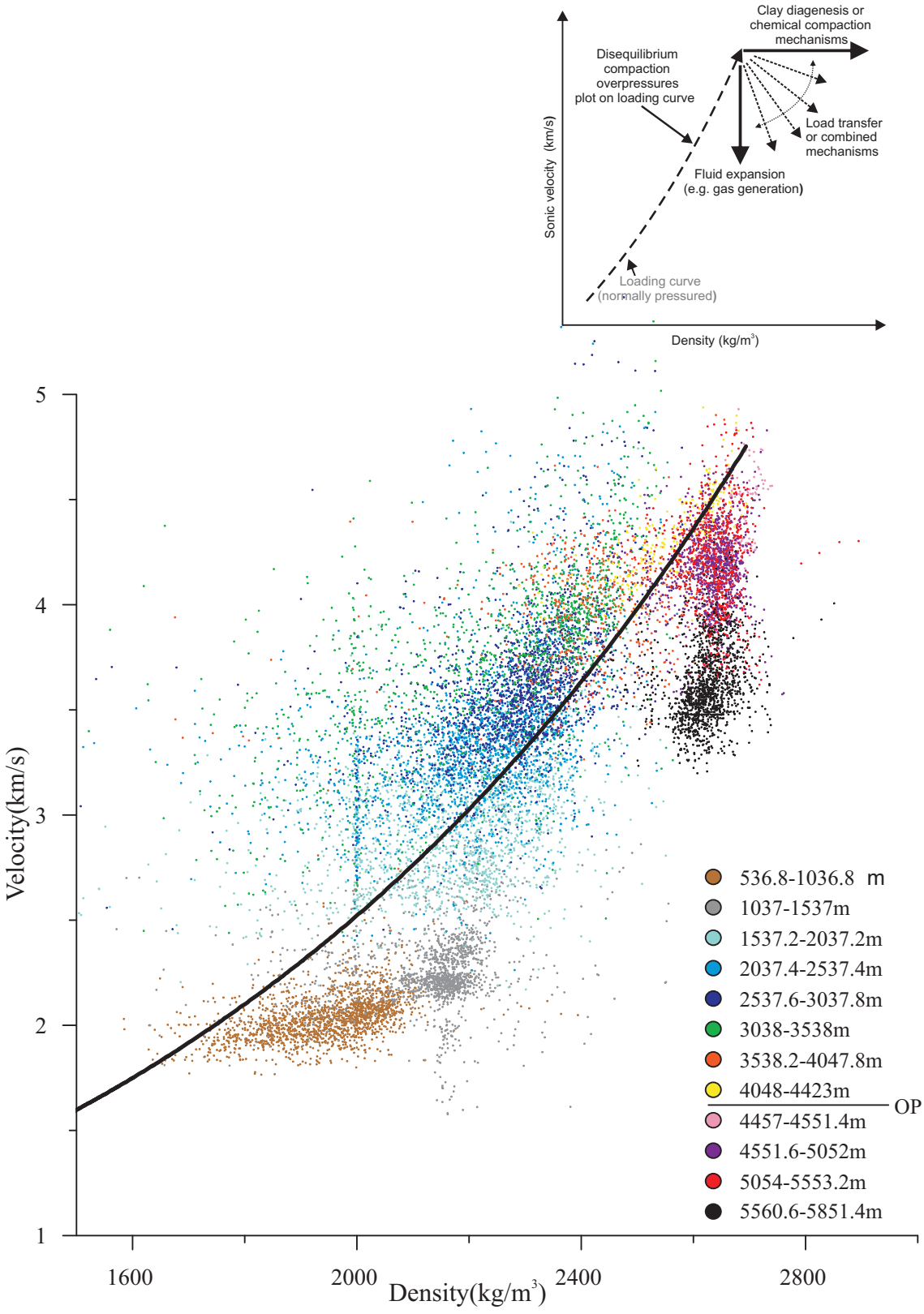

Figure 3.19.2 Graph #3 of a velocity vs. density plot for Venture B-43.

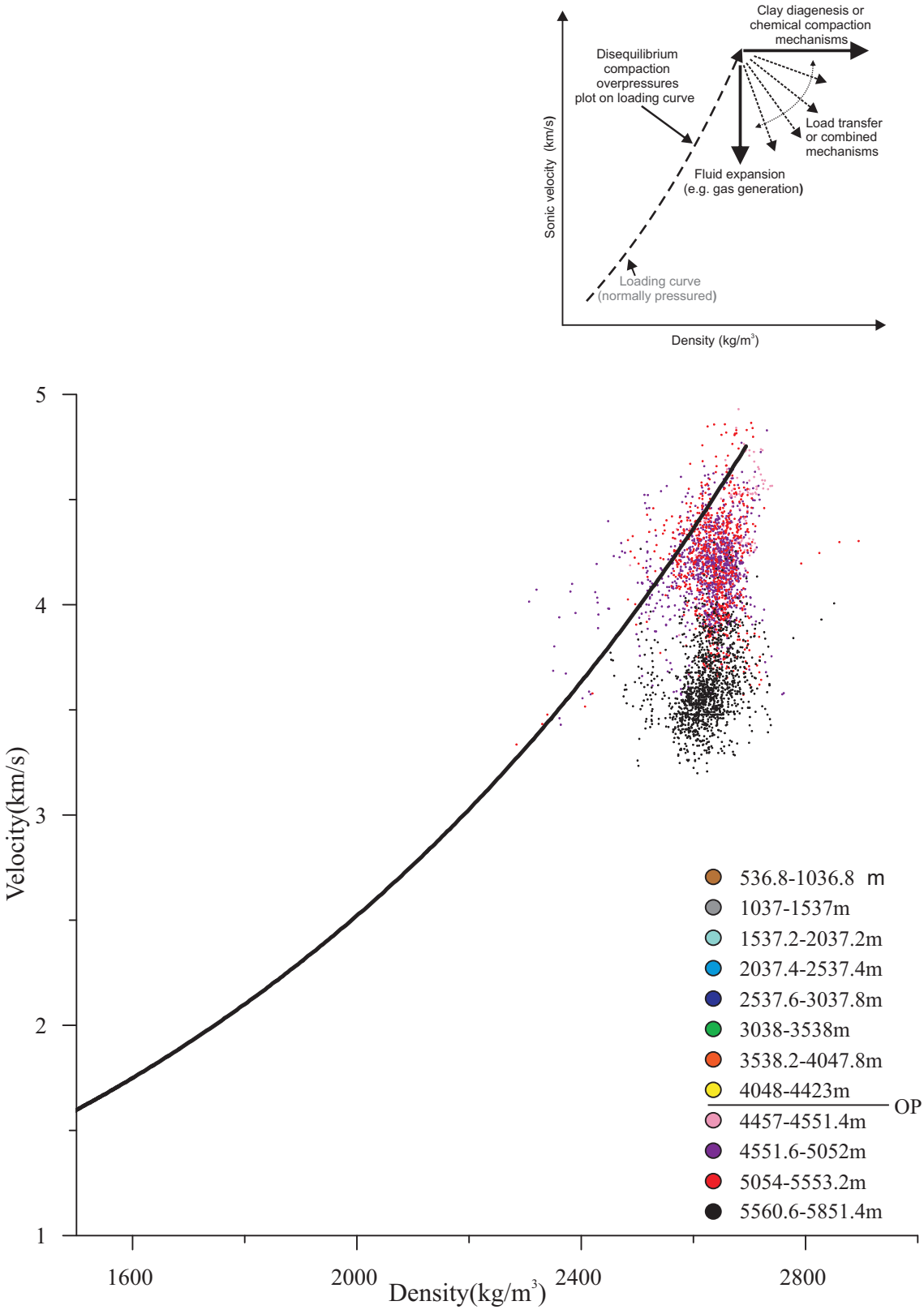

Figure 3.19.3 Graph #4 of a velocity vs. density plot for Venture B-43.

below the trend line in a somewhat vertical shape. The overall shape is similar to type 3 pattern (Fig. 3.1.1).

3.20 Venture B-52

Venture B-52 is located within the Venture field to the east of the Sable Sub-Basin. Overpressure starts at ~4478 m and continues to a TD of 5960 m. The top of overpressure occurs in a sandy-silty interval indicated by the East Coast Basin Atlas (MacLean and Wade, 1993). Overpressure is significant because points reach lithostatic as indicated by the BASIN database plot (Fig. 3.20.1). There was a recorded overpressure and the well discovered gas, condensate, and water.

Graph #3 (Fig. 3.20.2) shows a normal loading curve of increasing velocity and density with increasing depth, to a maximum near the top of overpressure. Below that, velocity decreases with little change in density.

Graph #4 (Fig. 3.20.3) shows a similar pattern to Venture B-43 because there are many pink, purple, and red points clustered together. Pink points are below the trend line but start the highest. Red points fall below the pink and obscure many purple points. There is an observable transition between red and black points. The graph is a type 3 pattern (Fig. 3.1.1),

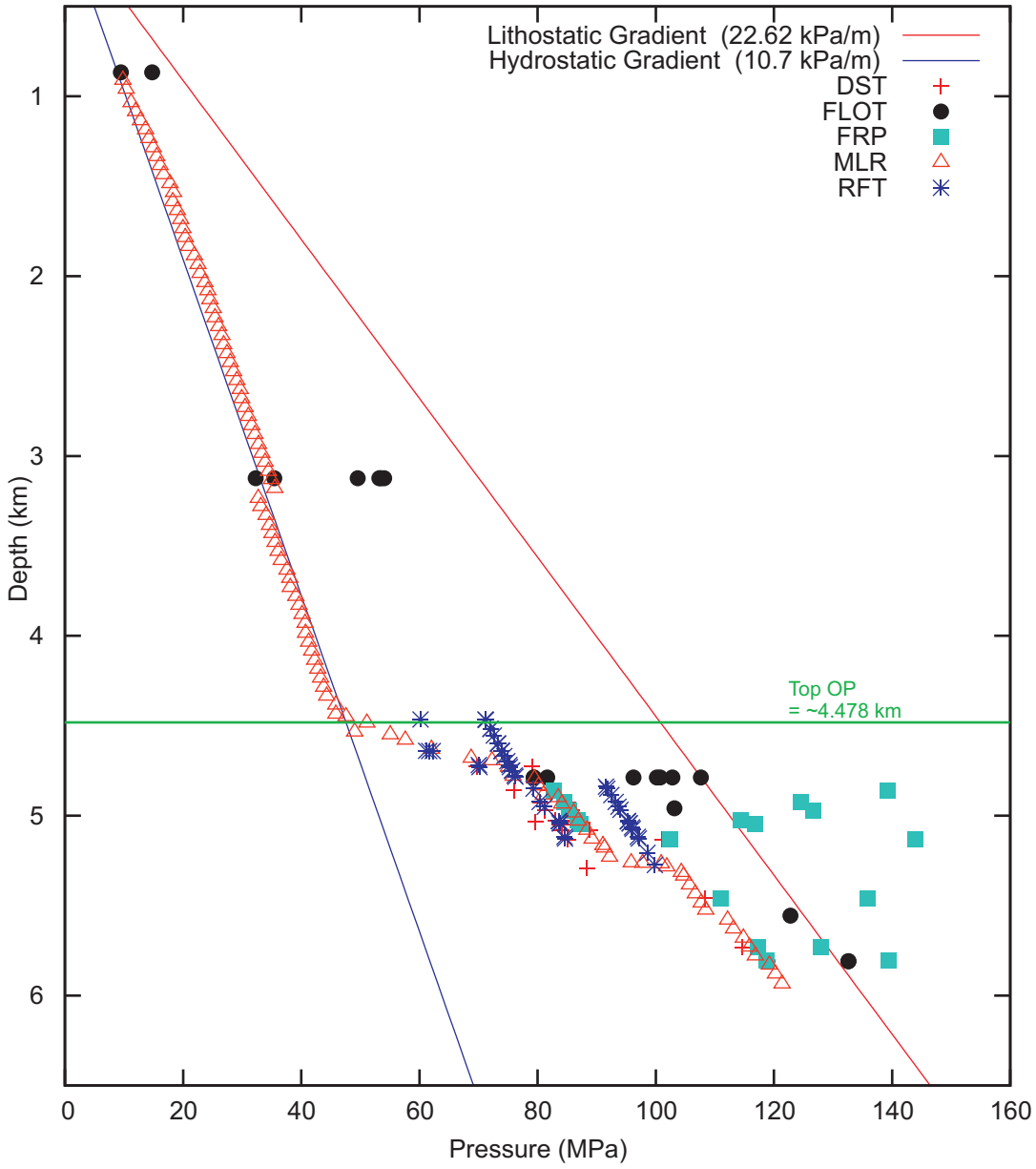

Figure 3.20.1 Depth vs. Pressure graph for Venture B-52 modified from NRCAN Basin Database.

Testing types of pressure:

BDP = Breakdown Pressure
DST = Drillstem test
DMR = Drilling Mud Record
FLOT = Formation Leak-Off Test
FRP = Feedrate Pressure
MDT = Modular Formation Dynamics Tester
MLR = Mudloggers Report
PIT = Pressure Integrity Test
RFT = Repeat Formation Tester
WK = Well Kick

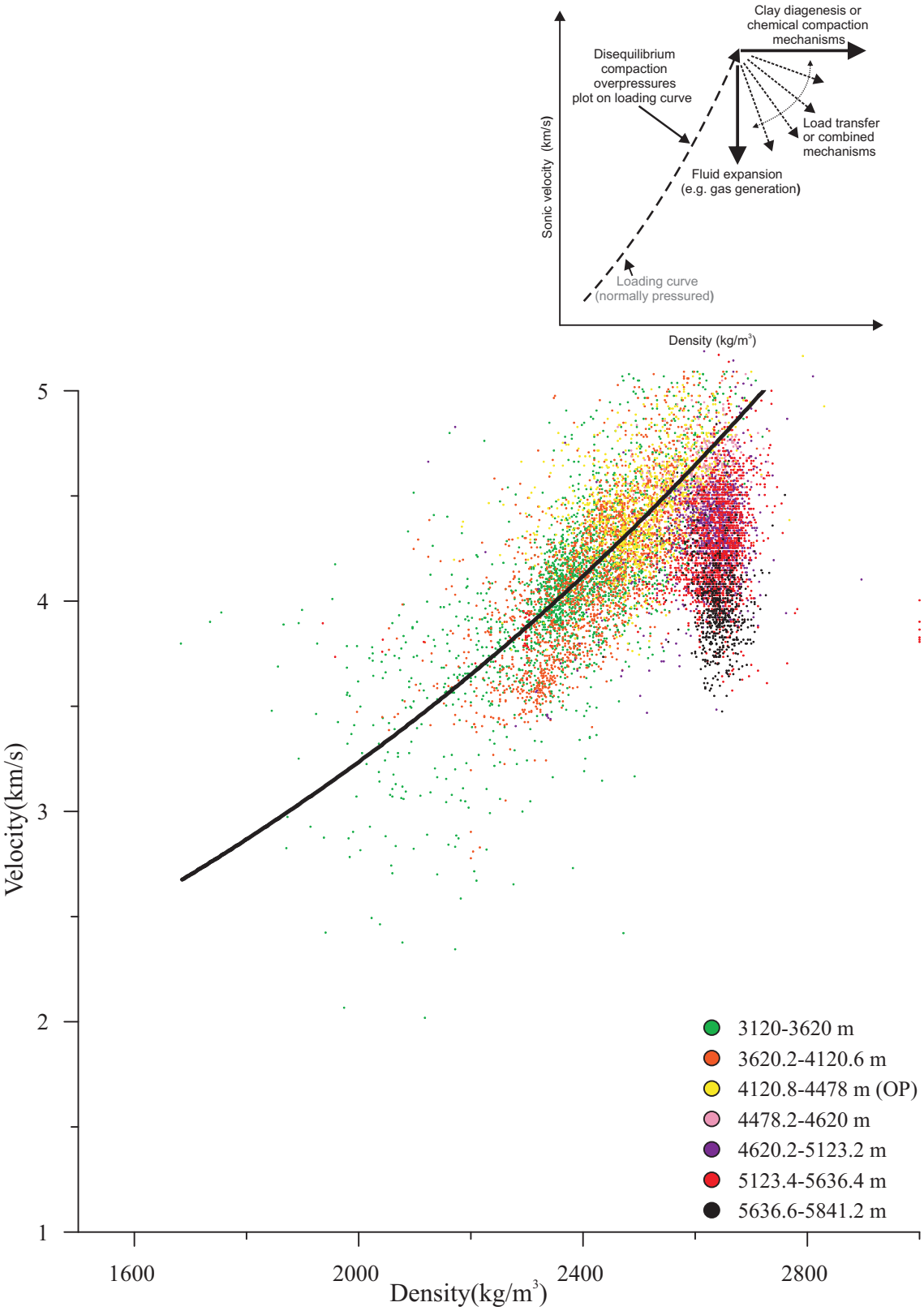

Figure 3.20.2 Graph #3 of a velocity vs. density plot for Venture B-52.

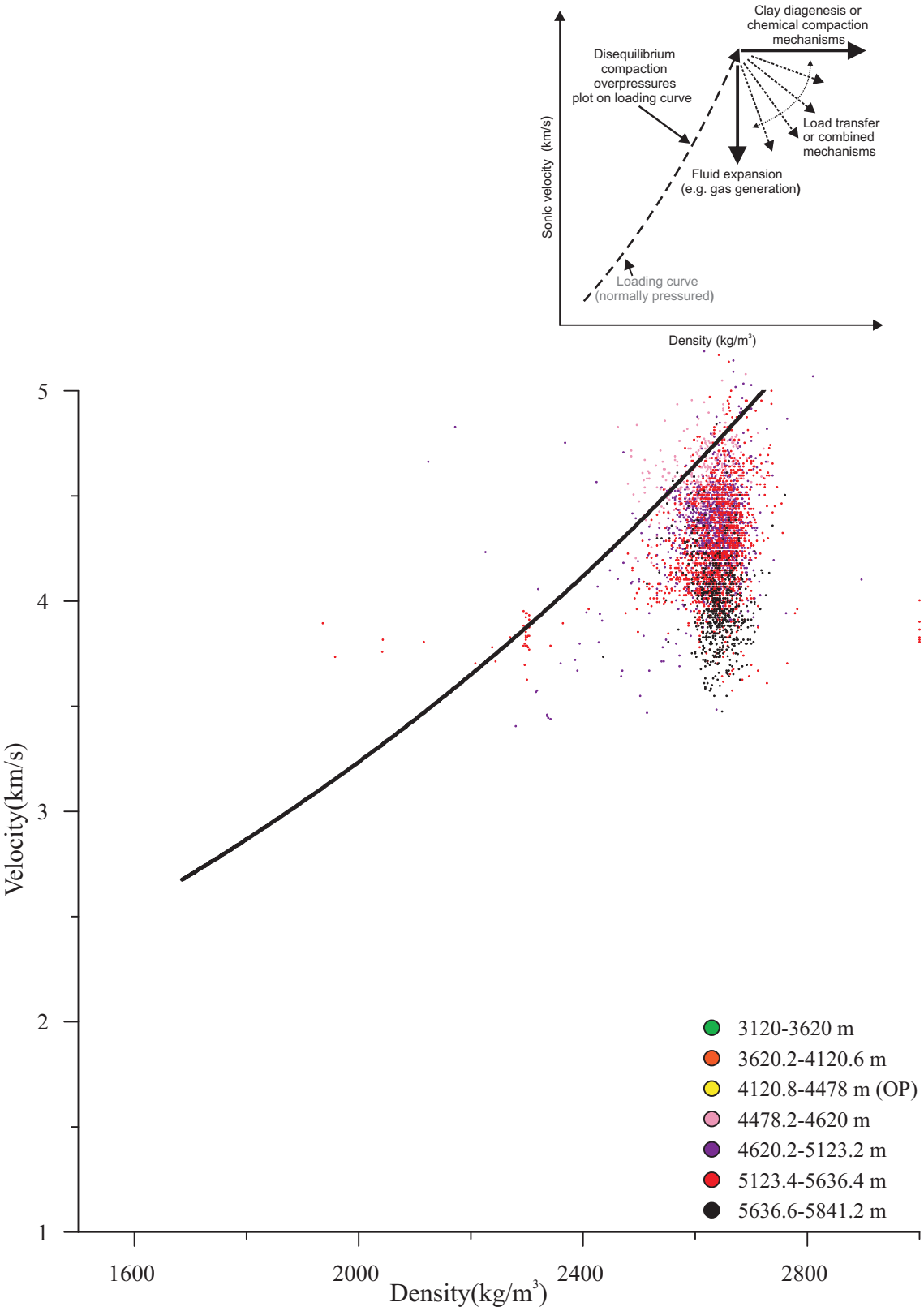

Figure 3.20.3 Graph #4 of a velocity vs. density plot for Venture B-52.

3.21 Venture H-22

Venture H-22 is located within the Venture field to the east of the Sable Sub-Basin. Overpressure starts at ~4480 m and continues to a TD of 5943.6 m. The top of overpressure occurs within a shale unit unlike the other two Venture wells. Again there is significant overpressure indicated by points almost reaching the lithostatic gradient (Fig. 3.21.1). The well discovered gas, condensates, and water.

Graph #3 (Fig. 3.21.2) shows a nice transition between points below the top of overpressure and has a similar shape to graphs from other Venture wells. Graph #4 (Fig. 3.21.3) has samples ~0.2-373 m below overpressure (pink points) reach the highest on the graph. They mostly sit below the trend line in a vertical shape. Samples ~391-891 m below overpressure (purple points) form a sparse cluster at the tip of the pink points. Samples ~891-1391 m below overpressure (red points) are in a vertical cluster at the tip of the purple points. Samples ~1391-1443 m below overpressure (black points) are few in number and are on top of the tip of the red points. There is a very nice trend going downwards from pink to black. There are not many black points but it is enough to see they represent the deepest depth. The graph shows a type 3 pattern (Fig. 3.1.1),

3.22 West Esperanto B-78

West Esperanto B-78 is located within the Abenaki Sub-Basin. Overpressure starts at ~4870 m and goes down to the bottom of the well at a TD of 5703 m. The top of overpressure occurs within a dominantly shale interval and is fairly significant with points

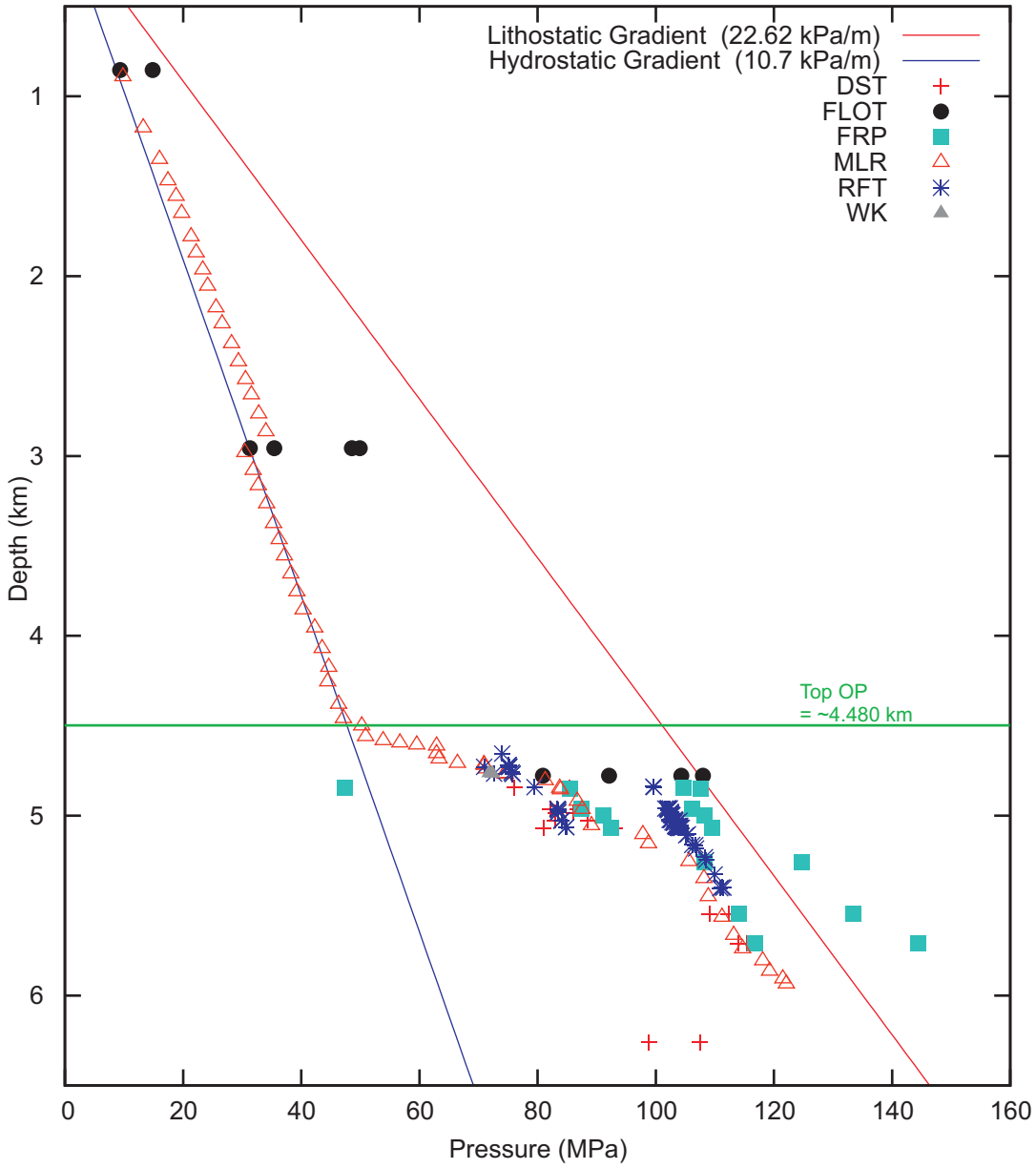

Figure 3.21.1 Depth vs. Pressure graph for Venture H-22 modified from NRCAN Basin Database.

Testing types of pressure:

BDP = Breakdown Pressure
DST = Drillstem test
DMR = Drilling Mud Record
FLOT = Formation Leak-Off Test
FRP = Feedrate Pressure
MDT = Modular Formation Dynamics Tester
MLR = Mudloggers Report
PIT = Pressure Integrity Test
RFT = Repeat Formation Tester
WK = Well Kick

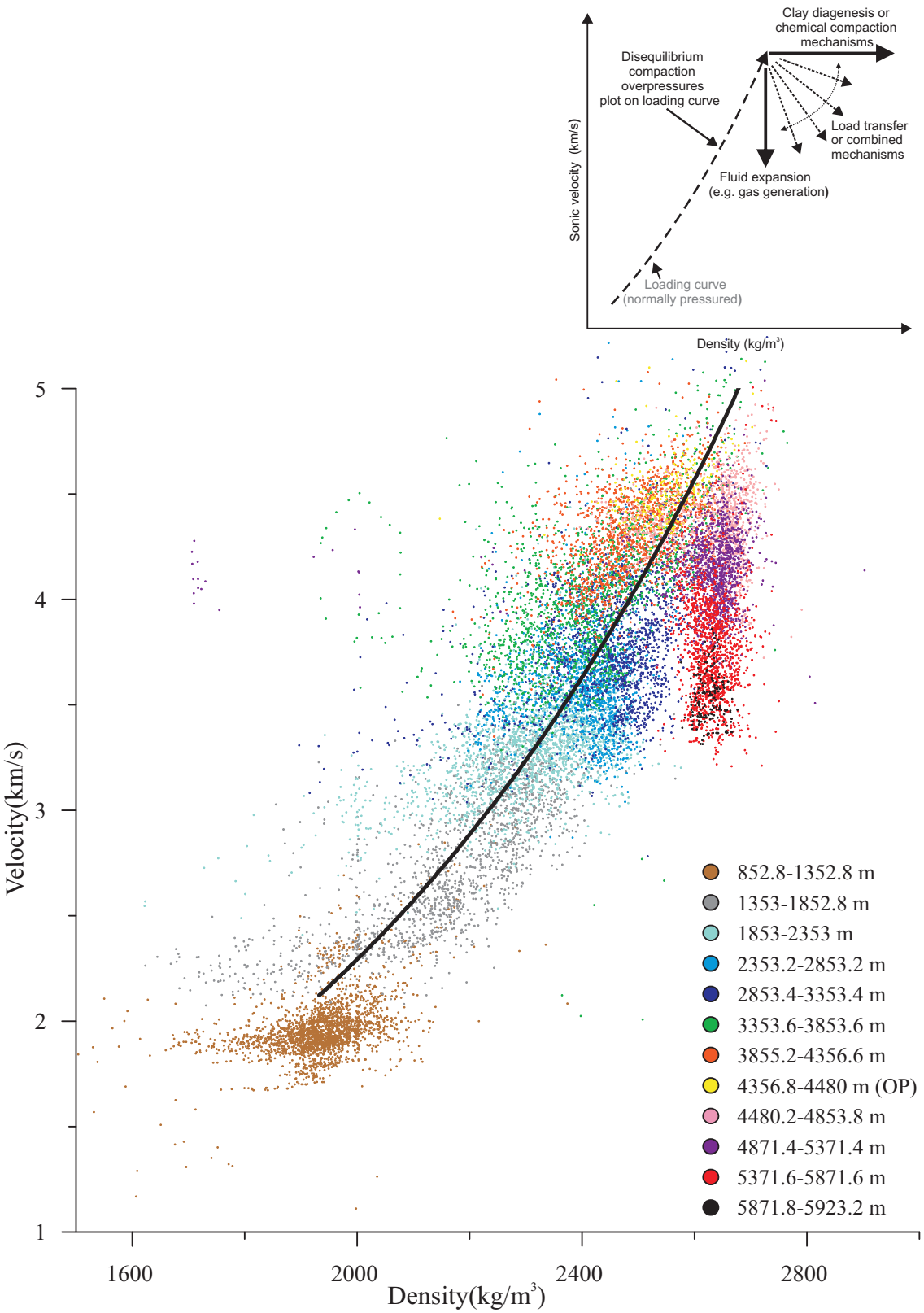

Figure 3.21.2 Graph #3 of a velocity vs. density plot for Venture H-22.

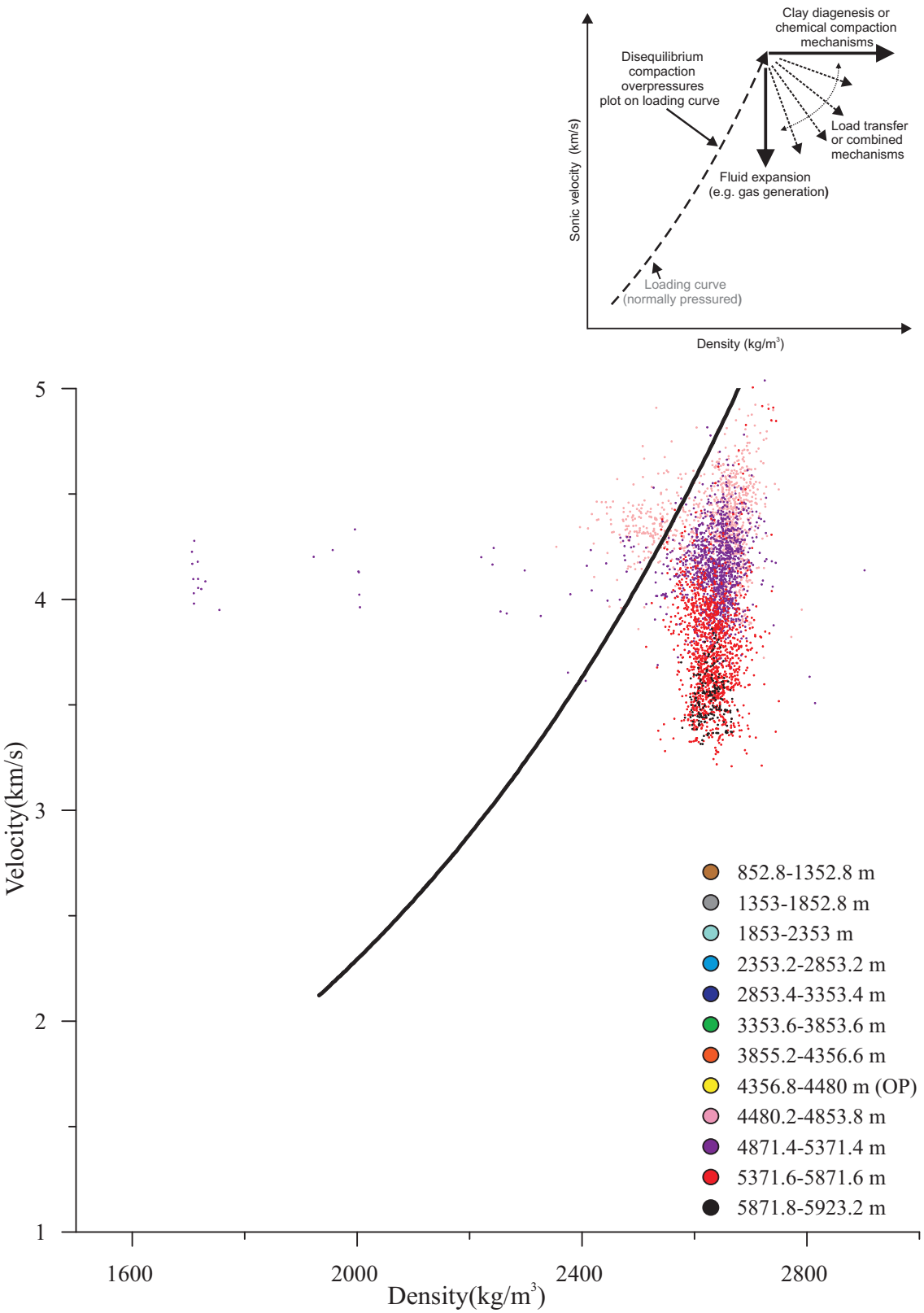

Figure 3.21.3 Graph #4 of a velocity vs. density plot for Venture H-22.

falling in at ~60 % between hydrostatic and lithostatic (Fig. 3.22.1). The well has been found to be dry.

Graph #3 (Fig. 3.22.2) follows a normal loading curve to the top of overpressure. Many points of low-intermediate depths are spread over an area encompassing velocities of 2-5 (km/s) and densities of 1550-2650 (kg/m^3).

Graph #4 (Fig. 3.22.3) shows red points spread out above and below the loading curve. Black points are found in two clusters, one below and one mostly above. This is the first time there has been two distinct clusters of black points. The first black cluster sits higher on the trend line at ~ 2700 km/m^3. The second black cluster is entirely below the trend line at ~ 2500 kg/m^3. The graph represents a type 8 pattern (Fig. 3.1.1).

3.23 West Venture C-62

West Venture C-62 is located within the Venture field to the east of the Sable Sub-Basin. Overpressure starts at ~4445 m and continues to the bottom of the hole at a TD of 5522 m. The top of overpressure occurs within a sandy-shaly section. The overpressure is significant, almost reaching the lithostatic gradient (Fig. 3.23.1). The well discovered gas, condensates, and water,

Graph #3 (Fig. 3.23.2) does not follow a normal loading curve as was previously seen in other graphs. Instead the colored clusters of points are stacked on top of each other. The thing to notice about this graph is that the orange points (shallow) are below the red and black points (deep) but all of the points are around approximately the same

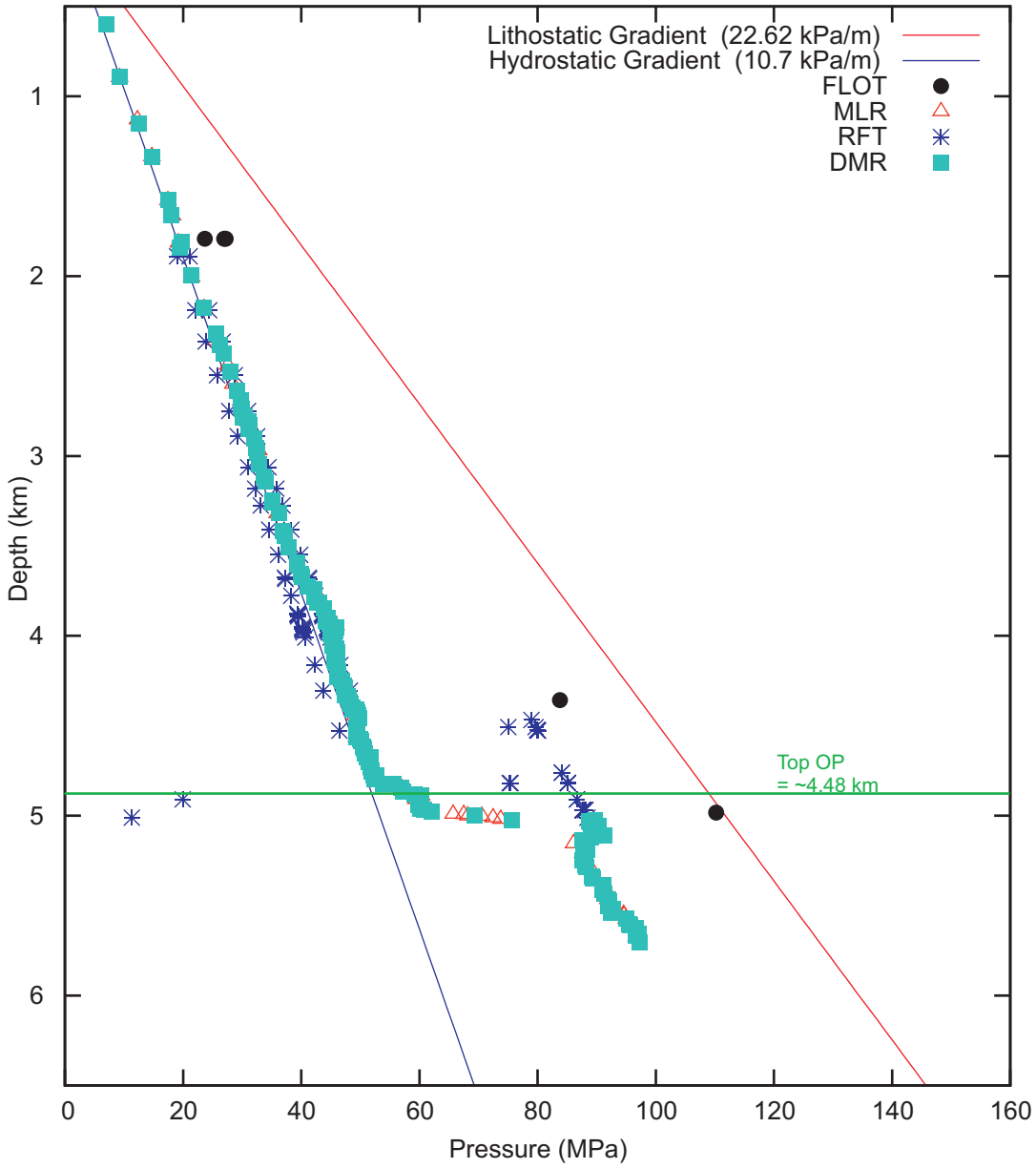

Figure 3.22.1 Depth vs. Pressure graph for West Esperanto B-78 modified from NRCAN Basin Database.

Testing types of pressure:

BDP = Breakdown Pressure
DST = Drillstem test
DMR = Drilling Mud Record
FLOT = Formation Leak-Off Test
FRP = Feedrate Pressure
MDT = Modular Formation Dynamics Tester
MLR = Mudloggers Report
PIT = Pressure Integrity Test
RFT = Repeat Formation Tester
WK = Well Kick

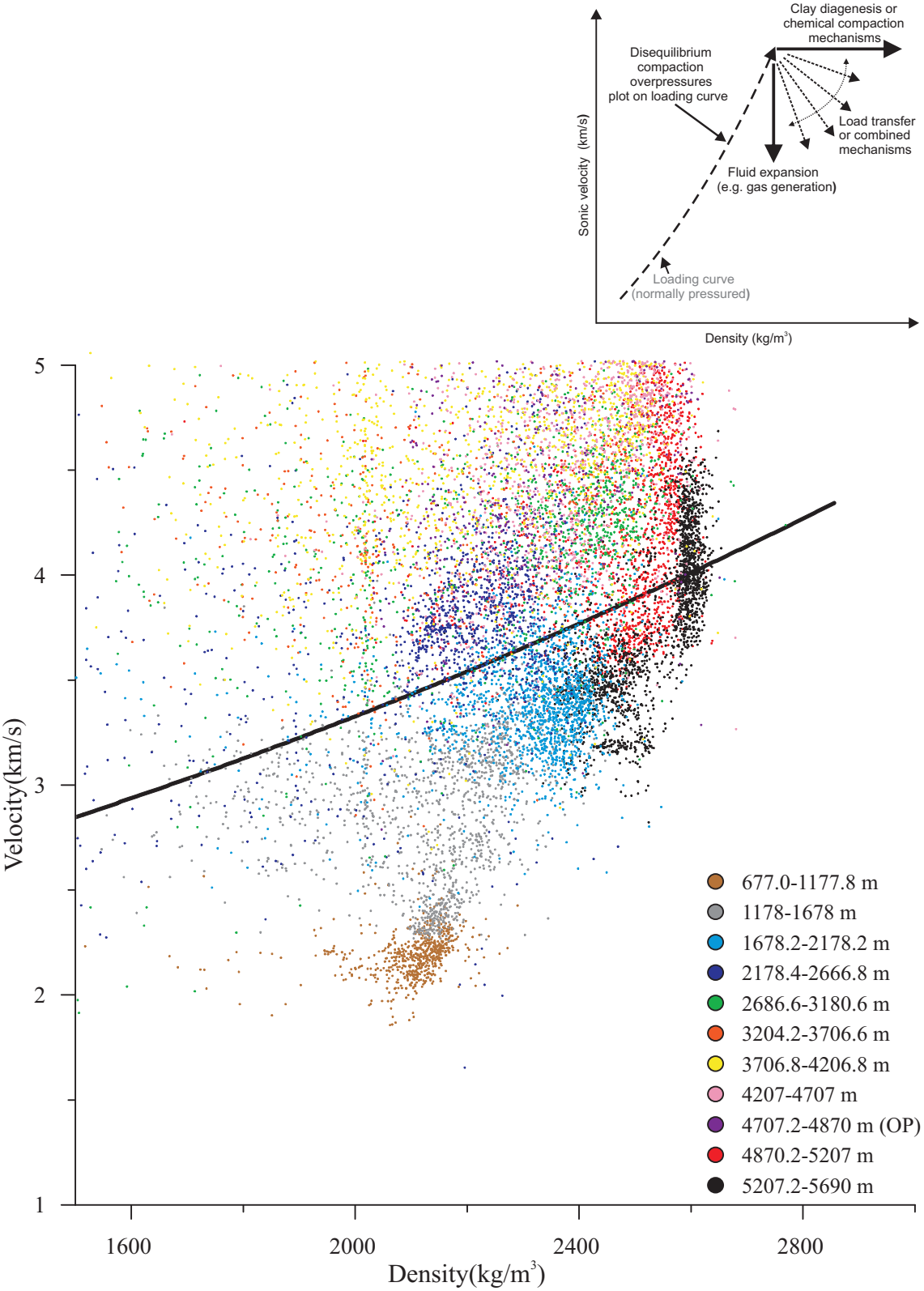

Figure 3.22.2 Graph #3 of a velocity vs. density plot for West Esperanto B-78.

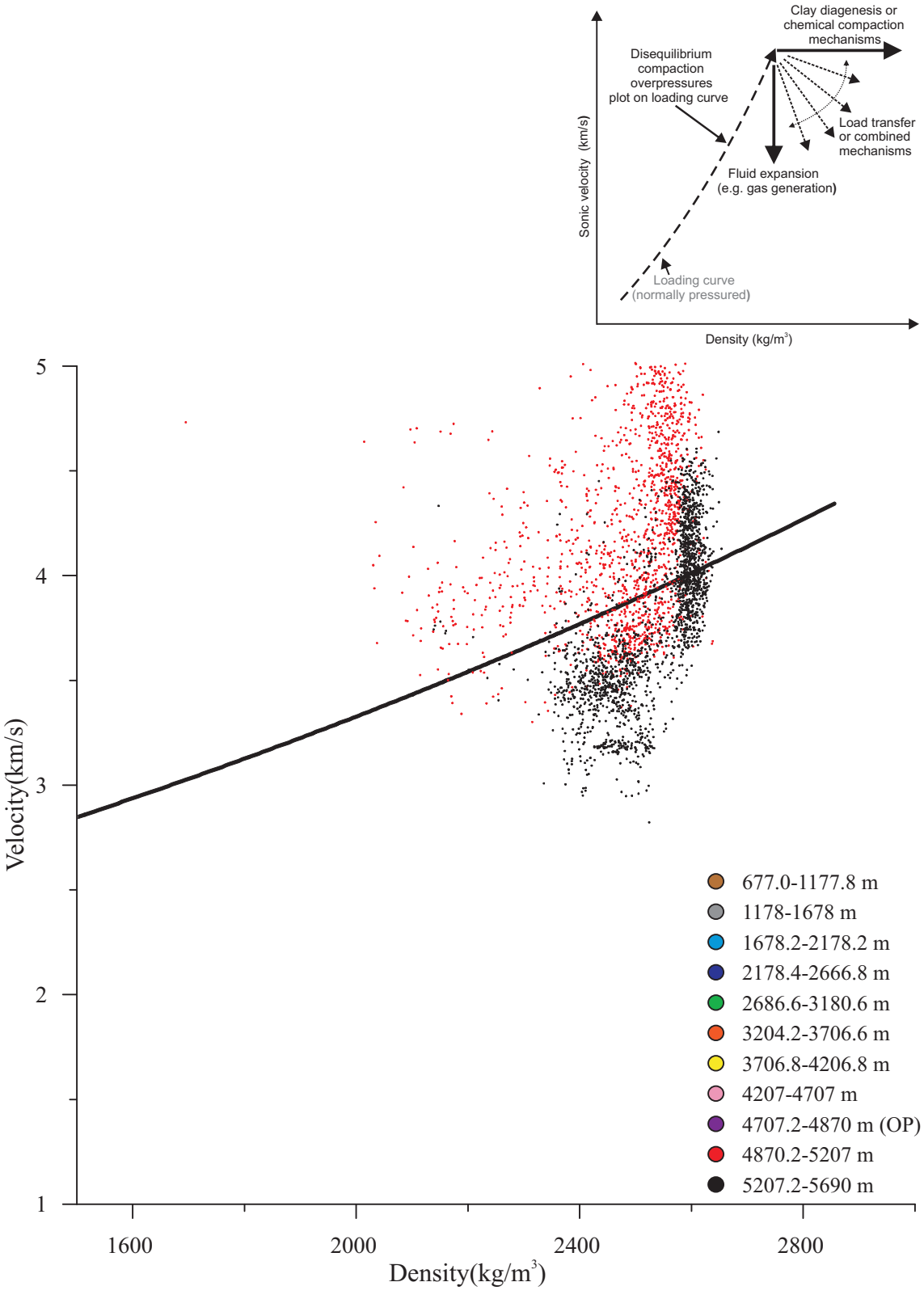

Figure 3.22.3 Graph #4 of a velocity vs. density plot for West Esperanto B-78.

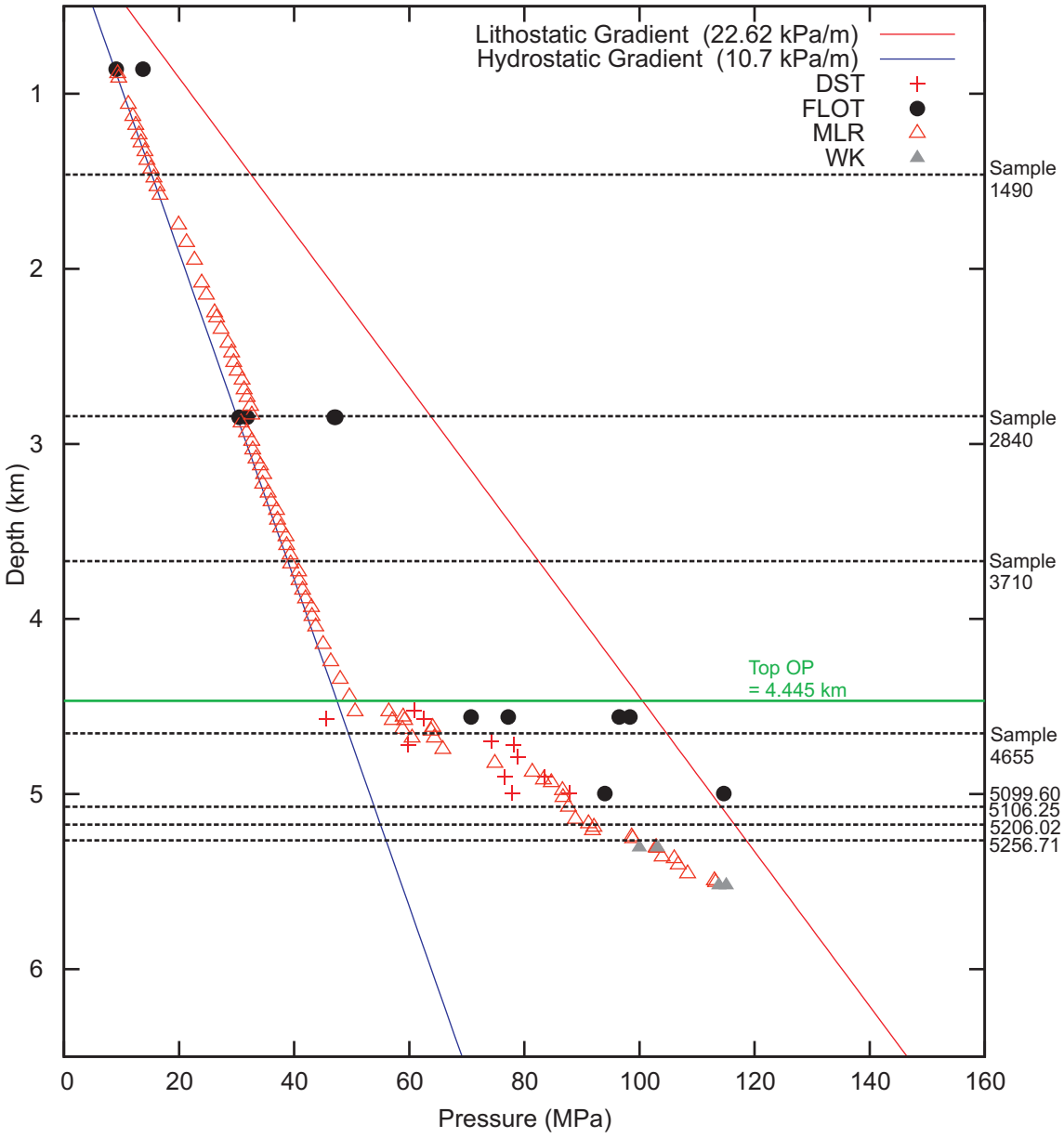

Figure 3.23.1 Depth vs. Pressure graph for West Venture C-62 modified from NRCAN Basin Database.

Testing types of pressure:

BDP = Breakdown Pressure
DST = Drillstem test
DMR = Drilling Mud Record
FLOT = Formation Leak-Off Test
FRP = Feedrate Pressure
MDT = Modular Formation Dynamics Tester
MLR = Mudloggers Report
PIT = Pressure Integrity Test
RFT = Repeat Formation Tester
WK = Well Kick

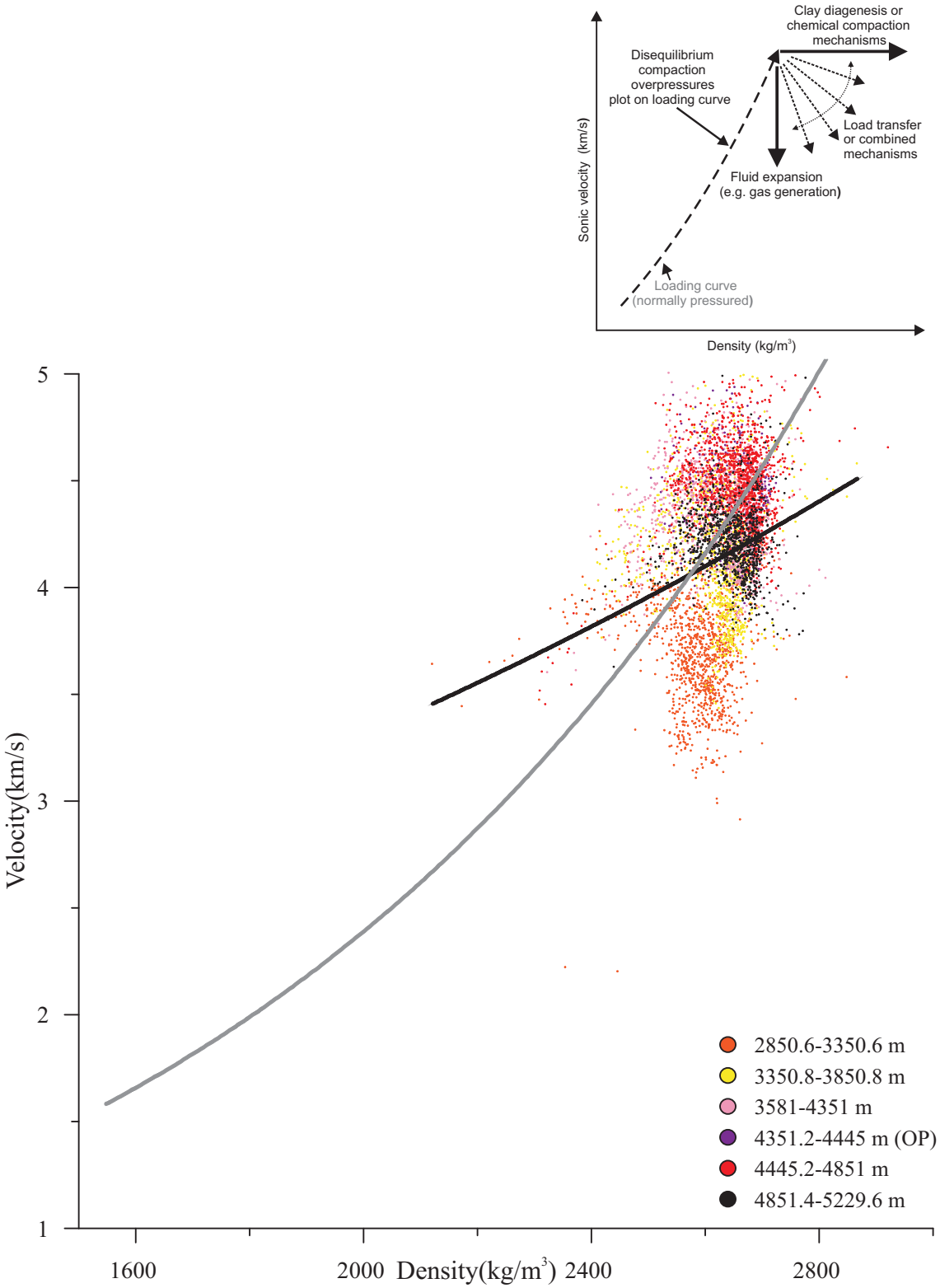

Figure 3.23.2 Graph #3 of a velocity vs. density plot for West Venture C-62. The grey trendline is from Sable Island C-67, located nearby and with complete shallow data.

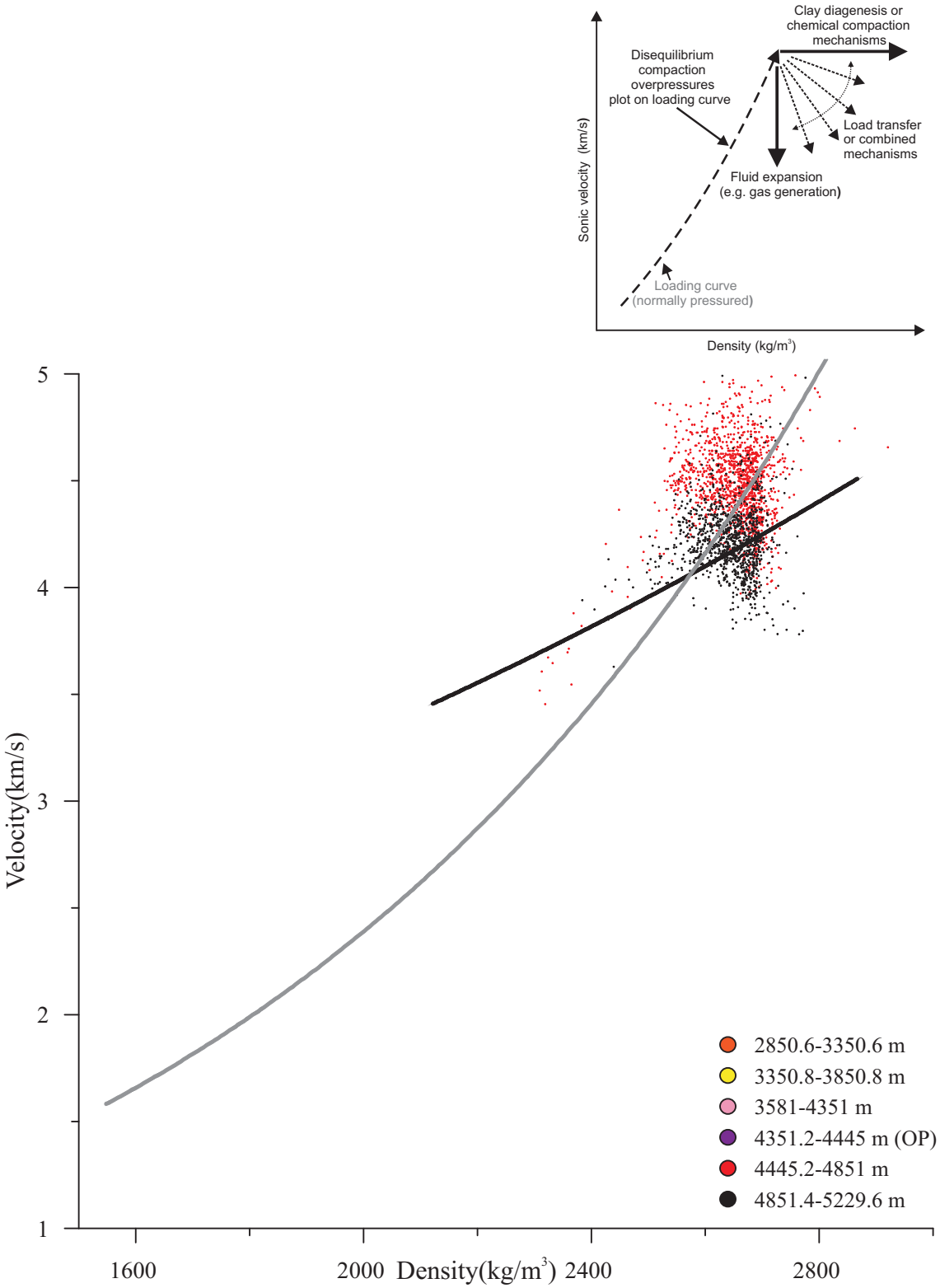

Figure 3.23.3 Graph #4 of a velocity vs. density plot for West Venture C-62. The grey trendline is from Sable Island C-67, located nearby and with complete shallow data.

density (~2600 kg/m^3). Usually there is a separation or disconnect between shallow points and deep points.

Graph #4 (Fig. 3.23.3) shows the majority of points above the top of overpressure sitting above the trend line. There is a clear transition from red points to black points in a vertical shape but they mask shallower green points underneath. The graph may represent a type 7 pattern.

3.24 West Venture N-91

West Venture N-91 is located within the Venture field in the eastern Sable Sub-Basin. The East Coast Basin Atlas (MacLean and Wade, 1993) states that top of overpressure starts at ~4423 m and continues to the bottom of the well at 5547 m. The depth vs. pressure graph from the BASIN database (Fig. 3.24.1) shows points approaching the lithostatic gradient, which indicates a significant overpressure. The top of overpressure occurs within a sandy-silty section. The well discovered gas.

Graph #3 (Fig. 3.24.2) shows shallow points (orange and yellow) arranged in horizontal lines corresponding to different velocity data. This results from changing our data to two decimal places. Pink points are placed primarily above the trend line and masked by deeper points. The most data is found within the interval corresponding to purple points. They are mostly clustered above the trend line but a fair number are found below. The purple points are oriented in a linear fashion that is similar to what has been previously seen throughout this chapter. There is less data within the red and black intervals. The important thing is that these points occur below the purple cluster, first red,

then black. The red and black points are at slightly less density than the purple cluster. All of the points leading up to and after overpressure seem to fit the trend line quite well, with the exception to the shallowest points.

Graph #4 (Fig. 3.24.3) shows a sparse cluster of red points that sits mainly below the trend line. The points are found above and below the trend line and if they are to be taken as a cluster, it is oriented almost perpendicular to the trend line. The red points are down and to the left of the purple and the black points are down and to the left of the red. This looks similar to Louisbourg J-47, in how once the top of overpressure is reached the velocity drops with little change in density. Therefore, this well exhibits a type 8 pattern.

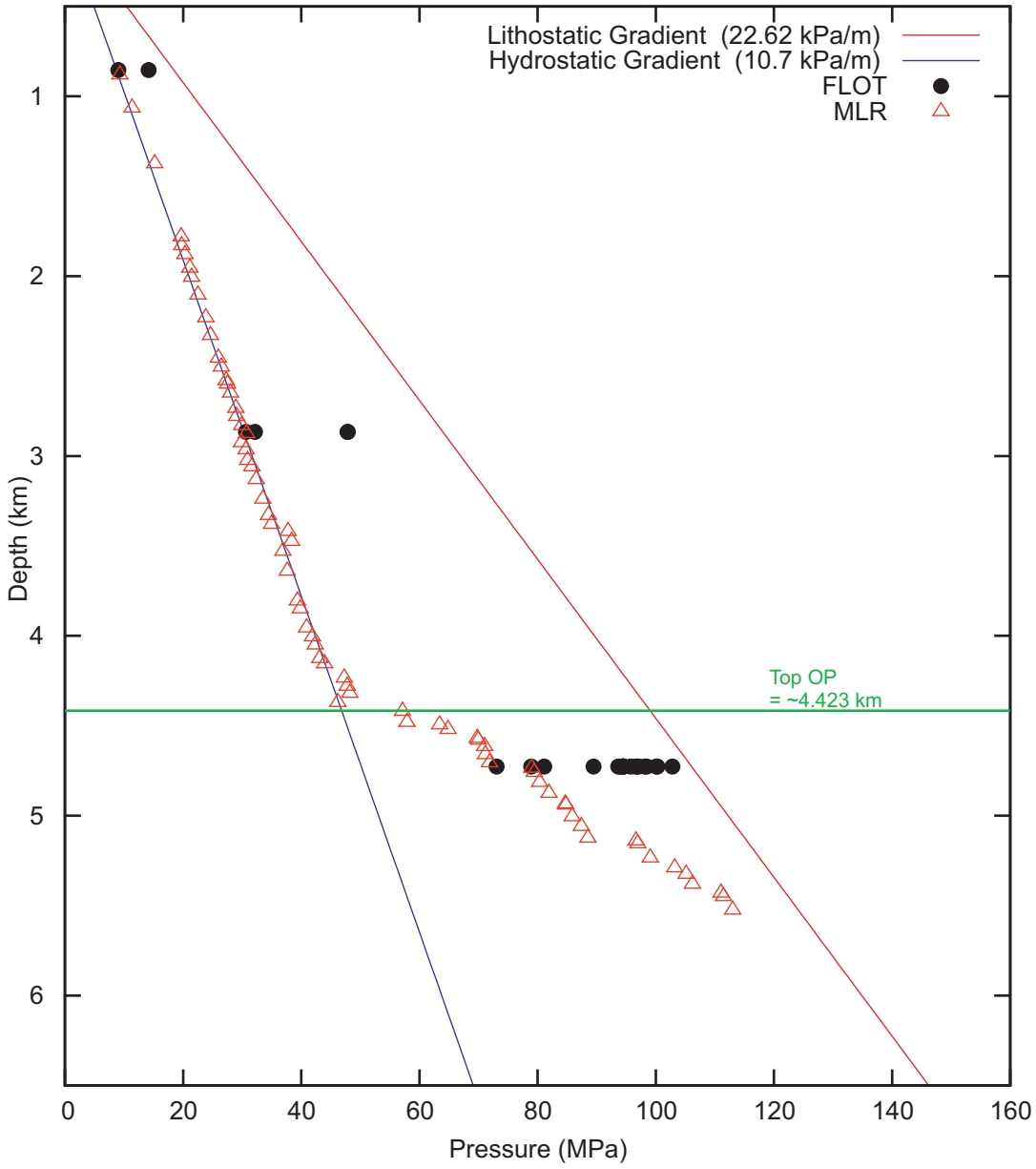

Figure 3.24.1 Depth vs. Pressure graph for West Venture N-91 modified from NRCAN Basin Database.

Testing types of pressure:

BDP = Breakdown Pressure
DST = Drillstem test
DMR = Drilling Mud Record
FLOT = Formation Leak-Off Test
FRP = Feedrate Pressure
MDT = Modular Formation Dynamics Tester
MLR = Mudloggers Report
PIT = Pressure Integrity Test
RFT = Repeat Formation Tester
WK = Well Kick

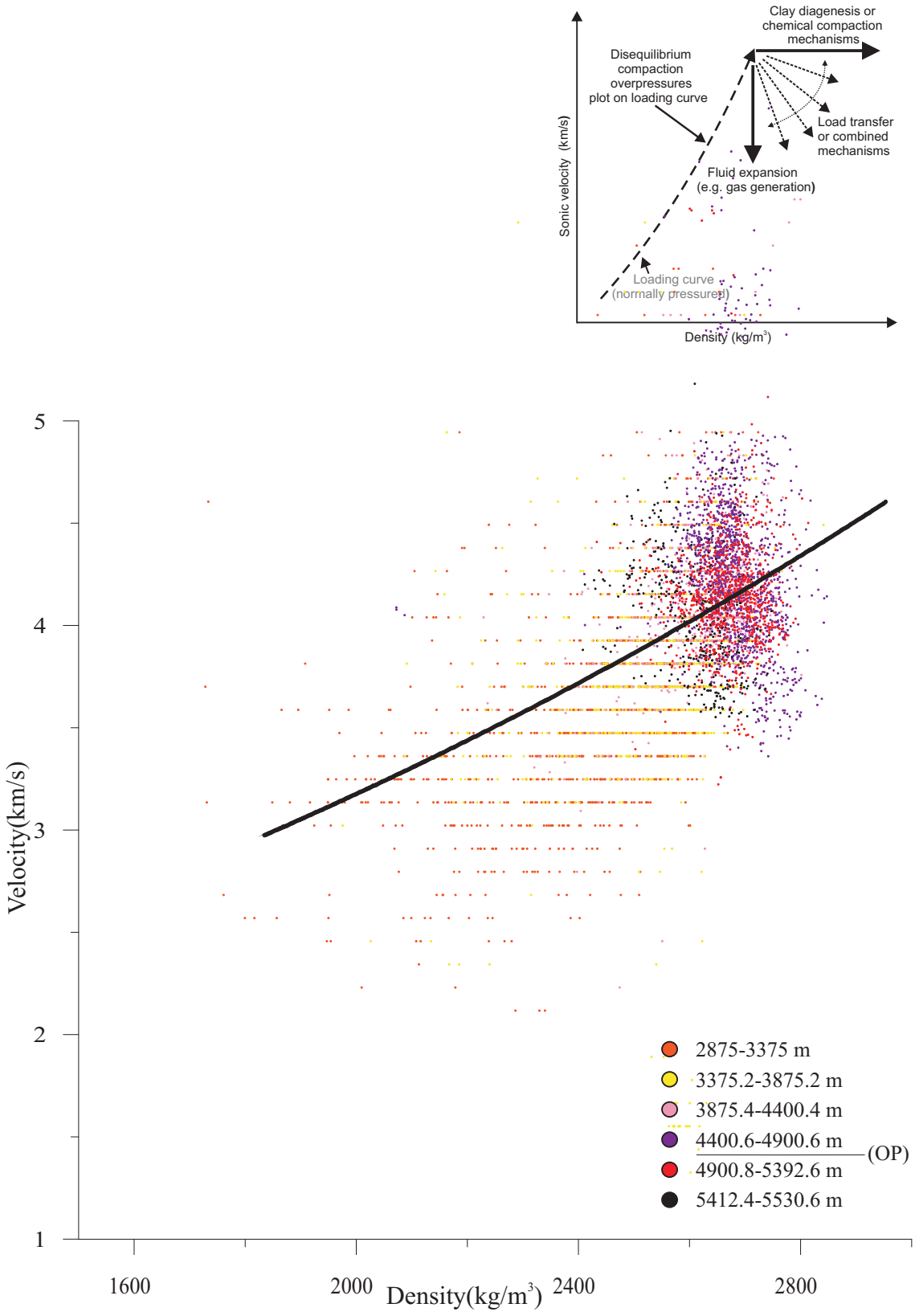

Figure 3.24.2 Graph #3 of a velocity vs. density plot for West Venture N-91.

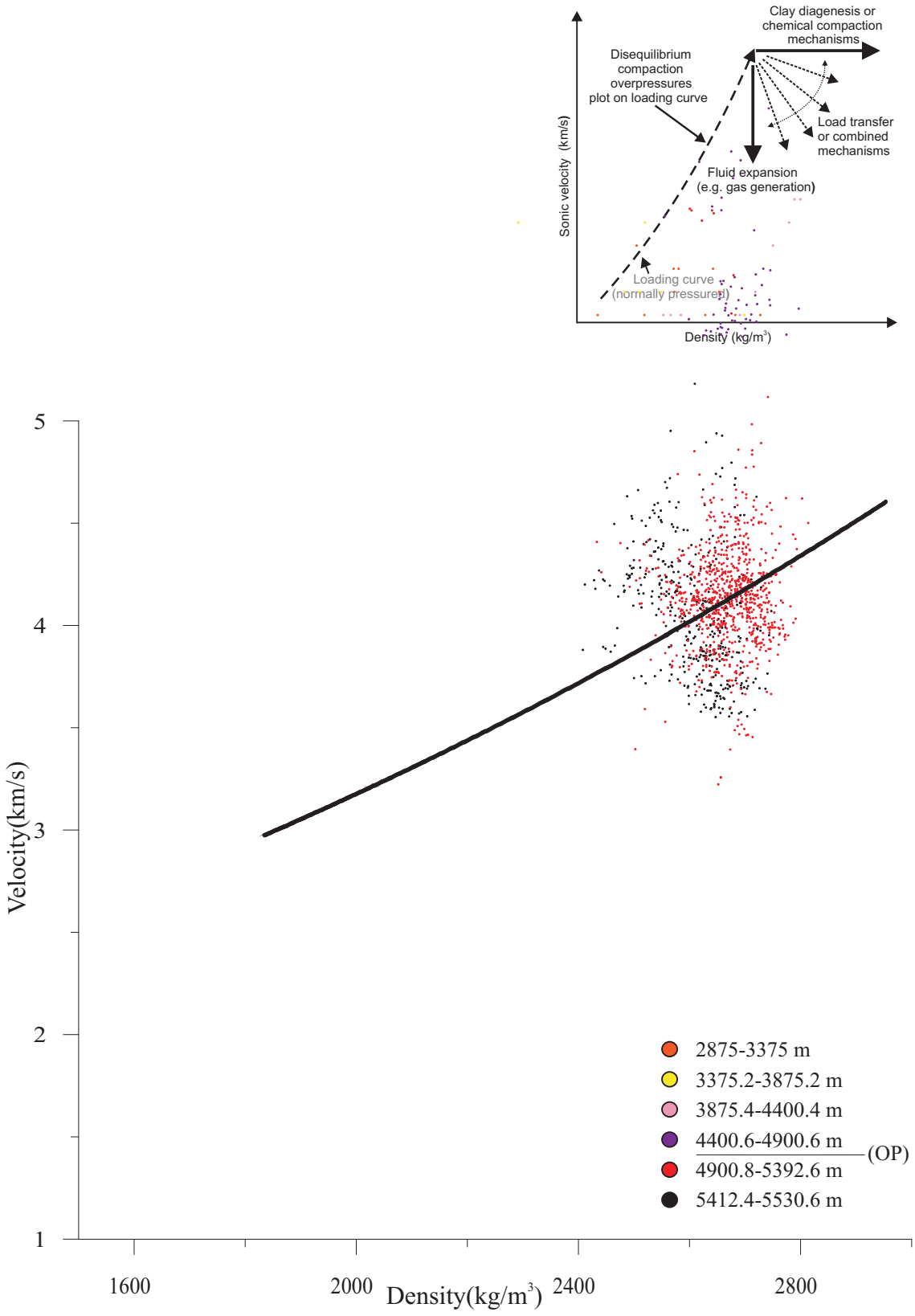

Figure 3.24.3 Graph #4 of a velocity vs. density plot for West Venture N-91.

Chapter 4.0 Diagenesis

4.1 Introduction

In this chapter, the focus will be on the second objective outlined in section 1.4, which deals with diagenesis and how it relates to overpressure. As was previously mentioned in chapter 1, diagenetic mineral reactions have been a proposed mechanism for producing overpressure. Because of this known association, it is important that more information can be garnered to help our understanding of overpressure. Such transformations are both temperature and pressure dependent; therefore knowledge of the thermal basin history will provide information into which transformations are likely to occur in particular areas.

Diagenetic mineral reactions can cause a number of processes, which include growth of minerals and cementation, thus affecting permeability and influencing overpressure (Osborne and Swarbrick 1997). Release of water from dehydration of smectite, transformation of smectite to illite, and transformation of gypsum to anhydrite all produces a volume expansion that may be responsible for overpressure. Smectite is a common mineral in shales and contains interlayered water within its crystal structure (Osborne and Swarbrick 1997). The well known diagenetic reaction of smectite to illite has been referenced in many papers (Mudford 1988, Wade and Maclean 1990, Osborne and Swarbrick 1997, O'Connor et al. 2011, Tingay et al. 2013) and was one of the more popular ideas relating overpressure and diagenesis. It was generally thought that the dehydration of smectite as well as the transformation of smectite into illite could release enough water to produce overpressure, in a sealed area. Osborne and Swarbrick (1997) have found that the volume expansion in the above reactions is not enough to produce significant overpressure. However, they have acknowledged that the release of water and

the collapse of the smectite framework may cause changes in the rheology of the rock. Thus, diagenetic mineral reactions may cause disequilibrium compaction.

The reaction of gypsum to anhydrite will not be looked at in this thesis because it occurs at relatively shallow depths and is not associated with deep overpressures. The majority of wells in this thesis have overpressure starting below 3 km. Another reason why the conversion of gypsum to anhydrite will not be focused on is that this reaction unlikely occurred in the area of study. Therefore, it is doubtful that overpressure is being produced in this way.

The effect of diagenesis in this study, as already discussed in section 2.8 will be examined using X-ray diffraction on clay material < 2 microns. This method thus will allow us to observe which clay minerals are occurring in the shale samples taken at varying depths.

4.2 X-Ray Diffraction Analysis of < 2 micron fraction

Samples were taken from six wells and their < 2 micron clay fraction was studied by XRD analysis. The wells are: Louisbourg J-47, Evangeline H-98, Glenelg E-58, Venture H-22, West Venture C-62, and South Griffin J-13. Twenty-six samples were selected in total for XRD analysis from the six wells, eight of which were from core and eighteen were from cuttings. The samples were selected over a range of depths because we wanted to observe any differences below and above the overpressured interval. Previous clay mineral analysis has been done in overpressured wells within the Scotian basin (Strathdee, 2012, Aneja, 2013), but less focus was placed on overpressure. Aneja (2013) looked at wells in the southwest Scotian Basin including Mohican I-100 and also incorporated samples from Strathdee (2012) into his report. Strathdee (2012) studied

some of the same wells in this thesis using XRD, which include South Desbarres O-76, Thebaud C-74, I-93, Chebucto K-90, North Banquereau I-13, and Peskowesk A-99. His samples were heated to varying temperatures and this will help observe diagenetic changes with temperature. Their XRD results will be compared to our own. Hopefully, comparisons and characteristics can be observed between the three studies that will lead to a better understanding between the overpressure and diagenesis.

Well	Depth(m)	Formation
Alma K-85[2]	2449.4	Logan Canyon (Cree Mb)
Alma K-85[2]	2904.15	Missisuaga Upper Mb
Alma K-85[2]	3039.88	Missisuaga Upper Mb
Alma K-85[2]	3104.1	Verrill Canyon Fm
Chebucto K-90[2]	2220	Logan Canyon (Marmora Mb)
Chebucto K-90[2]	4585	Missisuaga Fm
Chebucto K-90[2]	5120	Missisuaga Fm
Cohasset A-52[1]	2418.75	Naskapi Mb
Evangeline H-98[3]	1490	Banquereau Fm
Evangeline H-98[3]	2565	Dawson Canyon Fm
Evangeline H-98[3]	3090	Shortland Shale
Evangeline H-98[3]	4750	Shortland Shale
Evangeline H-98[3]	5000	Shortland Shale
Glenelg E-58[3]	2390	Logan Canyon (Cree Mb)
Hercules G-15[2]	646.18	Logan Canyon (Cree Mb)
Louisbourg J-47[3]	1875	Logan Canyon (Sable Mb)
Louisbourg J-47[3]	2425	Logan Canyon (Cree Mb)
Louisbourg J-47[3]	4076.03	Missisauga Middle Mb
Louisbourg J-47[3]	4085.4	Missisauga Middle Mb
Louisbourg J-47[3]	5437.61	Mic Mac Fm
Louisbourg J-47[3]	5710	Mic Mac Fm
MicMac H-86[1]	4717.78	Mohican Fm
Moheida P-15[1]	3747.21	Iroquois Fm
Mohican I-100[1]	2539.05	Artimon/Roseway
Mohican I-100[1]	2840.49	Abenaki (Misaine Mb)
Mohican I-100[1]	3960.6	Iroquois Fm
Mohican I-100[1]	3696.55	Mohican Fm
Mohican I-100[1]	3697.95	Mohican Fm
Mohican I-100[1]	4332.43	Eurydice Fm

Naskapi N-30[2]	1469	Missisauga Upper Mb
North Banquereau I-13[1,2]	3248.8	Logan Canyon (Naskapi Mb)
Panuke B-90[1]	2235.37	Naskapi Mb
Panuke B-90[1]	2241.57	Naskapi Mb
Panuke B-90[1]	2245.78	Naskapi Mb
Panuke B-90[1]	2247.21	Naskapi Mb
Panuke B-90[1]	2255.49	Naskapi Mb
Panuke B-90[1]	2256.56	Naskapi Mb
Panuke B-90[1]	2278.21	Naskapi Mb
Peskowesk A-99[2]	2209.25	Logan Canyon (Cree Mb)
Peskowesk A-99[2]	2479.35	Missisauga Upper Mb
Peskowesk A-99[2]	2927.36	Missisauga Middle Mb
Peskowesk A-99[2]	3812.64	Mic Mac Fm
Sable Island C-67[1,2]	2830.45	Naskapi Mb
Sable Island C-67[1,2]	2835.42	Naskapi Mb
Sable Island C-67[1,2]	3373.45	Missisauga Middle Mb
South Desbarres O-76[2]	3815.1	Missisauga Lower Mb
South Desbarres O-76[2]	5956.8	Mic Mac Fm
South Griffin J-13[3]	3485	Missisauga Fm
South Griffin J-13[3]	4450	Missisauga Fm
South Griffin J-13[3]	5010	Mic Mac Fm
South Griffin J-13[3]	5670	Mic Mac Fm
Thebaud C-74[2]	1825	Logan Canyon (Sable Mb)
Thebaud C-74[2]	2560	Logan Canyon (Naskapi Mb)
Thebaud C-74[2]	3780	Missisauga Lower Mb
Thebaud C-74[2]	4335	Missisauga Lower Mb
Thebaud I-93[2]	3080.38	Missisauga Middle Mb
Venture H-22[3]	4987.4	Missisauga Lower Mb
West Venture C-62[3]	1490	Wyandot Fm
West Venture C-62[3]	2840	Logan Canyon (Cree Mb)
West Venture C-62[3]	3710	Missisauga Middle Mb
West Venture C-62[3]	4655	Missisauga Lower Mb
West Venture C-62[3]	5099.6	Missisauga Lower Mb
West Venture C-62[3]	5106.25	Missisauga Lower Mb
West Venture C-62[3]	5206.02	Missisauga Lower Mb
West Venture C-62[3]	5256.71	Missisauga Lower Mb
Wyandot E-53[1]	2877.03	Mohican Fm

Table 2. Selected < 2 μm samples with corresponding depth and formation. Numbers indicate samples from three sources, 1 = Aneja (2013), 2 = Strathdee (2012), and 3 = this thesis.

4.3 Clay Mineral Identification

X-ray diffraction measures the intensity of diffraction from the principal crystallographic planes and displays the variation of intensity against the spacing of crystallographic planes (Carroll, 1970). The distance between atomic planes in a mineral is called d-spacing and is measured in angstroms (Å). Each mineral has a specific set of d-spacings that produce a diffraction peak. The d-spacings are related to crystal structure by their Miller indices. Oriented clay mounts as used in this study enhance diffractograms from the 00ℓ planes in platy clay minerals. For example, the 001 planes in illite have a d-spacing of 10 Å, the 002 planes 5 Å and the 003 planes 3.33 Å. Mixed-layer clays have complex diffraction patterns at high d-spacings and may partly mask the simpler clays. Also, some peaks of different minerals are so close together that it becomes harder to separate individual minerals. For example, the Kaolinite 002 and Chlorite 004 peaks at 3.57 and 3.54 Å are almost indistinguishable when they occur as one peak, but it is possible to identify them by running the XRD slower, which will produce a clearer separation.

Minerals Present

Quartz:

Quartz is present in all of the samples and its peak positions occur at 4.26 Å by itself and at 3.35 Å with Illite 003.

Zincite:

Zincite was used as a standard. It has d-spacings at 2.48 Å as well as 2.6 Å, and 2.8 Å.

Smectite:

Smectite is recognized by a broad peak around 14-16 Å in air-dried samples, which shifts to 17 Å on glycolation. It is found in varying amounts in the shallowest samples in all the wells studies in detail in this thesis, and was also found in varying amounts by Strathdee (2012) in Alma K-85, Hercules G-15, Peskowesk A-99, South Desbarres O-76, Thebaud C-74, and Thebaud I-93. The smectite peaks in Evangeline H-98 are much larger then Louisbourg and West Venture but altogether are generally broad, which may indicate they are less crystallized. The d-spacing occurs between 16-18 Å. Strathdee (2012) found that samples with smectite had a significant loss of peak height from 110°C to 300°C. The peak height in general decreases in height with depth in all wells except Peskowesk A-99 and Alma K-85 (Strathdee, 2012).

Mixed layer smectites:

Illite-smectite (I-S) and illite-chlorite (I-C) mixed layer clay. Many diffractograms show a small discrete peak at 11 Å on a broader shoulder from 12-10 Å, and also a corresponding 002 peak at 5.5 Å. This shoulder, and the 11 Å peak, are reduced in height but still present in glycolated samples. The overall reduction in height suggests that much of this shoulder consists of illite-smectite (I-S) mixed layer clay. The small 11 Å peak is unchanged by heating or glycolation (Strathdee, 2012) and is probably an illite-chlorite (I-C) mixed layer clay that overlaps with the illite-smectite mixed layer clay. The illite-

chlorite 001 and 002 peaks are highly variable in height and show no systematic change with depth in the well. South Griffin J-13 samples have the most prominent peaks.

Chlorite:

Chlorite has characteristic diffractions at d-spacings of 14, 7, 4.7, and 3.54 Å, and thus overlaps with the Kaolinite 001 peak at 7.1 Å and 002 peak at 3.54 Å. Fe-rich chlorites have relatively stronger 002 and 004 diffractions, whereas Mg-rich chlorites have relatively stronger 001 and 003 diffractions. Generally the Chlorite 001 peak decreases with increasing depth. In contrast, Strathdee (2012) suggested that there was not an observable connection between depth and Chlorite peak height in his samples.

Illite:

The diffractograms show three different illite peaks. Illite 001 is found at 10.1 Å and appears to start out as a stand alone peak but with increasing depth forms a composite illite and illite-smectite peak. The illite 002 peak is present at 5 Å. The Illite 002 and chlorite 003 peaks are broader and overlap in shallower samples but separate into two distinctly observable peaks with increasing depth. There is also an Illite 003 + quartz peak at 3.35 Å. Since it remains a single peak as depth increases, it is very difficult to distinguish if it is illite 003 or quartz.

Kaolinite:

A Kaolinite 001 + Chlorite 002 peak is found at 7.1 Å, which is present in all of the samples. The Kaolinite 001 + Chlorite 002 peak does not show a systematic change with increasing depth. In some wells, smaller peaks are observed at deeper depths, while the

opposite also occurs. The Kaolinite 002 + chlorite 004 peaks are broad and overlap at 3.35 Å in shallower samples but separate into two distinctly observable peaks with increasing depth.

Unknown:

There are several unknown peaks that occur in both glycolated and unglycolated samples. Their positions are present at 7.9 Å, 3.9-4.0 Å, 3.7 Å, and 3.1 Å.

4.4 Relationship between depth and clay mineral changes

To understand how smectite and smectite mixed layer clays are changing with increasing depth and temperature, diffractograms of the < 2 micron fraction were studied using a method by Sachsenhofer et al. (1998) (Fig. 4.3.1). This involved combining diffractograms corresponding to each well and stacking them from shallowest to deepest depth. The end result of this stacking helps to explain and visualize the smectite to illite transformation.

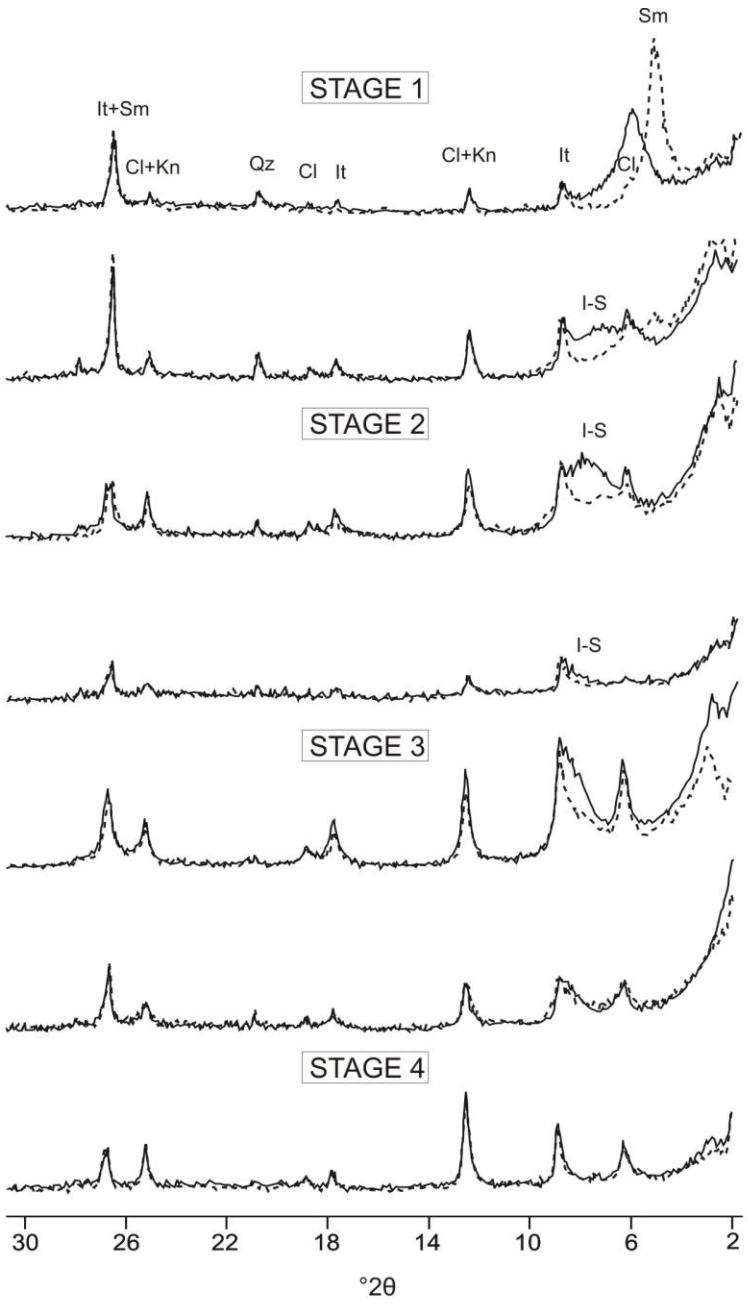

Figure 4.3.1 Diffractograms of air-dried (solid line) and glycolated (dotted line) < 2 μm samples. Cl = chlorite, Sm = smectite, I-S = mixed-layer illite-smectite, Kn = Kaolinite, Qz = quartz. The gradual evolution of smectite to illite is sub-divided into four stages (Modified from Sachsenhofer et al. 1998).

Sachsenhofer et al. (1998) described four stages based on XRD patterns of smectite, illite-smectite, and illite. Stage 1 has a characteristically dominant smectite peak around 16-18 Å in glycolated samples. Stage 2 is characterized by the formation of a mixed layer I-S peak between 13 and 10.5 Å that partly collapses on glycolation. This mixed peak is clearly separated from the illite peak at 10 Å. In stage 3 the I-S peak merges with the illite peak at 10 Å but there is some collapse of the I-S shoulder with glycolation. Stage 4 is characterized by the disappearance of smectite and the I-S peak, leaving a dominant illite peak at 10 Å and little or no change with glycolation. Diffractograms of samples from Table 2 were stacked by increasing depth and by using Figure 4.3.1 and previous research from Aneja (2013) as a reference; the stages of smectite evolution were identified. Aneja (2013) used samples from Strathdee (2012) (Table 2) to produce figures of stacked diffractograms. These figures will be compared to our results because they include samples from wells for which velocity-density plots are presented in chapter 3 of this thesis.

Louisbourg J-47:

J-47 1875 and J-47 2765 correspond to stage 1 of the Sachsenhofer et al. (1998) diagram. A smectite peak is observable in these two samples at 16 Å, but it looks like it is forming an I-S peak that is separate from the illite peak at 10 Å. This may reflect the later phase of stage 1 as it passes into stage 2.

J-47 2425, J-47 4047.03, J-47 4085.40, and J-47 5437.61 all correspond to stage 3 of the Sachsenhofer et al. (1998) diagram. The I-S peak continues on its way to merge with the illite peak at 10 Å. Sample J-47 2425 is between J-47 1875 and J-47 2765 but resembles a

stage 3 (Fig. 4.3.3). This is curious because one would expect the stages to increase with increasing depth as in the case with samples from Aneja (2013).

Evangeline H-98

H-98 1490 and H-98 3090 both closely resemble stage 1 of the Sachsenhofer et al. (1998) diagram. There are distinct smectite peaks at 16 Å.

H-98 2565 corresponds to stage 2 of the Sachsenhofer et al. (1998) diagram. The I-S has formed and is distinct from the illite 001 peak.

H-98 4750 is similar to stage 3 of the Sachsenhofer et al. (1998) diagram. The I-S peak merged with the illite peak at 10 Å.

H-98 5000 matches up with stage 4 of the Sachsenhofer et al. (1998) diagram. The disappearance of smectite and I-S, accompanied with a dominant illite peak at 10 Å makes this stage significantly different from the others.

South Griffin J-13:

J-13 1575 is similar to stage 1 of the Sachsenhofer et al. (1998) diagram. There is a distinct smectite peak at 16 Å.

J-13 3485 resembles stage 2 of the Sachsenhofer et al. (1998) diagram. The formation of an I-S peak separate from the illite peak is characteristic.

J-13 4450, J-13 5010, and J-13 5670 are all stage 3 from the Sachsenhofer et al. (1998) diagram. The I-S peak merges with the illite peak at 10 Å.

West Venture C-62:

C-62 1490 fits the model of stage 1 from the Sachsenhofer et al. (1998) diagram. There is a distinct smectite peak at 16 Å that is separate from the illite peak at 10 Å.

C-62 2840, C62 3710, C-62 5099.60, C-62 5106.25, C-62 5206.25, and C-62 5256.71 all resemble stage 3 of the Sachsenhofer et al. (1998) diagram. There is no smectite peak and the I-S peak has almost completely merged with the illite 001 peak.

C-62 4655 mirrors stage 4 of the Sachsenhofer et al. (1998) diagram. It is characterized by the absence of smectite and I-S peaks and the presence of a stand alone illite peak at 10 Å.

The important difference between the samples from this thesis and those from Aneja (2013) are that the stages do not necessarily descend in the expected sequence from 1 to 4 with depth. The samples from Aneja (2013) clearly progress through stages 1 to 4 as the depth becomes greater. That is not the case for wells Evangeline H-98 (Fig. 4.3.2) or West Venture C-62 (Fig. 4.3.5). In both wells there is not a clear transition from one stage to another. Figure (4.3.2) for example has a stage 2 sandwiched in between two stage 1 samples. Also, at greater depths, the stages progress from 1 to 2 to 4, apparently skipping 3. In West Venture C-62, at a depth of 4655 m, stage 4 is reached, but further down the well a stage 3 sample is present. The occurrence of later stages sandwiched in between

earlier ones could have several origins: (1) there might be downhole contamination by smectite cuttings from deeper sections of wells. (2) Alternatively, hot fluids moving through permeable sandstone from greater depths may have locally increased temperature and caused diagenetic transformations. (3) There may have been climatically controlled variation in supply of smectite by rivers.

In South Griffin J-13 and West Venture C-62, the sample immediately above the top of overpressure shows a greater collapse of the ~11 Å illite-smectite mixed layer peak on glycolation than immediately overlying samples, or samples well within the overpressure zone. In Louisbourg J-47, a sample that shows a similar behavior is from 5437.61 m, almost 1 km below the top of overpressure. In South Griffin J-13, the high I-S sample is distant from thick sandstone beds, but there is no similar relationship in the other two wells. The reason for this behavior is unknown.

Thyne et al. (2001) concluded from their research, that dissolution of K-feldspar provided potassium, which ultimately produced late-stage illite in sandstone reservoirs by the illitization of preexisting kaolinite. There may be a role of sandstone in providing potassium to produce illite.

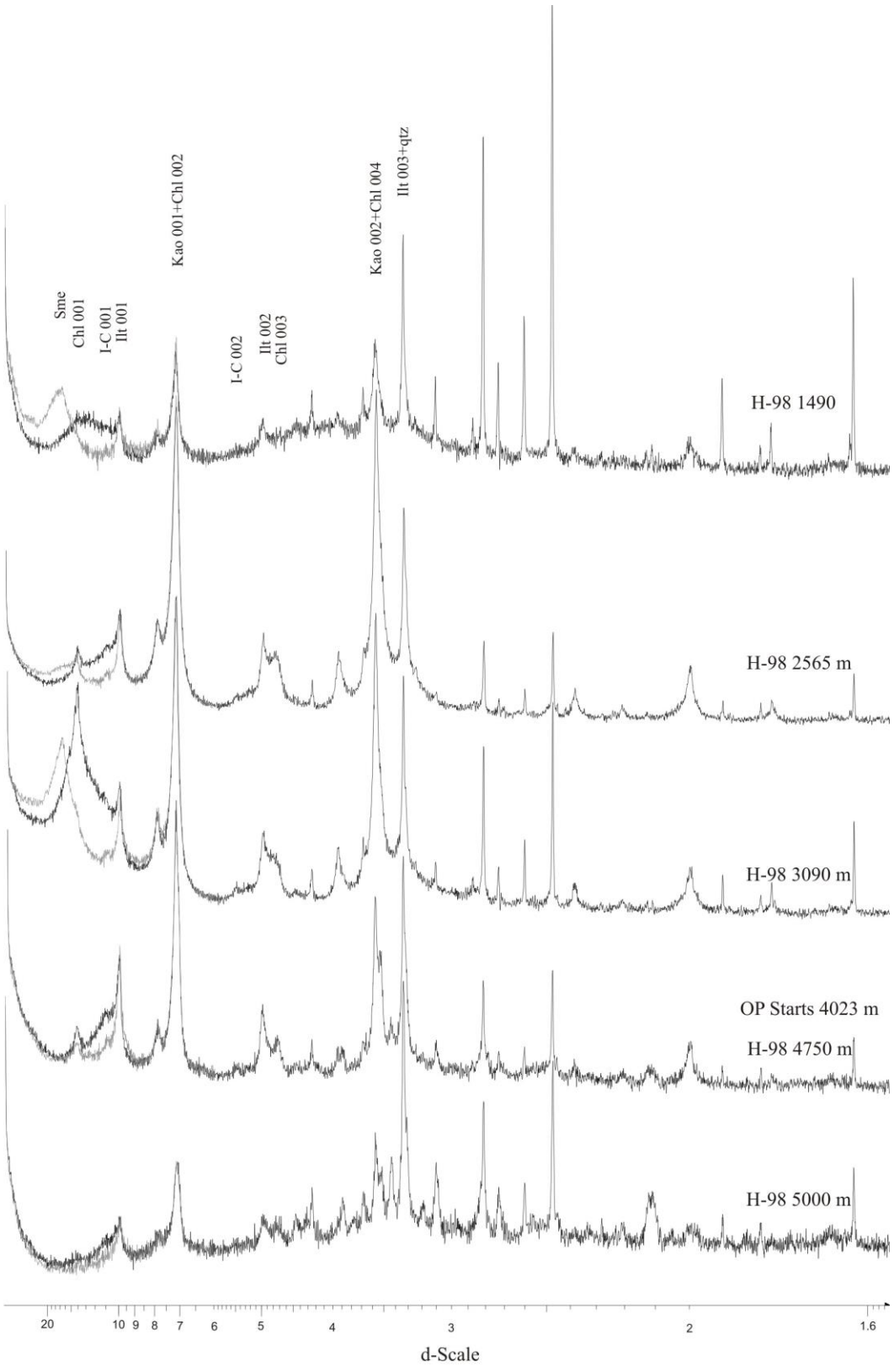

Figure 4.3.2 Stacked Diffractograms from Evangeline H-98 < 2μm clay samples. Solid black line indicates air-dried and grey line indicates glycolated.

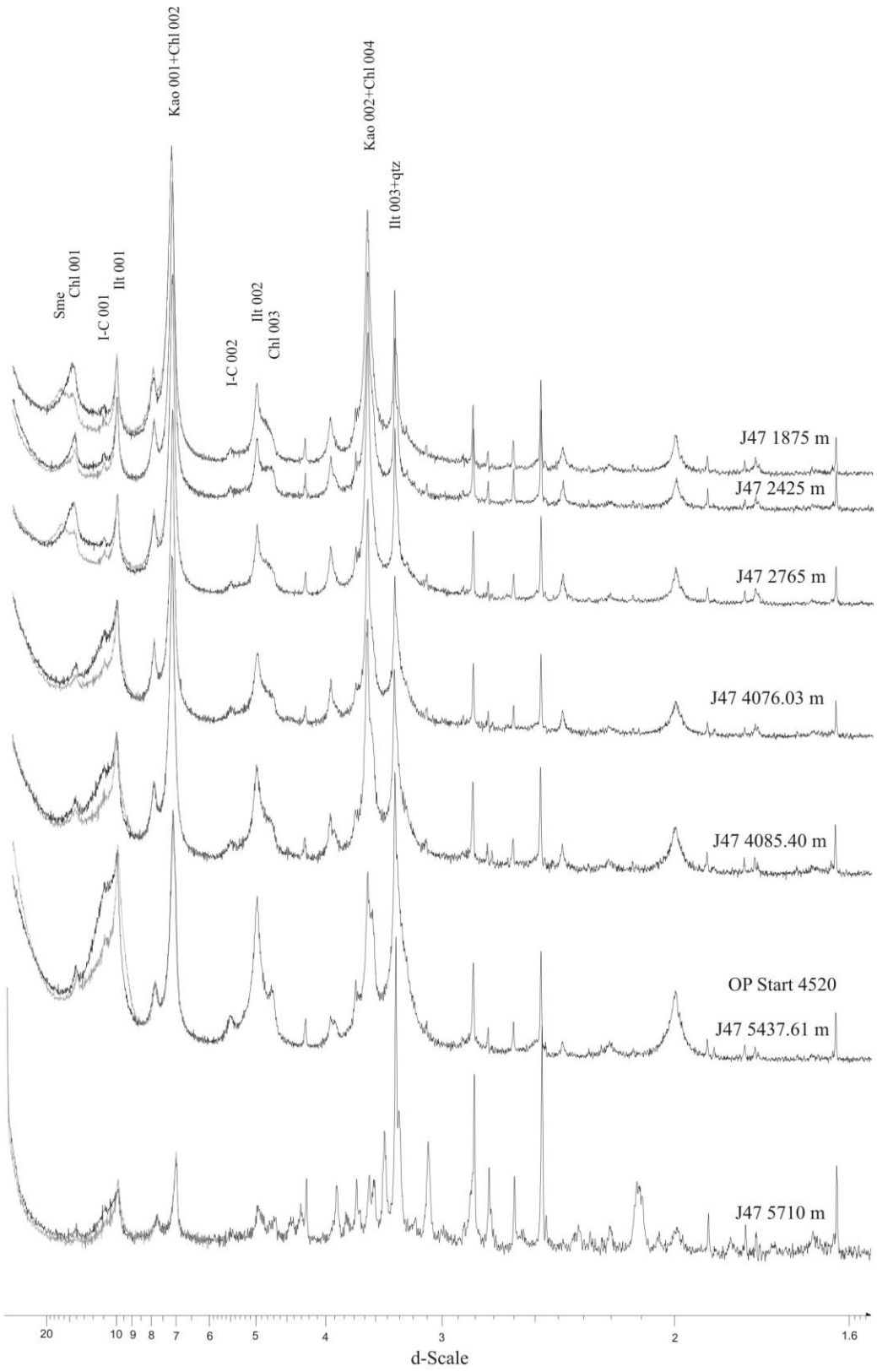

Figure 4.3.3 Stacked Diffractograms from Louisbourg J-47 < 2µm clay samples. Solid black line indicates air-dried and grey line indicates glycolated.

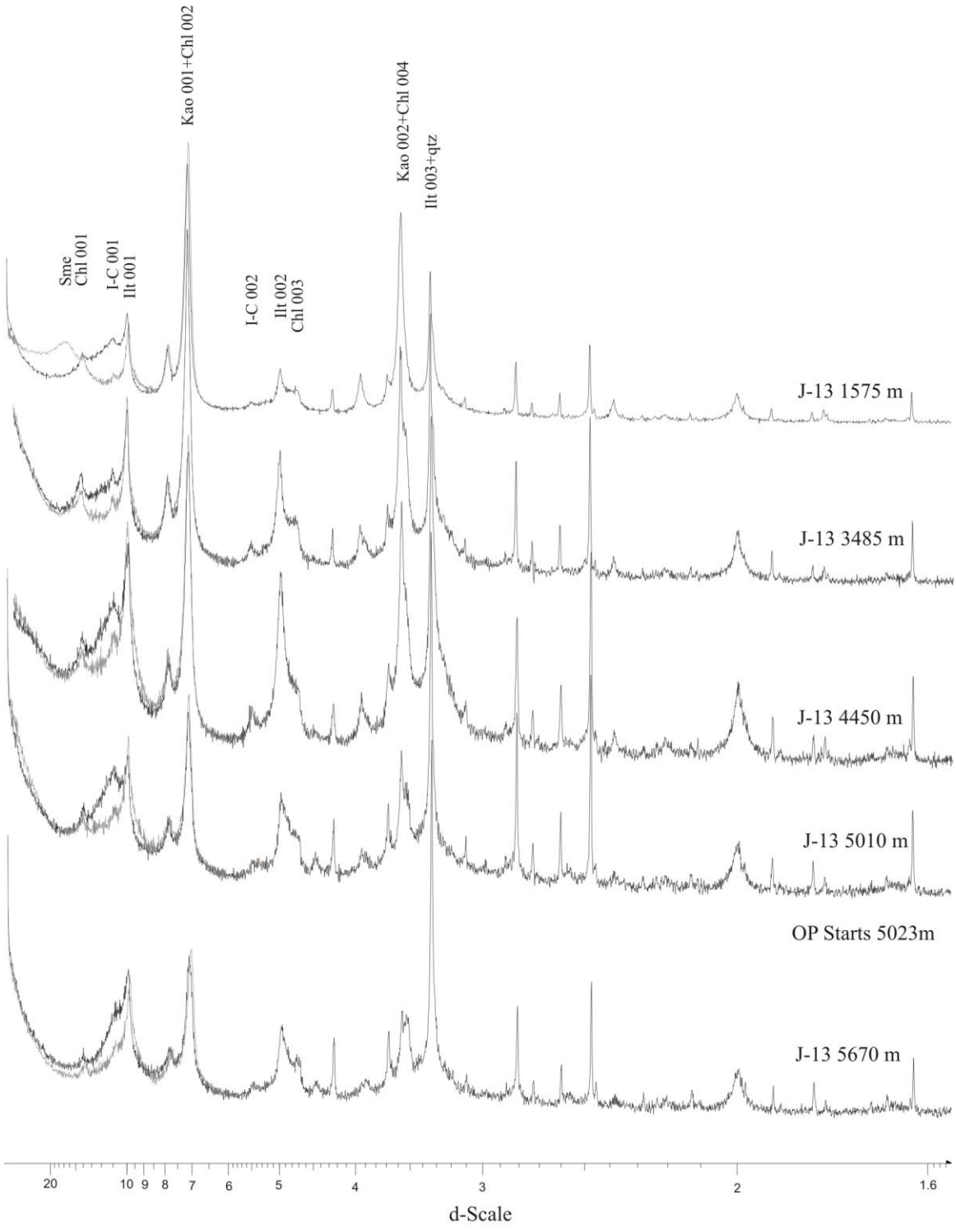

Figure 4.3.4 Stacked Diffractograms from South Griffin J-13 < 2μm clay samples. Solid black line indicates air-dried and grey line indicates glycolated.

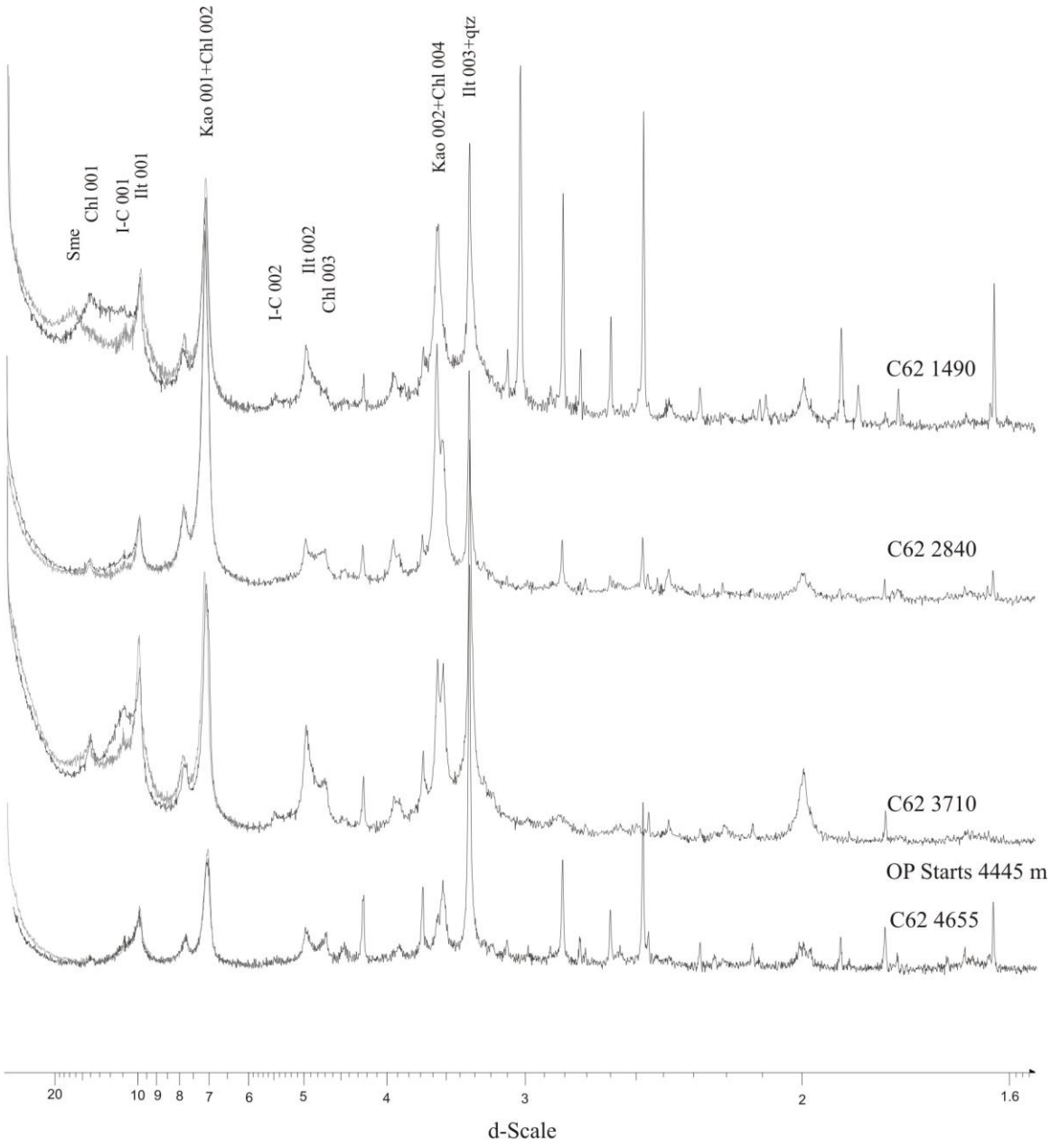

Figure 4.3.5a Stacked Diffractograms from West Venture C-62 < 2μm clay samples. Solid black line indicates air-dried and grey line indicates glycolated.

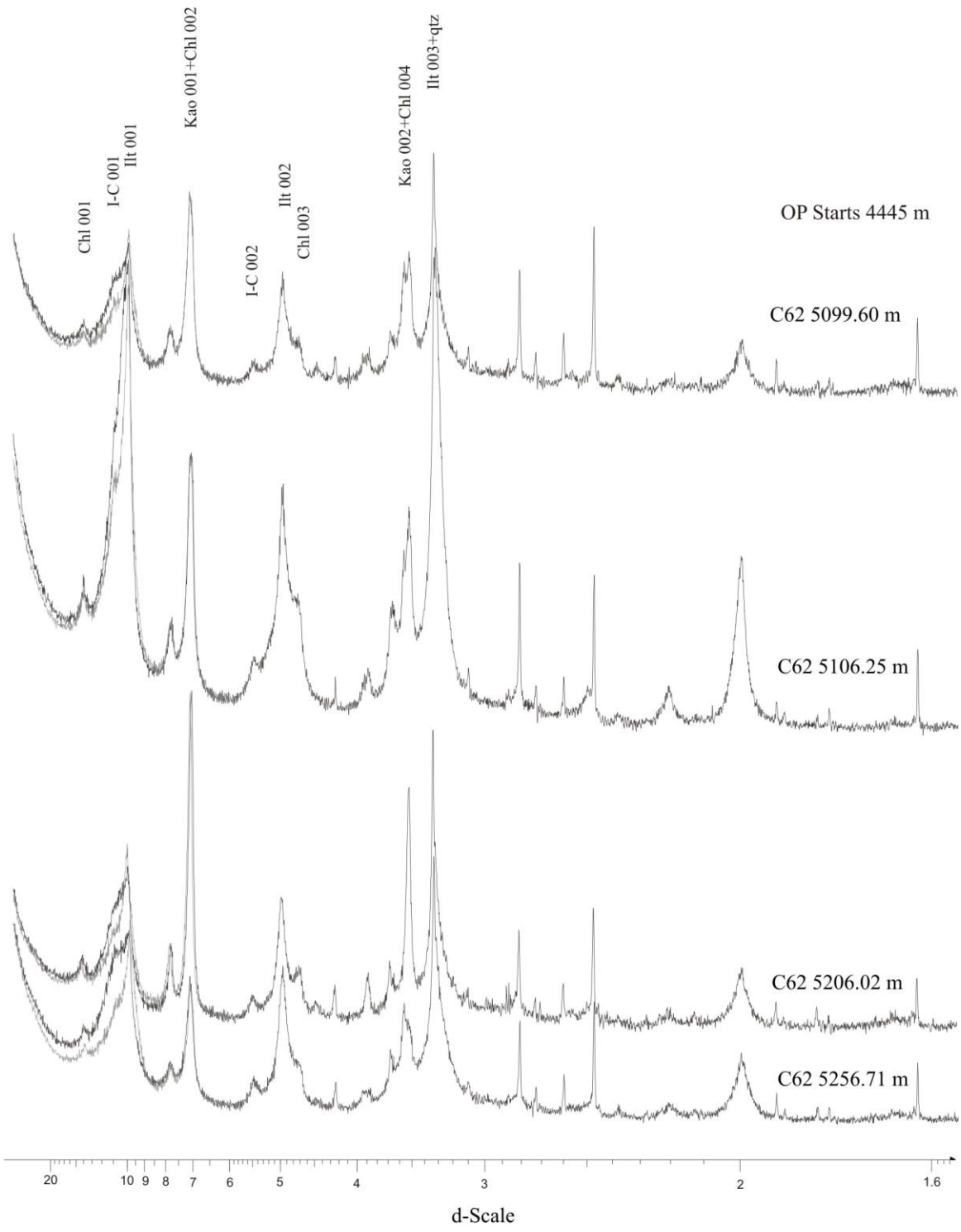

Figure 4.3.5b Stacked Diffractograms from West Venture C-62 < 2µm clay samples. Solid black line indicates air-dried and grey line indicates glycolated.

Chapter 5.0 Discussion

In this chapter, the mechanisms causing overpressure, if any, will be interpreted and compared with the petroleum discoveries in the well, if any. The studied wells show a range of observed velocity vs. density patterns in the overpressured zone, several of which have not been previously mentioned in the literature (Hoesni 2004, Lahann and Swarbrick 2011, O'Connor et al. 2011, Tingay et al., 2013). There is an apparent regular distribution of different velocity/density types; an example of this would be that all of the Venture wells show a similar pattern.

5.1 Lithologic controls on velocity and density

Velocity values can be determined by using a sonic log, which measures transit times of a formation. The log is a measure of how well a formation can transmit seismic waves. The interval transit time is dependent upon lithology and porosity, which will thus also affect velocity, which is the inverse of transit time. Interval transit time will decrease with increasing effective porosity (porosity that contributes to fluid flow).

The relationship

$$Vp = \sqrt{\frac{BM + 1.33SM}{p}}$$

where Vp = p-wave velocity, BM = bulk modulus, SM = shear modulus and p = density,

demonstrates how velocity depends on both moduli and density. The moduli effectively represent the elasticity of the rock, which tends to increase as pore-space is cemented. When porosity decreases, the moduli and P-wave velocity will both increase. At similar

porosities, the density of sandstone and shale are comparable, owing to the fact that clay minerals and quartz have similar densities. Sandstone and limestone that have been cemented by carbonates will be denser at similar porosities.

As sediments are buried, there is a progressive decrease in porosity. Muds undergo physical compaction and expulsion of pore fluids. Sandstones and limestones are compacted less, but porosity is reduced by cementation. Both compaction and cementation lead to an increase in density and velocity as burial depth increases. This can be observed by the normal compaction curve in Figure 3.1.1, also known as type 1 pattern. This pattern does not exhibit an increase or decrease in either velocity or density independent of the other. It is characterized by increasing velocity and density as you reach deeper depths. The normal compaction curve is associated with wells that do not experience overpressure. In shales, which are the subject of this thesis, density may be further increased by cementation (particularly by carbonates). Porosity may increase, and thus velocity and density decrease, if the shale develops open fractures filled with water or gas or if secondary porosity is created by corrosive fluids (as is common in many sandstones and limestones).

5.2 Effects of erosion in inboard wells

As noted in Chapter 3, there are higher velocities and densities in some proximal wells such as Kegeshook (Fig. 3.7.2) and West Esperanto (Fig. 3.22.3) than at the same depth in more distal wells such as Evangeline H-98 (Fig. 3.5.3) and Louisbourg J-47 (Fig. 3.8.3). There are several possible hypothesis that might explain the higher velocities and

densities at the same depth: (1) different lithologies in the more proximal wells; (2) the effects of overpressure in more distal wells, resulting in relatively low velocities and (3) glacial erosion of the upper part of the Banquereau Formation, so that the first sediments logged are more compacted than in most other wells. Lithological changes can be discounted, because only shaly intervals were analyzed for the velocity-density plots. The effect of overpressure would be applicable to deep parts of the section, but the interval in which the effect is most pronounced, from 1-3 km, is well above the overpressure zone in the distal wells. Seismic reflection profiles, for example from Maclean and Wade (1993) and Kendell (2012), show considerable erosion of the Banquereau Formation in the proximal parts of the Scotian Basin, consistent with the idea that parts of the succession were originally more deeply buried and compacted. Thus the higher velocities and densities in inboard wells are likely a consequence of Quaternary erosion.

5.3 Evidence from rock samples for controls on velocity

Velocity changes will depend on moduli and porosity. If porosity decreases because of greater crystallinity from such events as precipitation of minerals in fractures or pores, this will cause increase in velocity. Increasing porosity by opening fractures from gas generation, dehydration of minerals, or the formation of secondary porosity will cause a decrease in velocity. It is commonly observed that the onset of overpressure is marked by a decrease in velocity (Mudford, 1988). This can be detected from resistivity logs, which respond by decreasing in resistivity within the overpressured zone. This decrease in resistivity is caused by an increase in porosity and the resulting increase in water content

within shales in the overpressured region (Mudford, 1988). Sonic logs have also been used to detect the onset of overpressure because within an overpressured zone there may be a deviation to a lower velocity. This reduction in velocity is shown by types 3, 4, 8, and 9 in a velocity-density plot (Fig. 3.1.1). The increased porosity in the overpressured zone commonly results from bedding-parallel fractures, which open up parallel to the vertical direction of the least confining stress (Cobbold et al., 2013). However, a decrease in velocity does not necessarily occur at the top of the overpressure zone, as shown by types 5, 6, 7, and 10 in a velocity-density plot (Fig. 3.1.1).

Changes in velocity can also be inferred by looking at fractures and mineral precipitation occurring within shale samples. Figure 5.3.1a is a backscattered electron image, obtained using a scanning electron microscope, of a shale from West Venture C-62 at a depth of 5254.93 m, within the overpressure interval. There are obvious bedding-parallel fractures and variations in abundance of fractures may account for changes in velocity. There is also later cementation by pyrite, which would cause an increase in velocity and an increase in density. Pyrite grains have grown across fractures and this indicates that mineral growth occurred post fracture. Figure 5.3.1b is a back scattered electron image of a sandstone from South Desbarres O-76, almost 800 m above the top of overpressure. Like the shale sample, this sandstone shows bedding-parallel fractures. Lenses of barite as well as Mn-siderite, pyrite, and chlorite have precipitated within the fractures. These fractures were probably the result of hydraulic fracturing in the past, where the depth of this sample was previously within an overpressured zone (Pe-Piper et al., 2014).

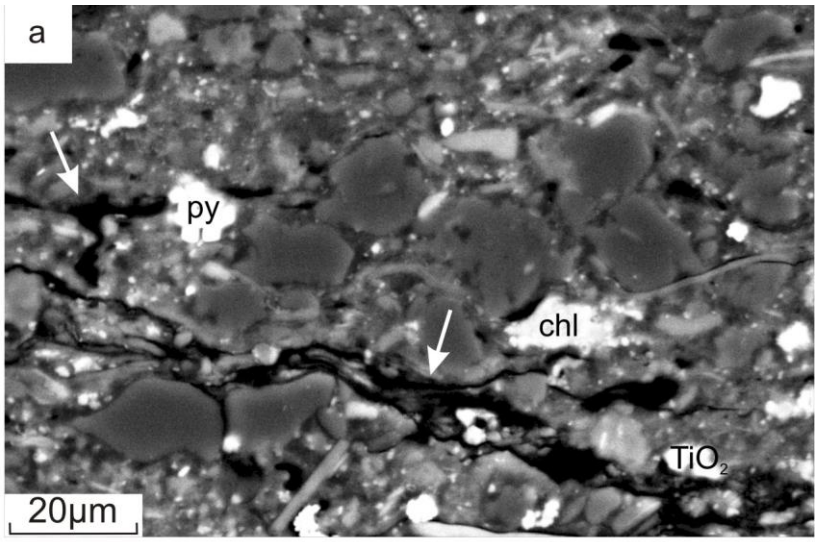

Figure 5.3.1a SEM image for sample C-62 5254.93 m site 1. The larger fracture does not cut through minerals, but pyrite(py) appears to cross-cut and post-date a fracture. Image taken by Yuanyuan Zhang (pers. comm. 2014). Fractures are indicated by white arrows.

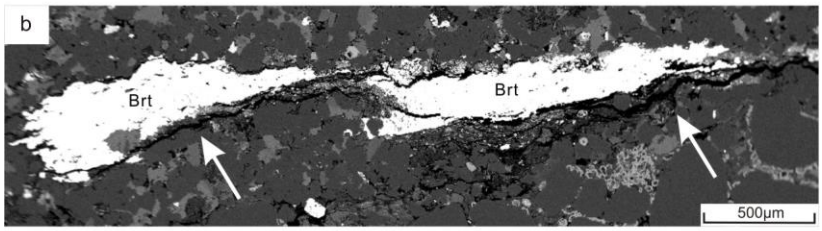

Figure 5.3.1b BSE image for sample O-76 3809.66 m site 1. Barite lenses and mineral precipitation (Mn-siderite, pyrite, and chlorite) within fractures indicate mineral precipitation post-dates the fractures (Pe-Piper et al., 2014). Fractures are indicated by white arrows.

5.4 Controls on Density

The velocity-density plots presented in Chapter 3 show that density may increase downwards within the overpressure zone, particularly for velocity-density types 4, 5, 6, and 8. Dehydration of clays and the associated expulsion and migration of water may lead to changes in density. So too will the diagenetic change from smectite to mixed layer I-S to illite demonstrated by X-ray diffraction in Chapter 4. This is because the grain density (i.e. water-free) of smectite is 2.08, whereas that of illite is 2.79. Fluids migrating through fractures precipitate minerals such as barite and sphalerite, causing cementation, may also cause changes in density, as illustrated in Figure 5.3.1 and discussed above.

5.5 Interpretation of the ten observed types of patterns (Fig. 3.1.1)

In Chapter 3, various patterns of data in density-velocity plots were distinguished and are summarized in Figure 3.3.1. This section interprets these patterns based on the observations on clay minerals and thin sections of shales, and on interpretations of density-velocity plots elsewhere in the literature.

Type 1 patterns follow a normal loading curve of increasing velocity and density with increasing depth in rocks that are normally pressured. Not all wells show similar patterns, but in general density increases more rapidly than velocity in the upper part of the well, and velocity more rapidly than density with deeper burial. For example, the deepest part of Peskowesk A-99 shown in red and black, shows features similar to type 3 plots, in which there is considerable range in velocity with little change in density, producing a vertically elongated cluster. Loading and consolidation above overpressure are not the focus of this thesis and Type 1 patterns are not considered further.

All other patterns refer only to overpressured sections of the wells. Type 2 patterns have been observed in Mohican I-100 (Fig. 3.9.2), Glenelg E-58 (Fig. 3.6.2), and Thebaud I-94 (Fig. 3.18.2). The type 2 pattern is essentially the same as type 1, suggesting that the processes involved in compaction are similar to those in the normally pressurized section. This is emphasized in the case of Mohican I-100, where the Shortland Shale from 1490 to 1990 m becomes progressively overpressured with depth, but the underlying strata to TD are normally pressurized (Fig. 3.9.1). The density-velocity plot in the overpressured interval shows a pattern intermediate between that above and below in normally pressured rocks (Fig. 3.9.2). There is no evidence in Mohican for

disequilibrium compaction in the moderately overpressured interval of the Shortland Shale.

Type 3 patterns are observed in Venture B-43 (Fig. 3.19.2), B-52 (Fig. 3.20.2), H-22 (Fig. 3.21.2), Thebaud I-93 (Fig. 3.17.2), and Alma F-67 (Fig. 3.3.1). Every type 3 pattern shows points below the top of overpressure decreasing in velocity with little to no change in density. O'Connor et al. (2011) interpreted this pattern as resulting from fluid expansion, usually caused by gas generation. Venture B-43, B-52, and H-22, have a vertical trend almost identical to the fluid expansion line in the plot by Tingay et al., (2013) shown as type 3 in Fig. 3.3.1. In contrast, Alma F-67 and Thebaud I-93 show a slight tendency for density to be higher at lower velocity, i.e. they trend slightly to the right downwards and are thus transitional to Type 4. All five wells showing the type 3 pattern discovered gas, condensate, and water and are from the three highest producing fields in the Scotian Basin. The pressure vs. depth graphs for these wells show points almost reaching lithostatic pressure indicating a large degree of overpressure. Thus a Type 3 pattern is restricted to wells that have high concentrations of gas and overpressures approaching lithostatic, confirming the interpretation of O'Connor et al. (2011) that this type is the result of fluid expansion

The Type 4 pattern is only seen in Sable Island C-67 (Fig. 3.12.1). It is characterized by the deepest points arranged at an angle with higher density at lower velocity, unlike a type 3, which points straight down. Given that Alma F-67 and Thebaud I-93 show a similar but smaller angular trend, Type 4 is probably related to a combined mechanism, involving fluid expansion and another process. That process may be load transfer (O'Connor et al., 2011), related to weakening of the framework of the rock by

partial dissolution of grains of kerogen and K-feldspar that help support the framework. However, a study of late barite and sphalerite cements by Pe-Piper et al. (2014) showed that these cements were more common in Sable Island C-67 than in the Thebaud field, and least common in the Venture field. It is therefore possible that the increase in density with decreasing velocity represents patchy cementation by these dense minerals of fractures opened by gas. Type 4 is thus identified as due to both fluid expansion and cementation.

Throughout this study a type 5 pattern has not been found. Type 5 is indicative of clay diagenesis or chemical compaction (O'Connor et al., 2011), in the absence of significant changes in velocity. There is petrographic evidence for chemical compaction, i.e. cementation by minerals brought in by formation water (e.g. sphalerite, barite) and for significant clay diagenesis involving illitization of smectite (Chapter 4). These effects are apparently masked by other processes that result in changes in velocity.

Type 6 patterns occur in Evangeline H-98 (Fig. 3.5.2), and South Griffin J-13 (Fig. 3.14.2). Based on graphs #4 (Fig. 3.5.3 and Fig. 3.14.3) for the wells mentioned above, a mechanism of overpressure generation could not be visually estimated because the points below the top of overpressure showed a high degree of scatter. The scattering effect is most likely due to a small interval in which the deepest points are located. If more points were available, it might be possible to reclassify these two wells.

Type 7 patterns are observed in Chebucto K-90 (Fig. 3.2.2), and West Venture C-62 (Fig. 3.23.2). These patterns are associated with changes in velocity and little to no changes in density. The type 7 may be due to opening and closing of fractures within the

subsurface, as there are increases and decreases in velocity with very little change in density. This specific type has not been previously mentioned in the literature. Both wells show a rapid increase in overpressure with depth, similar to that in wells in the Venture, Thebaud and Alma fields. Both were rated as significant discoveries of gas, but unlike the Type 3 fields, were never produced, suggesting that gas abundance was less. Thus Type 7 is interpreted to involve principally fluid expansion, but less than in Type 3.

Type 8 patterns are observable in Louisbourg J-47 (Fig. 3.8.2), and West Esperanto B-78 (Fig. 3.22.2). The increase in density with no change in velocity may be the result of cementation or precipitation of a dense mineral. The progressively lower density with increasing depth in the deepest samples (red and black) (Fig. 3.8.1 and Fig. 3.22.2) is unusual, but this may be a consequence of variable abundance of calcareous shale, which will tend to have higher density and velocity than pure shale. Louisbourg and South Griffin are the two wells studied with abundant interbedded limestone in the overpressure interval, but none is reported from West Esperanto. Lahann and Swarbrick (2010, 2011) postulated that if pore-pressure gradients were to reduce with depth within the overpressure zone, gas generation would cause velocity and density values to return to the loading curve; this is the likely cause of type 7.

Type 9 patterns, which are the exact opposite of type 7, are seen in Thebaud C-74 (Fig. 3.16.2) and South Desbarres O-76 (Fig. 3.13.2). In both wells the velocity decreases when the top overpressure is reached and then increases slightly when the deepest points are encountered, with a slight increase in density. The pattern is similar to Type 3 over most depths, resulting from fluid expansion, but at greatest depths the fractures may not

be as large or may be partly cemented, thus increasing velocity and slightly increasing density.

Type 10 patterns are shown by North Banquereau I-13 (Fig. 3.10.1) and Tantallon M-41 (Fig. 3.15.2). This pattern looks similar to type 2 in that it follows the loading curve shown in Figure 3.1.1. The difference is that the deeper points start to orient themselves vertically and continue above the original figure created by Hoesni (2004). The continuation of small increases in velocity and density may be due to increased disequilibrium compaction with depth.

5.6 Relationship to hydrocarbons

The conversion of kerogen to hydrocarbons has been a suggested mechanism to generate a high degree of overpressure. This is because it was generally thought that a large volume expansion was associated with this reaction. In order to maintain overpressure there would need to be a good seal.

Most of the offshore production is from Venture, Thebaud, and Alma. These fields contain wells that display type 3 velocity-density plots. The wells all discovered gas, with some finding condensates, and water. The amounts of each discovery varied with each well. They also displayed a large degree of overpressure as shown by data points almost reaching the lithostatic gradient in pressure vs. depth plots for corresponding wells. There may thus be a connection between gas discovery, large degree of overpressure, and type 3 velocity-density pattern.

Cohasset A-52, Glenelg E-58, and Louisbourg J-47 have found gas but in lesser amounts. The wells have very different degrees of overpressure as well as velocity-density types. Cohasset A-52 does not have overpressure and thus is a type 1. This may have to do with oil being more prominent and gas being minor. Glenelg E-58 has a small degree of overpressure and shows a type 2 pattern. This may be the effect of small amounts of gas and oil discovered in the well. Louisbourg J-47 has a large degree of overpressure and is classified as a type 8 based on its velocity vs. density plot. There was a gas show with minor oil.

There are a number of wells throughout the Scotian Basin that are dry and also have varying degrees of overpressure, or none at all. The majority of these wells have medium degrees of overpressure, with a few exceptions. South Desbarres O-76 and West Esperanto K-78 both have large degrees of overpressure even though South Desbarres O-76 has a type 9 velocity-density plot and West Esperanto K-78 has a type 8 velocity-density plot. Kegeshook G-67 and Peskowesk A-99 have no overpressure and thus have type 1 velocity-density plots. Tantallon M-41 has a small degree of overpressure and a type 10 velocity-density plot.

Well	Velocity-Density type	Degree of overpressure	Well Discoveries
Alma F-67	3	L	Producing Field, Gas+Cond
Chebucto K-90	7	M	Sig Disc of Gas+Unrated Oil+Cond
Cohasset A-52	1	N	Oil+Minor gas
Evangeline H-98	6	M	Dry
Glenelg E-58	2	S	Gas Field, Unrated Gas and Oil
Kegeshook G-67	1	N	Dry
Louisbourg J-47	8	L	Gas show, unrated Oil
Mohican I-100	2	M-S	Dry
North Banquereau I-13	10	M	Dry
Peskowesk A-99	1	N	Dry
Sable Island C-67	4	M	Gas+Oil shows
South Desbarres O-76	9	L	Dry
South Griffin J-13	6	M	Dry
Tantallon M-41	10	S	Dry
Thebaud C-74	9	L	Producing Field, Gas+Cond
Thebaud I-93	3	L	Producing Field,Gas+Cond
Thebaud I-94	2	M	Producing Field,Gas+Cond
Venture B-43	3	L	Producing Field,Gas+Cond
Venture B-52	3	L	Producing Field,Gas+Cond
Venture H-22	3	L	Producing Field,Gas+Cond
West Esperanto B-78	8	L	Dry
West Venture C-62	7	L	Sig Disc of Gas+Unrated Oil+Cond
West Venture N-91	8	L	Sig Disc of Gas+Unrated Oil+Cond

Table 3: Wells with their velocity-density type, degree of overpressure and discoveries. N = none, L = large, M = medium, S = small. Cond = condensates.

5.7 Relationship to clay diagenesis

The transformation of smectite to illite has been a suggested mechanism of producing secondary overpressure. Swarbrick and Osborne (1997) have stated that this is unlikely to happen because the volume of water expelled is not enough to generate significant overpressures and dehydration is impeded by overpressure build up. If smectite to illite dehydration were to occur, the presence of a seal would be needed in order to have any pressure increase. Smectite dehydration on its own may not be able to produce large overpressures but the release of intercrystalline water may lead to disequilibrium compaction. Swarbrick and Osborne (1997) stated that the release of water by collapsing of the smectite framework would influence the compressibility of the sediments. If the rock becomes more compressible, the overlying sediments will cause compaction and the pore water created by smectite dehydration will leave the rock. On the other hand, if water is not released, overpressure results from pore water supporting the increased overlying sediments and disequilibrium compaction is produced by mineral dehydration.

Three wells, Evangeline H-98 (velocity-density type 6), Louisbourg J-47 (type 8) and West Venture C-62 (type 7) have more than one clay mineral sample within the overpressure zone and show variations between Sachsenhofer et al. (1998) types 3 and 4. Although there is no precise correlation between smectite abundance and rock density, each of these three types of velocity-density plot involves variations in density that could result from variations in smectite abundance in I-S clays.

Evangeline 4750 (3) to 5000 (4).

Louisbourg 5437 (3) to 5710 (4).

West Venture 4655 (4) to 5099 (3) to 5106 (4) to 5206 (4) to 5256 (3).

The reaction of gypsum to anhydrite is another possible mechanism thought to produce overpressure in evaporite sections. It has been suggested by Swarbrick and Osborne (1997) that this transformation releases 39% of bound water. This is a greater volume expelled than the smectite to illite transformation. The reaction occurs during shallow burial at around 40-60 °C and is unlikely to generate overpressures at great depth (Swarbrick and Osborne 1997). This reaction would be unlikely occurring in the studied wells because overpressure occurs at significant depths.

5.8 Relationship of velocity-density patterns to degree of overpressure

As was mentioned before, processes such as diagenesis of smectite may not be able to generate significant overpressures, while gas formation, load transfer, and disequilibrium compaction could possibly generate larger overpressures. A way to visualize the degree of overpressure is to use pressure vs. depth graphs such as the ones throughout Chapter 3. If points follow the hydrostatic line without moving off it, as in the case of Kegeshook G-67 (Fig. 3.7.1), this indicates no overpressure. When points move off the hydrostatic line and approach the lithostatic line it means there is overpressure. How far the points come off the hydrostatic line can also tell you the degree of overpressure. In the case of Venture B-43 and Glenelg E-58 (Fig. 3.19.1 and Fig. 3.6.1), Venture B-43 has a higher overpressure because the points almost reach lithostatic, while Glenelg E-58 has a much lower overpressure because the points are closer to the hydrostatic line.

The onset of overpressure will encounter a transition zone with increasing depth. Pressure vs. depth plots with overpressure (Fig. 5.8.1) reveal a transition zone where

Keen and Williams (1990) interpreted this as indicating interconnected permeable reservoirs. Mudford (1988) said that the transition zone is an area of very high pressure gradient and below it is the hard overpressure zone, which is characterized by having a constant pressure gradient that is less than the transition zone but greater than the hydrostatic gradient. The transition zone can be seen on pressure vs. depth plots of wells that have overpressure. It is characterized by a semi-horizontal "plateau" as pressure initially lifts off the hydrostatic pressure gradient (Fig. 3.19.1).

Based on the study of velocity-density graphs and their proposed types, high overpressures (large degree) are found to correspond to types 3, 7, 8, and 9 (Table 3). Moderate overpressure (medium degree) showed the most variation in velocity-density types. The different types were 2, 4, 6, 7, and 10. Two wells that showed low overpressure (small degree) and corresponded to types 2 and 10. Wells that did not have overpressure were referred to as type 1.

Chapter 6.0 Conclusions

The purpose of this thesis was to test the methodology of velocity-density cross plots in the Scotian Basin. The goal was to use these plots to possibly further understand the secondary mechanism of overpressure generation occurring throughout the study area. X-ray diffraction was also used hoping to find the link between clay diagenesis and overpressure generation in some of the studied wells.

1. The method of cross plot creation and analysis to determine secondary overpressure generation mechanisms does indeed have some merit. Many of the velocity-density cross plots from this study show trends almost identical to those proposed by Hoesni 2004, O'Connor et al. 2011, and Tingay et al. 2013. That being said, using cross plot analysis solely to determine what is causing the overpressure would not be enough. This method combined with others pressure determination methods would be beneficial. The studying of overpressure, no matter where, may be aided by cross plot analysis.

2. The studied wells show a range of observed velocity vs. density patterns within the overpressured zone, several of which have not been previously mentioned in the literature (Hoesni 2004, Lahann and Swarbrick 2011, O'Connor et al. 2011, Tingay et al. 2013). The original figure from Hoesni (2004) showed five possible trends or pattern types as we call them in this study. We have added to the figure another five trends observed in our samples, totaling thus ten trends or types.

3. There is an apparent regular distribution of different velocity-density types; an example of this would be that all of the Venture wells show a similar pattern. This

could be further tested by adding wells from the same fields that were not included in this thesis. For example, more wells from the Alma, Thebaud, and Glenelg fields.

4. Local geological/petrophysical factors dictate how velocity and density will change within the overpressure zone. The data from this study have shown that each specific pattern can be explained in terms of the following physical parameters: rock lithology, porosity, fluid circulation including hydrocarbons, diagenetic changes and erosion.

5. Thus fractures and cementation may have an influence on velocity and density downwell. The fractures may be due to the buildup of overpressure and its eventual release. The opening of fractures would cause a decrease in velocity and that would be observable in velocity-density plots. From SEM analysis of mudstones, fractures were observed within the overpressure zone from West Venture C-62.

6. The XRD patterns of smectite, illite-smectite, and illite did not always descend in the expected sequence from 1 to 4 with depth. In some wells, later stages are sandwiched between earlier ones. This may be due to: a) downhole contamination by smectite cuttings from the upper sections of the wells. b) Locally increase of temperature by circulating fluids causing these diagenetic transformations and c) changes in the supply of smectite by rivers that was climatically controlled.

References

Aneja, N., 2013. Clay mineral analysis of shales from the Mesozoic strata, Scotian Basin. Technical Report, Department of Geology, Saint Mary's University, p. 1-21.

CNSOPB, 2000. Technical Summaries of Scotian Shelf Significant and Commercial Discoveries, November 2000 edition, 275p.

Cobbold, P.R., Zanella, A., Rodrigues, N., Loseth, H., 2013. Bedding-parallel fibrous veins (beef and cone-in-cone): Worldwide occurrence and possible significance in terms of fluid ovepressure, hydrocarbon generation and mineralization. Marine and Petroleum Geology, v. 43, p. 1-20.

Drummond, K.J., 1986. Geopressure in Venture and Sable Island area; Program and Abstracts, Canadian Society of Petroleum Geologists, 1986 Convention, June 1–4, 1986 Calgary Alberta, p. 40.

Forbes, P.L., Ungerer, P., Mudford B.S., 1992. A Two-Dimensional Model of Overpressure Development and Gas Accumulation in Venture Field, Eastern Canada. The American Association of Petroleum Geologists Bulletin, v. 75, p. 318–338.

GSC Atlantic, 2014. NRCAN Basin Database. http://basin.gdr.nrcan.gc.ca/wells

Hoesni, J.M., 2004. Origins of Overpressure in the Malay Basin and its influence on petroleum systems: PhD thesis, University of Durham, Durham United Kingdom. Available at Durham E-Thesis Online: http://etheses.dur.ac.uk/1755/

Keen, M.J.(ed), Williams, G.L.(ed), 1990. Geology of the continental margin of eastern Canada. Geological Survey of Canada, Geology of Canada Series no. 2, p.855.

Kendell K.L., 2012. Variations in salt expulsion style within the Sable Canopy Complex, central Scotian Margin. Canadian Journal of Earth Science, v. 49, p. 1504-1522.

Lahann, R.W., Swarbrick, R.E., 2011. Overpressure generation by load transfer following shale framework weakening due to smectite diagenesis. Geofluids, v. 11, p. 362-375.

MacLean, B.C., and Wade, J.A., 1993. Seismic Markers and Stratigraphic Picks in the Scotian Basin Wells. East Coast Basin Atlas Series, Geological Survey of Canada, 276p.

Mudford, B.S., 1990. A One–Dimensional, Two Phase Model of Overpressure Generation in the Venture Gas Field, Offshore Nova Scotia. Bulletin of Canadian Petroleum Geology, v. 38, p. 246–258.

Mudford, B.S., Best, E.M., 1989. Venture Gas Field, Offshore Nova Scotia: Case Study of Overpressuring in Region of Low Sedimentation Rate. AAPG Bulletin, v. 73, p. 1383–1396.

Mudford, S.B., 1988. Modeling the Occurrence of Overpressure on the Scotian Shelf, Offshore Eastern Canada. Journal of Geophysical Research, v. 93, p. 7845–7855.

O'Connor, S., Swarbrick, R., Hoesni, J., Lahann, R., 2011. Deep Pore Prediction in Challenging Areas, Malay Basin, SE Asia. Indonesian Petroleum Association.

Osborne, M.J., Swarbrick, R.E., 1997. How Overpressure and Diagenesis Interact in Sedimentary Basins – Consequences for Porosity Preservation in HPHT Reservoir Sandstones. Indonesian Petroleum Association.

Osborne, M.J., Swarbrick, R.E., 1997. Mechanisms for Generating Overpressure in Sedimentary Basins: a reevaluation. AAPG Bulletin, v. 81, p. 1023–1041.

Sachsenhofer, G.R.F., Rantitsch, C., Russegger B., Jelen, B., 1998. Smectite to illite diagenesis in early Miocene sediments from the hyperthermal western Pannonian Basin. Clay Minerals 33, 523-537.

Strathdee, G, 2012. Origin and significance of clay minerals in Mesozoic shales of the Scotian Basin. M.Sc. thesis, Department of Geology, Saint Mary's University.

Thyne, G., Boudreau, B.P., Ramm, M., Midtbo, R.E., 2001. Simulation of potassium feldspar dissolution and illitization in the Statfiord Formation, North Sea. The American Association of Petroleum Geologists, v. 85, p. 621–635.

Tingay, M.R.P., Morley, C.K., Laird, A., Limpornpipat O., Krisadasima K., Pabchanda S., Macintyre H.R., 2013. Evidence for overpressure generation by kerogen-to-gas maturation in the northern Malay Basin. The American Association of Petroleum Geologists, v. 97, p. 639–672.

Wade, J.A. and MacLean, B.C., 1990. The geology of the southeastern margin of Canada, Chapter 5 in Geology of the Continental Margin of Eastern Canada, M.J. Keen and G.L. Williams (ed.); Geological Survey of Canada, Geology of Canada, no. 2, p. 190–238.

Williamson, M.A., 1995. Overpressures and hydrocarbon generation in the Sable sub-basin, offshore Nova Scotia. Basin Research, v. 7, p. 21–34.